RESEARCH IN PHARMACY AND MEDICINE
PHARMEDICINE
JOURNAL

ISSN: 3023-6967

Regulatory Effects of Plant-Derived Phenolic Compounds on Ferroptosis: A Novel Paradigm in Cancer Therapy

Talip Sahin

Therapeutic Properties of Alpha Lipoic Acid and Quercetin on Methotrexate-Induced Oxidative Stress in Rat Liver

Seyma Savas
Esin Ak
Sarfraz Ahmad
Sehkar Oktay

Micellar Pseudo-Models for Biological Membranes: Spectrophotometric Analysis of Micellar Binding of Antiviral (Oseltamivir Phosphate) and Anticoagulant (Enoxaparin Sodium)

Seher Guclu
Sinem Gokturk

Integrative Analysis of Molecular Interactions and Repurposable Drugs in Primary Biliary Cholangitis

Duygu Sari-Ak
Nazlı Helvaci-Kurt
Fatih Con
Alev Kural

03

Volume 3 Issue 1 February 2026

www.pharmedicinejournal.com

RESEARCH IN PHARMACY AND MEDICINE
PHARMEDICINE
JOURNAL

Editorial Team

RESEARCH IN PHARMACY AND MEDICINE
PHARMEDICINE
JOURNAL

CONTENTS

REVIEW

ORIGINAL ARTICLES

RESEARCH IN PHARMACY AND MEDICINE
PHARMEDICINE JOURNAL

2026; 3(1):1-26. doi: 10.62482/pmj.53

Review

Regulatory Effects of Plant-Derived Phenolic Compounds on Ferroptosis: A Novel Paradigm in Cancer Therapy

Talip Sahin

Adıyaman University, Faculty of Arts and Sciences, Department of Biology, Adıyaman, Türkiye

Corresponding Author: Talip Sahin (**E-mail:** talipsahin34@gmail.com)

Received: 2026.01.16; **Revised:** 2026.02.19 **Accepted:** 2026.02.22 **Published:** 2026.02.28

Abstract

Ferroptosis is a recently identified, iron-dependent form of regulated cell death characterized by excessive lipid peroxidation and membrane damage, and it has emerged as a promising therapeutic target in cancer treatment. In recent years, increasing attention has been directed to plant-derived phenolic compounds due to their potent redox-modulating, metal-chelating, and signaling-regulatory properties. This review provides a comprehensive overview of the molecular mechanisms by which phenolic compounds regulate ferroptosis in cancer cells. Phenolics modulate ferroptosis through multiple pathways, including suppression of glutathione peroxidase 4 (GPX4), depletion of intracellular glutathione (GSH), disruption of iron homeostasis via ferritinophagy, and acceleration of lipid peroxidation mediated by acyl-CoA synthetase long-chain family member 4 (ACSL4) – and arachidonate lipoxygenase (ALOX)-dependent pathways. In addition, redox-sensitive signaling axes, particularly the nuclear factor erythroid 2-related factor 2 (NRF2) pathway, play a dual role by conferring cytoprotective effects in normal cells while promoting ferroptosis resistance in tumor cells. Recently, in silico, network pharmacology, and omics-based studies further reveal that phenolic compounds exert their effects via complex multi-target networks rather than single protein inhibition. Moreover, nanotechnological carrier systems significantly improve the bioavailability, tumor selectivity, and ferroptosis-inducing efficacy of phenolic compounds. Collectively, the available preclinical evidence highlights plant-derived phenolics as promising ferroptosis modulators and potential adjuvant agents in cancer therapy. Unlike previous reviews that focus primarily on either ferroptosis signaling or general anticancer effects of polyphenols, this review integrates molecular mechanisms, systems-level analyses, and delivery strategies to present a unified framework for phenolic-driven ferroptosis modulation in cancer.

Keywords: Cancer therapy, ferroptosis, lipid peroxidation, network pharmacology, phenolic compounds

1. Introduction

Cancer is the second leading cause of mortality worldwide after cardiovascular diseases, with millions of new cases diagnosed each year (1). Despite advances in conventional treatment strategies such as surgery, chemotherapy, and radiotherapy, tumor heterogeneity, multidrug resistance (MDR), therapy-associated systemic toxicity, and high recurrence rates significantly limit the overall efficacy of cancer treatment (2-4). Therefore, in recent years, the identification and therapeutic targeting of novel regulated cell death mechanisms independent of apoptosis have become a priority area in oncological research (5).

In this context, ferroptosis was defined in 2012 as an iron-dependent, lipid peroxidation-driven, non-apoptotic form of cell death, opening a new era in cancer biology (6,7). Ferroptosis is characterized by intracellular free iron accumulation, excessive production of reactive oxygen species (ROS), peroxidation of polyunsaturated fatty acids, and the collapse of antioxidant defense systems (7,8). In this process, glutathione peroxidase 4 (GPX4) and intracellular glutathione (GSH) levels play a central regulatory role. Inhibition of GPX4 activity or depletion of GSH irreversibly commits cells to ferroptotic death (9).

Due to their increased metabolic activity, elevated iron demand, and pronounced oxidative stress burden, cancer cells are considerably more susceptible to ferroptosis than normal cells (5). In aggressive tumor types such as hepatocellular carcinoma, pancreatic adenocarcinoma, triple-negative breast cancer, glioblastoma, and lung cancer, pharmacological modulation of ferroptosis pathways has been reported to yield significant antitumor effects (7,10). However, the identification of agents capable of selectively inducing ferroptosis while exhibiting minimal toxicity in healthy tissues remains a major unmet research need.

Natural products, particularly plant-derived secondary metabolites, occupy an important place in cancer chemoprevention and therapy owing to their multi-target mechanisms of action and low toxicity profiles (11-13). Among these compounds, plant phenolics represent a broad phytochemical class encompassing phenolic acids, flavonoids, stilbenes, and lignans (14,15). Traditionally recognized for their strong antioxidant properties, phenolic compounds have recently been shown to function not only as free radical scavengers but also as bioactive molecules capable of bidirectionally regulating cellular redox homeostasis (16-18).

An increasing number of molecular and cellular studies demonstrate that plant phenolics can regulate ferroptosis through direct or indirect mechanisms (17,19-21). Phenolic compounds influence ferroptosis via multiple pathways, including modulation of iron homeostasis (21), regulation of ferritin metabolism (22, 23), inhibition of GPX4 activity or suppression of GSH synthesis (24) and activation nonheme iron-based arachidonate lipoxygenase (ALOX)-dependent lipid peroxidation pathways (25). Moreover, activation of redox-sensitive signaling cascades such as nuclear factor erythroid 2-related factor 2 (NRF2) plays a central role in the bidirectional regulatory effects of phenolics on ferroptosis (26-28).

It has been reported that certain phenolic compounds such as resveratrol, quercetin, epigallocatechin gallate (EGCG), and curcumin increase intracellular free iron accumulation, suppress GPX4 activity, and trigger lipid ROS production in cancer cells, thereby inducing ferroptotic cell death (21,29-31). Morever, phenolic acids such as gallic acid, chlorogenic acid, and rosmarinic acid have been shown to reduce iron-mediated oxidative damage limit lipid peroxidation, and suppress ferroptosis by stabilizing the GSH-GPX4 axis in normal cells (33-35), This bidirectional regulatory effect clearly indicates that the phenolic-ferroptosis interaction is highly dependent on the type of compounds, dose, and cellular context.

The heightened susceptibility of cancer cells to ferroptosis, coupled with the ability of phenolics to protect healthy cells, highlights the exceptional therapeutic selectivity of these compounds. Indeed, preclinical studies have demonstrated that the combination of phenolic compounds with conventional chemotherapeutics can enhance therapeutic responses, suppress chemotherapy resistance, and potentiate ferroptosis-mediated cell death (36,37).

Nevertheless, the clinical translation of phenolic compounds is hindered by major limitations such as low bioavailability, rapid metabolism, limited tissue penetration, and unfavorable pharmacokinetic properties. To overcome these challenges, nanotechnological delivery systems based on polymeric nanoparticles, lipid-based carriers, chitosan, alginate, and liposomes have been developed in recent years, and these systems have been shown to significantly enhance the ferroptosis-modulating efficacy of phenolic compounds (38,39).

Collectively, these findings indicate that plant phenolics are not merely conventional antioxidant molecules, but rather multifunctional and selective natural anticancer agents capable of regulating ferroptosis through iron metabolism, lipid peroxidation, and antioxidant defense systems. When

the unique position of ferroptosis in cancer biology is combined with the pleiotropic redox-modulatory effects of phenolics, it becomes evident that these compounds may occupy a central role in next-generation ferroptosis-based therapeutic strategies.

In this review, the chemical classes of plant phenolics, the molecular mechanisms of ferroptosis, the cellular and molecular regulatory roles of phenolic-ferroptosis interactions, current preclinical evidence, and the clinical translation potential of nanotechnological carrier systems are comprehensively addressed from an integrated perspective. Thus, this work aims to elucidate how phenolic-based approaches targeting ferroptosis may establish a new paradigm in cancer therapy.

2. Ferroptosis

Ferroptosis is a regulated, iron-dependent, lipid peroxidation–driven and non-apoptotic form of cell death that was first described by Dixon et al. in 2012. Unlike apoptosis, necrosis, and autophagy, ferroptosis does not involve classical apoptotic hallmarks such as caspase activation, DNA fragmentation, or formation of apoptotic bodies (6,7). At the morphological level, ferroptotic cell death is characterized by mitochondrial shrinkage, loss of cristae, and increased density of the outer mitochondrial membrane, while nuclear integrity is largely preserved (40).

From a biochemical perspective, the fundamental determinants of ferroptosis can be summarized as intracellular Fe^{2+} accumulation, increased production of ROS, peroxidation of polyunsaturated fatty acids (PUFAs), and collapse of antioxidant defense systems (8). The complex molecular landscape of ferroptosis presents a vital frontier for medical research. Emergent data have identified innovative regulatory targets, paving the way for advanced pharmacological interventions to mitigate or harness this cell death pathway in various clinical contexts.

2.1. Central Regulators of Ferroptosis

2.1.1. Iron Homeostasis

Iron homeostasis is a tightly controlled cellular process that ensures sufficient iron availability for essential metabolic functions while preventing iron-induced oxidative damage. At the core of ferroptosis lies the expansion of the intracellular labile iron pool (LIP). Iron catalyzes the formation of highly reactive hydroxyl radicals (•OH) from hydrogen peroxide via the Fenton reaction, thereby initiating the lipid peroxidation cascade and cell death (41).

Multiple iron-regulatory pathways converge to modulate ferroptosis sensitivity. Enhanced iron uptake via the transferrin-transferrin receptor 1 (TFR1) axis increases intracellular iron loading, while endosomal ferrireductases such as six-transmembrane epithelial antigen of prostate 3 (STEAP3) facilitate the conversion of Fe^{3+} to the more reactive Fe^{2+} form (41). Simultaneously, impairment of iron storage mechanisms, particularly through the downregulation of ferritin heavy chain-1 (FTH1), limits iron sequestration and further enlarges the LIP. A critical contributor to this process is ferritinophagy, a selective form of autophagy mediated by nuclear receptor coactivator 4 (NCOA4), which promotes lysosomal degradation of ferritin and releases stored iron into the cytosol. Therefore, excessive activation of ferritinophagy causes intracellular iron overload, which further triggers oxidative stress and ferroptosis (42).

In addition to increased iron import and mobilization, ferroptosis is further reinforced by reduced iron export. Suppression of ferroportin-1 (FPN1), the sole known cellular iron efflux transporter, leads to intracellular iron retention and amplifies oxidative stress (43). Collectively, these alterations establish a pro-ferroptotic iron landscape characterized by sustained Fe^{2+} accumulation and heightened vulnerability to lipid peroxidation.

Notably, cancer cells exhibit profound alterations in iron metabolism, including elevated iron demand, increased TFR1 expression, and dysregulated ferritin dynamics, which render them particularly susceptible to ferroptosis (44). This iron-addicted phenotype creates a therapeutic window in which modulation of iron homeostasis can selectively induce ferroptotic death in malignant cells while sparing normal tissues. Consequently, targeting iron regulatory networks has emerged as a promising strategy for ferroptosis-based cancer therapies and for enhancing the efficacy of ferroptosis-inducing agents.

2.1.2. Lipid Peroxidation

The execution phase of ferroptosis is governed by the iron-dependent oxidative degradation of PUFAs within membrane phospholipids. Due to their bis-allylic hydrogen atoms, PUFAs are highly susceptible to radical-mediated peroxidation, rendering cellular membranes particularly vulnerable under conditions of redox imbalance. Lipidomics studies have identified phosphatidylethanolamine (PE) species containing arachidonic acid (AA) and adrenic acid (AdA) as the most critical lipid substrates driving ferroptotic cell death (45).

Chain reactions of lipid peroxidation initiated by free radicals and Fe^{2+} cause irreversible damage to the cell membrane, disrupt membrane integrity, and trigger cell death (6). Toxic aldehydes generated as a result of lipid peroxide decomposition, such as 4-hydroxynonenal (4-HNE) and malondialdehyde (MDA), further exacerbate cellular dysfunction by forming covalent adducts with proteins and DNA (16).

Enzymatic incorporation of these PUFAs into membrane phospholipids by ACSL4 and lysophosphatidylcholine acyltransferase 3 (LPCAT3) further sensitizes cells to ferroptosis (46).

Ferroptosis is a highly regulated ROS-dependent type of cell death, derived from free iron overload. Lipid peroxidation is initiated when Fe^{2+} catalyzes the formation of highly reactive oxygen species, which abstract hydrogen atoms from PUFA-containing phospholipids, generating lipid radicals (7). These radicals rapidly react with molecular oxygen to form lipid peroxyl radicals, thereby propagating self-amplifying chain reactions across the membrane bilayer. The uncontrolled accumulation of lipid hydroperoxides leads to irreversible membrane damage, increased membrane permeability, and loss of membrane integrity, ultimately culminating in ferroptotic cell death (47).

Beyond membrane disruption, the decomposition of lipid hydroperoxides yields highly reactive secondary products, including electrophilic aldehydes such as 4-hydroxynonenal (4-HNE) and MDA (48). These toxic products exacerbate cellular dysfunction by forming covalent adducts with proteins, lipids, and nucleic acids, thereby impairing enzyme activity, altering signaling pathways, and inducing genomic instability (47). The accumulation of such lipid-derived aldehydes represents a point of no return in ferroptosis, reinforcing oxidative damage and amplifying cell death signaling.

Under physiological conditions, lipid peroxidation is tightly controlled by antioxidant defense systems, most notably the GPX4 pathway, which detoxifies phospholipid hydroperoxides using reduced GSH. However, impairment of GPX4 activity or depletion of GSH results in unchecked lipid peroxide accumulation, establishing lipid peroxidation as the central lethal event in ferroptosis (9,24,41).

2.1.3. GSH–GPX4 Antioxidant System

The most critical regulatory mechanism of ferroptosis is the GSH-GPX4 system. GPX4 reduces phospholipid hydroperoxides to non-toxic lipid alcohols and thereby suppresses lipid peroxidation (5). Intracellular GSH serves as an essential cofactor for GPX4 and ensures the continuity of this enzymatic antioxidant defense line. The regulation of ferroptosis through iron homeostasis, lipid peroxidation, and the GSH-GPX4 axis is schematically illustrated in Fig 1.

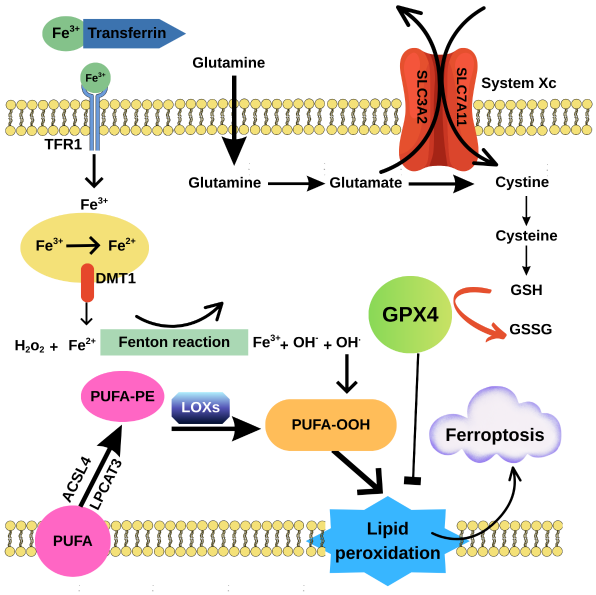

Figure 1. Schematic representation of the molecular regulation of ferroptosis mediated by iron homeostasis, the Fenton reaction, the GSH-GPX4 axis, and lipid peroxidation. TFR1, transferrin receptor 1; DMT1, divalent metal transporter 1; GPX4, glutathione peroxidase 4; LOXs, lipoxygenases; PUFAs, polyunsaturated fatty acids; PE, phosphatidylethanolamine; ACSL4, acyl-CoA synthetase long-chain family member 4; LPCAT3, lysophosphatidylcholine acyltransferase 3; SLC7A11, solute carrier family 7 member 11; SLC3A2, solute carrier family 3 member 2; GSH, glutathione; GSSG, glutathione disulfide.

In physiological conditions, cellular iron uptake is primarily mediated by transferrin-bound ferric iron (Fe^{3+}), which enters the cell through TFR1. Within endosomes, Fe^{3+} is reduced to Fe^{2+} and transported into the cytosol via divalent metal transporter 1 (DMT1), thereby increasing the labile iron pool (40,42). Abnormal distribution and excess intracellular Fe^{2+} catalyzes the Fenton reaction with hydrogen peroxide (H_2O_2), generating highly reactive hydroxyl radicals (•OH), which initiate lipid peroxidation cascades (47).

Polyunsaturated fatty acids (PUFA's) are esterified into membrane phospholipids through the coordinated action of ACSL4 and LPCAT3, generating PUFA-containing phosphatidylethanolamine (PUFA-PE) (45). These PUFA-PE species serve as preferred substrates for lipid peroxidation. Iron-dependent LOXs further catalyze the oxidation of PUFA-PE, producing phospholipid hydroperoxides (PUFA-OOH) (49).

Concurrently, glutamine metabolism contributes to ferroptosis sensitivity by fueling glutamate production (6). Glutamate is exported in exchange for cystine via the cystine/glutamate antiporter System Xc^-, composed of SLC7A11 and SLC3A2 subunits. Inhibition or downregulation of System Xc^- leads to reduced cystine uptake, limiting intracellular cysteine availability and consequently impairing GSH synthesis (50). Depletion of GSH or direct inhibition of GPX4 results in uncontrolled accumulation of lipid peroxides (7,8,51).

2.1.4. ACSL4 – and ALOX-Dependent Ferroptosis Pathway

The biosynthesis of lipid substrates involved in ferroptosis is primarily regulated by ACSL4. ACSL4 catalyzes the esterification of AA and AdA into membrane phospholipids, thereby increasing the susceptibility of the cell membrane to ferroptosis (7,49).

The enzymatic arm of lipid peroxidation is mainly mediated by ALOXs. ALOXs, a family of enzymes, produce oxygen lipids from PUFAs, including ALOXE3, ALOX5, ALOX12, ALOX12B, ALOX15, and ALOX15B (52). ALOX12 and ALOX15 are particularly known to mediate p53-induced ferroptosis in cancer cells after an alternative stimuli (52,53). These enzymes directly oxidize PUFA-containing phospholipids, thereby accelerating lipid hydroperoxide formation and promoting the progression of ferroptosis. Inhibition of the ACSL4-ALOX axis confers a strong cytoprotective effect against ferroptosis (40).

2.1.5. NRF2 and Other Redox-Sensitive Signaling Pathways

Nrf2 is a significant transcription factor involved in regulating the intracellular antioxidant stress response and maintaining the stability of the intracellular environment. NRF2 regulates the transcriptional activation of genes involved in GSH synthesis, iron transport, heme regulation, GPX4 expression, and antioxidant enzyme systems, thereby forming a protective shield against ferroptosis (28,54).

While NRF2 mitigates ferroptosis by upregulating downstream antioxidant genes, this protective mechanism paradoxically supports the survival of both healthy and malignant cells. Over the past decade, extensive research has demonstrated that NRF2 activation in neoplastic tissues facilitates tumor progression and metastasis while simultaneously conferring resistance to conventional chemotherapy and radiotherapy (55).

In addition, the p53, mTOR, AMPK, and Hippo signaling pathways have been shown to indirectly modulate ferroptosis through their effects on System Xc^-, lipid metabolism, and intracellular GSH levels (40,56). These findings indicate that ferroptosis is not controlled by a single pathway but rather by a multilayered molecular network.

3. The Role and Mechanisms of Plant-Derived Phenolic Compounds as Ferroptosis Inducers in Cancer

Plant-derived phenolic compounds represent a broad class of phytochemicals synthesized as secondary metabolites and characterized by the presence of one or more hydroxylated aromatic rings. These compounds play central roles in plant defense mechanisms, ultraviolet protection, pigmentation, and resistance to pathogens (9,10). The chemical diversity of phenolics is extensive, and they are mainly classified into phenolic acids, flavonoids, stilbenes, and lignans. Structural differences among these compounds critically determine their bioavailability, intracellular targets, and biological activities (8).

Beyond their ecological functions, phenolic compounds have garnered significant attention in human health due to their potent antioxidant and iron-chelating properties. In the context of ferroptosis, phenolic compounds act as multi-targeted inhibitors. Their structural hydroxyl groups facilitate the scavenging of lipid peroxyl radicals, thereby interrupting the lethal chain reactions that compromise membrane integrity (29-31). Furthermore, many phenolics possess the capacity to sequester intracellular labile iron, preventing the Fenton chemistry-driven generation of hydroxyl radicals (21).

One of the most remarkable features of phenolic compounds in the regulation of ferroptosis is their ability to exert both antioxidant and pro-oxidant effects depending on the dose and the cellular microenvironment (Fig 2). At low concentrations, phenolics protect cells against oxidative damage through their free radical-scavenging and metal-chelating properties; however, at high concentrations or within the acidic and iron-rich microenvironment of cancer cells, they may shift toward a pro-oxidant mode of action (16). This bidirectional behavior enables phenolic compounds to suppress ferroptosis in healthy cells while inducing ferroptosis in cancer cells. From a therapeutic perspective, this unique characteristic endows phenolics with selective anticancer potential (5).

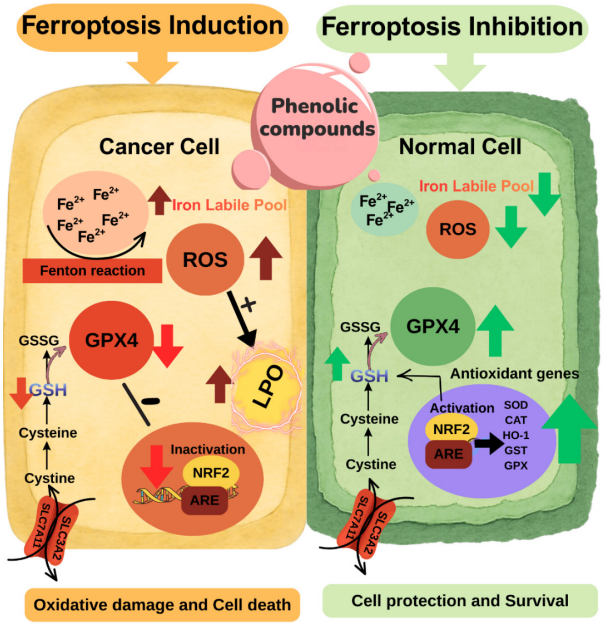

Figure 2. Dual role of phenolic compounds in the regulation of ferroptosis in cancer and normal cells. Phenolic acids (e.g., gallic acid, rosmarinic acid, quercetin) exert context-dependent effects on ferroptosis by differentially modulating iron metabolism, redox homeostasis, and lipid peroxidation pathways. In cancer cells, henolic compounds promote ferroptosis through expansion of the labile iron pool, enhancement of Fenton reaction-driven ROS generation, suppression of GPX4 activity, depletion of GSH, and inactivation of the NRF2/ARE antioxidant axis, leading to excessive LPO, oxidative damage, and cell death. In contrast,, phenolic compounds inhibit ferroptosis by limiting iron-dependent ROS production, activating NRF2/ARE signaling, upregulating antioxidant genes in normal cells (e.g., HO-1, SLC7A11, GPX4), restoring GSH homeostasis, and preventing lipid peroxidation, thereby promoting cellular protection and survival. ARE, antioxidant response element; CAT, catalase; GSH, Glutathione; GSSG, glutathione disulfide; GPX4, glutathione peroxidase 4; HO-1, heme oxygenase 1; LPO, lipid peroxidation; NRF2, Nuclear factor erythroid – 2; ROS, reactive oxygen species; SLC7A11, solute carrier family 7 member 11; SOD, superoxide dismutases; SLC3A2, solute carrier family 3 member 2.

3.1. Phenolic Acids

Phenolic acids are phenolic compounds that contain at least one hydroxyl group and a carboxylic acid function attached to a benzene ring. They are low-molecular-weight compounds derived primarily from the shikimate pathway and are subdivided into two main groups according to their carbon skeleton: Hydroxybenzoic acids (e.g., gallic, vanillic, syringic and protocatechuic acids) and hydroxycinnamic acids (e.g., caffeic, ferulic, sinapic, p-coumaric and chlorogenic acids) (14,15). Phenolic acids are widely distributed in cereals, fruits, vegetables, coffee, and medicinal plants and are well known for their strong antioxidant activities. However, recent studies have demonstrated that phenolic acids such as gallic acid, ferulic acid, caffeic acid, and chlorogenic acid not only act as antioxidants but also modulate ferroptosis by increasing iron uptake and ROS generation, and decreasing the GSH/GPX4 levels in cancer (Table 1).

Table 1. Experimental evidence of phenolic acids inducing ferroptosis in cancer models

Phenolic compound	Cancer cell line/model	Key ferroptosis markers	Main outcome	Reference
Gallic acid	HepG2	↓SLC7A11, and GPX4	**Inhibition of Wnt/β-catenin/SLC7A11/GPX4**	(57)
Gallic acid	HCT116 and Caco-2	↑Fe^{2+}, lipid ROS, MDA, ATF4 and TFR1 ↓SLC7A11, GPX4 and SIGMAR1	Growth inhibition of colon cancer cells by inducing ferroptosis	(58)
Gallic acid	HeLa, SH-SY5Y, and H446 cell	↑Fe^{2+}, lipid ROS	GA-induced cytotoxicity	(59)
Gallic acid	NSCLC (A549 and H1299)	↑ROS, MDA, ACSL4 ↓NRF2, SLC7A11, and GPX4	Enhancing NSCLC radiosensitivity by promoting ferroptosis	(60)
Chlorogenic acid	HepG2	↑Fe^{2+}, lipid ROS, MDA, PTGS2, ACSL4, and LPCAT3 ↓GPX4, GSH	Induction of ferroptosis through the PTGS2/AKR1C3/GPX4 axis	(64)
Rosmarinic acid	DLD-1 and LoVo cells	↑NCOA4 ↓SLC7A11, GPX4	Induction of apoptosis and ferroptosis pathway in cisplatin-induced cytotoxicity of CRC cells	(66)
Rosmarinic acid	MDA-MB-231	↑Fe^{2+}, ROS	Ferroptotic and apoptotic cell death via mitochondrial dysfunction and reduced mitochondrial activity	(67)
Rosmarinic acid	HCT-116	↑Fe^{2+}, ROS, MDA, AKR1C3, ACSL4, and LPCAT3 ↓GSH	Triggering ferroptosis via mitochondrial dysfunction and modulation of lipid metabolic pathways	(68)
Ferulic acid	TE-4 and EC-1	↑Fe^{2+}, ROS, MDA, ↓SLC7A11, GPX4, SOD, GSH	Ferroptosis by inhibiting SLC7A11 and GPX4 axis.	(72)
CAPE	MDA-MB 231	↑ROS, MDA ↓GSH	Ferroptosis via HO-1 induction	(74)
Para-coumaric acid (p-CA)	H460 and A549	↑Fe^{2+}, ROS, MDA ↓NRF2 GPX4, xCT, GSH	Induction of erroptosis through the GPX4, xCT, and NRF2 signaling pathways	(75)

ACSL4, acyl-CoA synthetase long-chain family member 4; ATF4, activated transcription factor 4; CAPE, caffeic acid phenethyl ester; GSH, glutathione; GPX4, glutathione peroxidase 4; HO-1, heme oxygenase 1; LPCAT3, lysophosphatidylcholine acyltransferase 3; MDA, malondialdehyde; NCOA4, nuclear receptor coactivator 4; NRF2, nuclear factor erythroid – 2; PTGS2, prostaglandin-endoperoxide synthase 2; ROS, reactive oxygen species; SIGMAR1, sigma-1 receptor; SLC7A11, solute carrier family 7 member 11; SOD superoxide dismutases; TFR1, transferrin receptor 1.

3.1.1. Gallic acid

Gallic acid is a widely distributed phenolic acid belonging to the hydroxybenzoic acid derivatives and it is found in grapes, tea, fruit peels, and many medicinal plants. Its antioxidant, anti-inflammatory, and cytoprotective properties have long been recognized. A recent investigation highlights the dual role of gallic acid (GA) in the regulation of ferroptosis, revealing that its biological effect is fundamentally determined by the cellular context. In malignant settings, GA has been identified as a potent inducer of ferroptosis. For example, in hepatocellular carcinoma (HCC) cells, GA triggers ferroptotic cell death by suppressing the Wnt/β-catenin signaling pathway, which subsequently leads to the downregulation of the cystine/glutamate antiporter SLC7A11 and the primary antioxidant enzyme GPX4 (57). Similarly, Hong et al. (2021) demonstrated that GA treatment significantly restricts the proliferation of colon cancer cells by inhibiting expression of ferroptosis-related proteins SLC7A11 and GPX4 (58). This mechanism leads to catastrophic accumulation of lipid peroxides and iron-dependent ROS, effectively bypassing conventional apoptotic resistance in tumor cells.

Beyond inducing ferroptosis, GA has been reported to exhibit a pleiotropic effect by simultaneously activating three different death mechanisms: apoptosis, necroptosis, and ferroptosis (59). This multifaceted approach allows for the elimination of malignant cells, even in the presence of single-path resistance, because GA disrupts mitochondrial integrity, activates caspases, and facilitates iron-dependent lipid peroxidation. Furthermore, GA may enhance the sensitivity of non-small cell lung cancer (NSCLC) cells to radiotherapy

by disrupting the NRF2-mediated antioxidant defense system, promoting iron accumulation and lipid peroxidation (60).

In contrast, GA functions as a ferroptosis inhibitor and cytoprotective agent in normal physiological contexts and non-cancerous injury models. Due to its strong radical scavenging and iron chelation properties, GA has been shown to protect healthy tissues (e.g., in traumatic brain injury or diabetic cardiomyopathy models) by neutralizing lipid peroxyl radicals and, binding unstable Fe^{2+} ions through their phenolic hydroxyl groups (33,61). By maintaining membrane integrity and preventing the initiation of the Fenton reaction, GA mitigates oxidative damage in normal cells. This differential activity-selectively promoting ferroptosis in neoplastic tissues while acting as a scaffold for cellular survival in healthy cells-highlights GA's therapeutic potential as a selective modulator in redox-based medicine.

3.1.2. Chlorogenic Acid

Chlorogenic acid (CGA) is an ester of caffeic acid and quinic acid and is abundantly found in coffee, apples, pears, and numerous medicinal plants. Traditionally, CGA has been characterized as a robust inhibitor of ferroptosis, primarily valued for its ability to mitigate iron-dependent oxidative stress in healthy tissues through the NRF2/GPX4 signaling axis (35,62,63). However, a recent study by Wu et al. (2025) has challenged this singular perspective, demonstrating that CGA can selectively function as a potent ferroptosis inducer within the context of HCC (64). According to Wu et al., CGA triggers ferroptotic cell destruction in HCC by regulating the reprogramming of arachidonic acid metabolism. This process occurs via the PTGS2/AKR1C3/GPX4 transport pathway, leading to disruption of the cell's antioxidant defense and subsequent lipid peroxidation. This important finding demonstrates that the role of CGA in ferroptosis is highly environment-dependent: while maintaining redox homeostasis and supressing lipid peroxidation in healthy organ models, it can be used to register overcoming cell death resistance in malignant tissues. By targeting the PTGS2/AKR1C3/GPX4 pathway, this research provides novel mechanistic insights into how CGA can serve as a dual-function therapeutic agent; acting as a scaffold for cytoprotection under normal conditions while effectively promoting ferroptotic abnormalities in cancer (64).

However, it should be noted that CGA concentrations used in in vitro studies often exceed plasma levels achievable through diet or conventional administration, due to its limited bioavailability and rapid metabolism. Therefore, while these findings provide valuable mechanistic information on CGA-mediated ferroptosis modulation, improved application strategies may be needed to translate these effects into physiologically and clinically relevant settings.

3.1.3. Rosmarinic Acid

Rosmarinic acid (RA) is a naturally occurring polyphenolic compound found in many plants (e.g., *Rosmarinus officinalis*, *Melissa officinalis*, and *Salvia* species with known antioxidant, anti-inflammatory, and anticancer properties (65). As a plant-derived polyphenolic compound, RA has emerged as a context-dependent regulator of ferroptosis, exhibiting opposing effects in cancerous and non-cancerous cells.

In various cancer models, RA has been shown to promote ferroptotic cell death by disrupting redox homeostasis through downregulation of key antioxidant systems such as GPX4 and SLC7A11, glutathione depletion, intracellular Fe^{2+} accumulation, and increased lipid peroxidation, ultimately making tumor cells susceptible to oxidative damage and chemotherapeutic agents (66-68). In colorectal cancer cell lines (DLD-1, LoVo), RA combined with cisplatin enhances cell death by promoting both apoptosis and ferroptosis. This is evidenced by downregulation of GPX4 and SLC7A11, key antioxidant regulators, and reversal of RA's effects by ferroptosis inhibitors (66).

In contrast, in normal or non-malignant cells exposed to pathological stress (e.g., ischemia-reperfusion injury, liver or kidney damage, and inflammatory conditions), RA functions predominantly as a ferroptosis inhibitor by activating cytoprotective signaling pathways, particularly the NRF2/HO-1 axis, preserving GPX4 activity, and suppressing iron-induced lipid peroxidation (69-71). Liu et al (2025)

reported that RA suppresses ferroptosis and protects neurons via activation of the NRF2 antioxidant pathway and inhibition of KEAP1, reducing oxidative injury cerebral ischemia-reperfusion injury (69). NRF2 protects cells against ferroptosis by transcriptionally activating genes involved in GSH synthesis, GPX4 expression, ferritin production, and antioxidant enzyme systems (26). In recent study, researhers found that RA mitigates acetaminophen-induced liver injury by enhancing antioxidant defense (NRF2/HO-1) and maintaining GPX4 and GSH levels, thereby preventing lipid peroxidation and ferroptosis in hepatocytes (70). This dual behavior highlights the redox-adaptive nature of RA, where its pro-oxidant, ferroptosis-inducing effects primarily manifest in the metabolically and oxidatively sensitive tumor microenvironment, while its antioxidant and ferroptosis-suppressive properties are dominant in normal tissues. This contextual selective regulation positions RA as a promising candidate for ferroptosis-based cancer therapy with a potentially favorable safety profile for non-malignant cells.

3.1.4. Ferulic acid

Ferulic Acid (FA), a ubiquitous dietary phenolic acid found in the cell walls of cereal grains, fruits, and vegetables, has long been celebrated for its potent antioxidant properties. However, recent pharmacological insights have repositioned FA as a context-dependent modulator of ferroptosis.

Emerging evidence indicates that FA can function as a pro-ferroptotic agent in malignant cells by amplifying oxidative stress, increasing intracellular reactive oxygen species and iron accumulation, and promoting lipid peroxidation while simultaneously suppressing key antioxidant defense systems. In esophageal squamous cell carcinoma (ESCC), FA treatment reduced cell viability, increased ROS and iron levels, elevated MDA, and downregulation of the SLC7A11/GPX4 axis; notably, these effects were partially reversed by ferroptosis inhibitors, like deferoxamine, suggesting FA's potential as a pro-ferroptotic anticancer agent (72). Conversely, in non-cancer contexts such as sepsis-induced acute lung injury and oxidative hepatocyte damage, FA mitigated ferroptosis by activating the NRF2/HO-1 antioxidant pathway, increasing GPX4 and GSH, reducing lipid peroxidation and iron overload, and preserving cellular function (73). These findings underscore FA as a compelling candidate for selective ferroptosis-based anticancer investigations with minimal toxicity to healthy cells.

3.2. Flavonoids

Flavonoids, a diverse class of plant secondary metabolites characterized by a polyphenolic a C6-C3-C6 skeleton, represent a cornerstone of natural product research due to their widespread presence in medicinal plants, fruits, and vegetables (76). Based on their chemical structures, flavonoids are classified into **flavonols** (quercetin, kaempferol, myricetin and fisetin), **flavones** (luteolin, apigenin), **flavanones** (naringenin, hesperetin), **flavanols** (catechin, epicatechin), **isoflavones** (genistein, daidzein), and **anthocyanins** (cyanidin, delphinidin) revealing further structural diversity arising from glycosylation and acylation at various hydroxyl and methyl sites (77).

Due to their redox-active chemical structures, flavonoids can modulate key molecular determinants of ferroptosis, including iron homeostasis, ROS formation, lipid peroxidation, and antioxidant defense systems (Table 2). Recent evidence suggests that flavonoids can act as both inducers and inhibitors of ferroptosis, depending on the context. In cancer cells, some flavonoids promote ferroptotic cell death by increasing intracellular unstable iron, enhancing ROS production, suppressing the SLC7A11/GSH/GPX4 axis, and remodeling PUFA-containing phospholipids, thus making tumor cells susceptible to ferroptosis-based therapeutic strategies (31,32). Conversely, in normal or non-malignant cells, flavonoids frequently exert ferroptosis-suppressing effects by activating cytoprotective pathways such as NRF2/ARE signaling, maintaining GPX4 activity, and limiting iron-induced lipid peroxidation (19,24). This dual, cell-context-dependent regulation highlights flavonoids as critical modulators of ferroptosis, emphasizing their potential to selectively target cancer cells while protecting normal tissues from oxidative damage.

3.2.1. Quercetin

Quercetin (QUE), one of the most abundant members of the flavonol subclass, is well known for its strong

antioxidant, anti-inflammatory, and anticancer properties (78). Recent studies have also demonstrated that quercetin promotes ferroptosis by increasing ROS, iron accumulation, and lipid peroxidation while suppressing ferroptosis regulators such as GPX4 and SLC7A11, leading to cancer cell death in lung cancer, glioblastoma, and colon cancer cell lines in association with increased ferroptosis markers.

In gastric cancer cells, QUE has been shown to increase lipid peroxidation and intracellular iron content, inhibit SLC1A5 expression, disrupt NRF2 nuclear translocation, and downregulate the NRF2/xCT/GPX4 axis, thereby triggering ferroptotic cell death and suppressing tumor progression (31). Zhu et al (2024) demonstrated that in oral squamous cell carcinoma models, QUE induced ferroptosis by suppressing SLC7A11, lowering GSH levels, and increasing ROS production in a mTOR/S6KP70-dependent manner (79). Additionally, QUE has been shown to induce ferritinophagy in breast and hepatic cancer cells by facilitating the transport of Transcription Factor EB (TFEB) to the nucleus, an event that triggers lysosomal degradation of ferritin, increasing free iron concentration, promoting ROS and lipid peroxidation, and highlighting its capacity to trigger ferroptosis (30,80). These reports are also corroborated by the results of studies on HEC-1-A endometrial cancer cells. Li et al (2022) showed that in endometrial carcinoma cells, QUE suppressed cell proliferation and migration by inducing ferroptosis (81). Collectively, these findings support quercetin as a pro-ferroptotic flavonoid in cancer models, acting through multiple molecular mechanisms that converge on iron dysregulation, antioxidant inhibition (e.g., GPX4, SLC7A11), and increased oxidative lipid damage.

Table 2. Experimental evidence of flavanoids inducing ferroptosis in cancer models

Phenolic compound	Cancer cell line / model	Key ferroptosis markers	Main outcome	Reference (s)
Quercetin	MCF-7, MDA-MB-231	↑ROS, MDA, Fe^{2+}	Induction of ferroptosis inducing TFEB-mediated ferritinophagy	(30)
Quercetin	AGS, MKN-45 cells	↑ROS, Fe^{2+} ↓NRF2 GPX4, SLC7A11, GSH	Induction of ferroptotic cell death	(31)
Quercetin	Oral squamous cell carcinoma	↑ROS, LPO ↓SLC7A11, GSH, GPX4	Ferroptosis via mTOR/S6KP70-dependent manner	(79)
Quercetin	HepG2 cells	↑ROS, Fe^{2+}, LPO ↓GPX4	TFEB-mediated ferroptosis and Bid-involved apoptosis	(80)
Quercetin	HEC-1-A	↑ROS, Fe^{2+}, TFR-1 ↓GPX4, xCT, ACO1 and FLC	Induction of ferroptotic cell death	(81)
Luteolin	HCT116, SW480, MC38/CT26 cells; colon cancer xenograft model	↑Lipid-ROS, ↓GPX4, GSH	Ferroptotic cell death	(82,83)
Luteolin	DU145 and PC-3 cells; prostate cancer xenograft model	↑ROS, MDA, Fe^{2+} ↓SLC7A11, GPX4, FTH1, and FTL1	Ferritinophagy-induced ferroptosis	(84)
Luteolin	Renal cell carcinoma cells	↑ROS, Fe^{2+}, MDA ↓GSH	Induction of ferroptosis	(85)
Luteolin	U87MG	↑ lipid-ROS ↓GSH	NRF2/xCT/GPX4-mediated ferroptosis	(86)
Naringenin	HOS, U2OS, and MG63; subcutaneous tumor model	↑ROS, Fe^{2+}, LPO ↓GPX4	Induction of STAT3-MGST2 signaling pathway	(87)
Naringenin	HepG2, Hep3B and SNU182 cells; liver cancer xenograft model	↑ROS, Fe^{2+}, MDA ↓GSH	Increasing the efficacy of ferroptosis inducers by attenuating aerobic glycolysis	(88)
Hesperetin	T24 (HTB-4) and 5637 (HTB-9)	↑ROS ↓GPX4	Promotion of apoptosis and ferroptosis	(89)
EGCG	A549 and H1299	↑ROS, MDA, Fe^{2+}, ACSL4 ↓SLC7A11, GPX4	Inhibition of GPX4/SLC7A11	(32)

ACO1, anti-aconitase 1; ACSL4, acyl-CoA synthetase long-chain family member 4; FTL1, ferritin light chain; FTH1, ferritin heavy chain 1; GSH, glutathione; GPX4, glutathione peroxidase 4; MDA, malondialdehyde; MGST2, microsomal glutathione S-transferase 2; NRF2, nuclear factor erythroid – 2; ROS, reactive oxygen species; SLC7A11, solute carrier family 7 member 11; TFR-1, transferrin receptor 1

3.2.2. Luteolin

Luteolin (3′,4′,5,7-tetrahydroxyflavone) is a naturally occurring flavonoid found in many fruits, vegetables, and medicinal herbs. While traditionally recognized for its antioxidant and anti-inflammatory properties, accumulated evidence indicates that luteolin can act as a potent ferroptosis inducer in various cancer types through multiple molecular mechanisms, including enhancement of ROS generation, disruption of iron homeostasis, activation of ferritinophagy, GPX4 suppression, and increased lipid peroxidation (Fig 3).

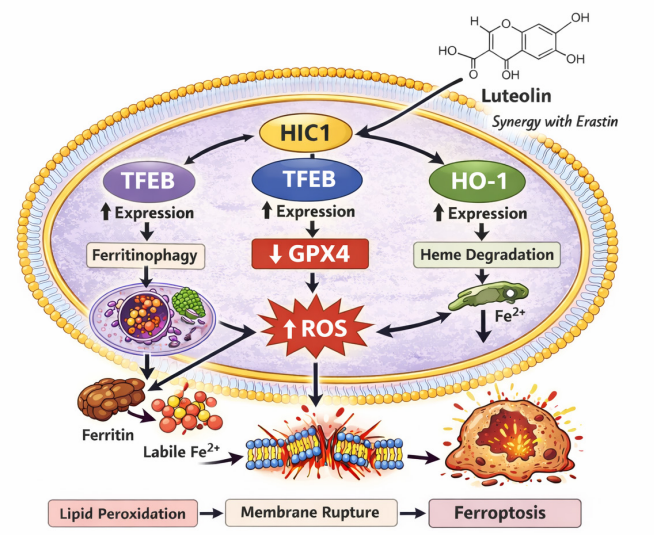

Figure 3. Luteolin-induced ferroptosis in cancer cells through multiple molecular mechanisms. Luteolin induces ferroptotic cell death through the coordinated regulation of antioxidant defense, iron metabolism, and lipid peroxidation pathways. Luteolin exhibits synergistic activity with ferroptosis triggers such as erastin, further intensifying ferroptotic signaling. HIC1, hypermethylated cancer 1; TFEB, transcription factor EB; GPX4, glutathione peroxidase 4; HO-1, heme oxygenase 1; ROS, reactive oxygen species.

Zheng et al. (2023) demonstrated that luteolin exhibits a potent ferroptosis-inducing effect in colon cancer cells primarily through transcriptional repression of GPX4. Mechanistically, luteolin activated the tumor suppressor hypermethylated cancer 1 (HIC1), which directly inhibits GPX4 expression, leading to excessive lipid hydroperoxide accumulation and ferroptotic cell death. Specifically, luteolin showed synergistic therapeutic efficacy with the ferroptosis-inducing erastin, significantly enhancing lipid peroxidation and ferroptosis-related cytotoxicity (82). Consistent with these findings, Cao et al. (2025) reported that luteolin induces GPX4-dependent ferroptosis in colon cancer models and simultaneously enhances antitumor immune activation. Luteolin treatment led to increased lipid peroxidation, disruption of membrane integrity, and upregulation of ferroptosis markers; suggesting that luteolin-induced ferroptosis may also contribute to immunogenic cell death, thereby enhancing antitumor immune responses (83).

In addition to GPX4 inhibition, luteolin promotes ferroptosis by altering intracellular iron metabolism. Fu et al. (2024) demonstrated that luteolin facilitates nuclear translocation of transcription factor EB (TFEB) in prostate cancer cells, leading to activation of the autophagy-lysosome pathway and increased ferritinophagy (84). Ferritin degradation increases the intracellular unstable Fe^{2+} pool, accelerating the formation of reactive oxygen species driven by Fenton chemistry and lipid peroxidation, ultimately triggering ferroptosis. Furthermore, Han et al. (2022) identified heme oxygenase-1 (HO-1) as a critical mediator of luteolin-induced ferroptosis in clear cell renal cell carcinoma (85). Luteolin-mediated upregulation of HO-1 promotes heme degradation, expanding the unstable iron pool and intensifying lipid peroxidation. The combined effects of iron loading and impaired antioxidant defenses make cancer cells highly susceptible to ferroptotic cell death.

Very recent evidence further supports the role of luteolin as a ferroptosis-inducing agent through the modulation of the NRF2/xCT/GPX4 signaling axis, a central pathway governing cellular redox homeostasis and ferroptosis resistance (Table 2). Luteolin has been shown to inhibit tumor growth by suppressing NRF2 activity, leading to downregulation of xCT (SLC7A11) and subsequent intracellular GSH depletion. in glioblastoma cells. Decreased GSH availability compromises GPX4 enzymatic activity, limiting the detoxification of lipid hydroperoxides and promoting excessive ROS accumulation (86). The resulting oxidative imbalance facilitates lipid peroxidation and makes glioblastoma cells susceptible to ferroptotic cell death. These findings demonstrate that luteolin disrupts ferroptosis defense mechanisms not only through transcriptional repression of GPX4 via

HIC1, but also by weakening the NRF2-driven antioxidant network, thus strengthening its role as a multi-target regulator of ferroptosis. Collectively, these studies demonstrate that luteolin triggers ferroptosis through multiple interconnected mechanisms, including GPX4 suppression, ferritinophagy-mediated iron release, HO-1-induced iron accumulation, and sustained lipid peroxidation. Thanks to its ability to target multiple ferroptosis regulatory axes simultaneously, luteolin, especially in combination with known ferroptosis inducers, emerges as a promising natural compound for ferroptosis-based anticancer strategies.

3.2.3. Naringenin and Hesperetin

Natural flavonoids such as naringenin and hesperetin have recently attracted significant attention as modulators of ferroptosis. Naringenin has been shown to exhibit ferroptosis-promoting effects through multiple signaling mechanisms in the context of cancer. In osteosarcoma cells, naringenin treatment significantly reduced cell viability and increased ferroptotic markers, including increased ROS, Fe^{2+} accumulation, and MDA levels; this indicates increased lipid peroxidation consistent with ferroptosis induction (87). Naringenin reduces the expression of MGST2, a gene normally involved in antioxidant defenses; this is associated with decreased GPX4 expression, thus reducing cellular antioxidant capacity and making cells susceptible to ferroptosis.

On the other hand, naringenin has been reported to enhance the efficacy of classical ferroptosis inducers by modulating cancer cell metabolism. In liver cancer cells, naringenin reduces aerobic glycolysis by activating the AMPK-PGC1α signaling axis and shifts cellular metabolism toward increased oxidative stress (88). This metabolic reprogramming lowers the threshold for ferroptosis induction by classical inducers, suggesting that naringenin may synergistically enhance ferroptosis through both metabolic effects and direct signaling pathway regulation.

Compared to naringenin, evidence regarding the direct role of hesperetin in ferroptosis is less extensive but emerging. Network pharmacology and molecular docking studies in bladder cancer cells show that hesperetin not only inhibits proliferation and migration via the PI3K/AKT pathway but also promotes cell death with features consistent with ferroptosis, such as ROS accumulation and decreased GPX4 expression (89). The role of PI3K/AKT signaling is important, as inhibition of this pathway has been associated with susceptibility to ferroptotic triggers in multiple cancer models.

In conclusion, these studies highlight that naringenin and hesperetin primarily influence ferroptosis through modulation of cellular redox balance, suppression of antioxidant defenses, and metabolic stress pathways. While naringenin's ability to inhibit the STAT3-MGST2 axis and enhance AMPK-mediated metabolic reprogramming clearly activates ferroptotic mechanisms, hesperetin's role appears to focus on PI3K/AKT signaling modulation and associated oxidative stress amplification, further supported by the emerging ferroptosis-inducing delivery systems. These flavonoids, alone or in combination with established ferroptosis inducers, stand out as promising natural compounds for ferroptosis-based anti-cancer strategies.

3.2.4. Epigallocatechin Gallate

Epigallocatechin-3-gallate (EGCG) is an important catechin found predominantly in green tea and also naturally occurring in various plant-based foods such as apples, blackberries, and carob. EGCG has been widely reported for its antioxidant, anti-inflammatory, and anticancer properties; however, its role in regulating ferroptosis has only recently begun to emerge. A recent study by Wang et al. (2024) reported that EGCG induced ferroptosis in non-small cell lung cancer (NSCLC). The authors demonstrate that EGCG inhibited the proliferation and survival of tumor cells through the downregulation of tsRNA-13502, a transfer RNA-derived small RNA involved in redox homeostasis. EGCG treatment was shown to activate ferroptotic cell disruption, leading to significant changes in ferroptosis-related markers, including increased lipid peroxidation and iron-dependent oxidative stress (32).

Suppression of tsRNA-13502 by EGCG disrupted cellular antioxidant defense systems, thereby enhancing susceptibility to ferroptosis. Although the precise downstream targets of tsRNA-13502 remain to be fully elucidated, its modulation was associated

with dysregulation of key ferroptosis regulators, suggesting that non-coding RNA–mediated control represents a novel layer of ferroptosis regulation by natural polyphenols. Importantly, restoration of tsRNA-13502 expression partially rescued cells from EGCG-induced ferroptotic damage, confirming the functional relevance of this pathway.

3.3. Stilbenes

Stilbenes represent a narrower group of phenolic compounds characterized by a C6–C2–C6 backbone consisting of two aromatic rings linked by an ethylene bridge. The most well-known member of this group is resveratrol, which is abundant in various plant sources, particularly grapes, peanuts, and red wine (11).

3.3.1. Resveratrol

In addition to its antioxidant, anti-inflammatory, and anticancer effects, resveratrol has attracted considerable attention in recent years for its ferroptosis-inducing effects, particularly in breast, colon, prostate, and liver cancer cells (29). Experimental studies have revealed that resveratrol increases intracellular labile iron levels, suppresses GPX4 activity, and accelerates lipid peroxidation, ultimately leading to ferroptotic cell death (90-98). These properties place stilbenes among the most promising natural compounds in ferroptosis-based anticancer strategies.

A review of the literature reveals that resveratrol exhibits a potent ferroptosis-inducing effect in a wide range of cancer types through multifaceted molecular mechanisms (Table 3). Resveratrol primarily promotes ferroptotic cell death by downregulating GPX4 and system Xc^- (xCT), leading to impaired glutathione metabolism and uncontrolled lipid peroxidation (91,93,95). In triple-negative breast cancer, resveratrol induces ferroptosis via NEDD4L-mediated ubiquitination and proteasomal degradation of GPX4, highlighting a post-translational regulatory mechanism (91). Similarly, in bladder cancer organoids and acute myeloid leukemia cells, resveratrol increases intracellular ROS accumulation and suppresses GPX4-dependent antioxidant defenses in a ROS-dependent manner (93, 95).

Resveratrol modulates ferroptosis not only by directly targeting GPX4, but also through iron metabolism, mitochondrial signaling, and oncogenic pathways. By increasing iron ion accumulation and lipid peroxidation, it sensitizes cancer cells to ferroptosis inducers such as sulfasalazine and cisplatin (96,97). Resveratrol also regulates ferroptosis by inducing autophagy-ferroptosis cross-interaction via EGFR/PI3K/AKT/GPX4, HMMR, and DHODH-mediated mitochondrial pathways and the USP36-SOD2 axis (92,94,98). Specifically, resveratrol has been shown to reshape the tumor microenvironment by increasing $CD8^+$ T cell cytotoxicity through ferroptosis regulation, further supporting its therapeutic importance (94).

In contrast, emerging studies highlight that resveratrol may also play a context-dependent protective role against ferroptosis, particularly in nonmalignant tissues or under conditions of excessive oxidative stress. This dual behavior largely stems from differences in basal ROS levels, iron availability, and antioxidant capacity between normal and cancer cells. In malignant cells, which typically exhibit high basal ROS levels and increased reliance on GPX4-mediated detoxification of lipid peroxides, resveratrol-induced disruption of redox balance and iron homeostasis can exceed cellular defense thresholds, thus promoting ferroptosis. Conversely, in non-malignant cells with lower basal oxidative stress, resveratrol, through its antioxidant capacity and iron chelation properties, maintains redox homeostasis and limits ferroptotic damage by activating antioxidant and cytoprotective pathways, including NRF2 signaling. In conclusion, these findings position resveratrol as a bidirectional ferroptosis regulator that can selectively induce ferroptotic cell death in cancer cells while maintaining normal tissue integrity (90).

3.4. Lignans

Lignans, found in seeds (especially flaxseed), whole grains, and various fruits and vegetables, are a class of plant-derived phenolic compounds formed through the dimerization of phenylpropanoid units. Some lignans, such as enterolactone and enterodiol, are converted by the gut microbiota into more biologically active metabolites. They have been extensively studied for

their antioxidant, anti-inflammatory, and anticancer activities. However, research linking lignans to ferroptosis regulation is extremely limited (Table 3). To date, only a few studies have begun to explore this link, with myrislignan emerging as the best-characterized example (99).

A recent study by Zhou et al. (2023) demonstrated that myrislignan, a naturally occurring lignan and a known NF-κB pathway inhibitor, effectively induced ferroptosis in glioblastoma cells. In this study, myrislignan treatment led to classic signs of ferroptotic cell death, including increased lipid peroxidation, disruption of redox homeostasis, and increased susceptibility to iron-dependent oxidative stress. Mechanistically, these effects were linked to the regulation of epithelial-mesenchymal transition (EMT) through the modulation of the transcription factor Slug (SNAI2), a key EMT driver. Specifically, myrislignan caused downregulation of Slug by suppressing NF-κB signaling, which in turn affected the expression of ferroptosis-related genes and increased susceptibility to ferroptotic triggers (99). While the precise downstream influencers linking key ferroptosis pathways such as Slug and GPX4, the system Xc^- (xCT), or iron metabolism are not fully defined, the study highlights a novel interaction between EMT regulation and ferroptosis susceptibility. EMT is increasingly recognized as a determinant of tumor cell plasticity and treatment resistance, and its modulation by myrislignan suggests that lignans may exert ferroptosis-promoting effects through indirect regulation of transcriptional networks governing redox balance and cell fate decisions.

Since the limited information in the literature, it is currently premature to generalize ferroptosis-regulating effects to all lignans. Further research is needed to elucidate whether other lignan subclasses share this capacity and to identify relevant molecular targets and signaling pathways, including their effects on GPX4 activity, iron homeostasis, and lipid peroxidation cascades.

Table 3. Experimental evidence of stilbenes, lignans, andother phenolic compounds inducing ferroptosis in cancer models

Phenolic compound	Cancer cell line/ model	Key ferroptosis markers	Main outcome	Reference (s)
Resveratrol	MDA-MB-231, SUM159, 4T1	↑ROS, Fe^{2+}, Lipid ROS, MDA ↓GPX4, GSH	Ferroptotic cell death through NEDD4L-mediated GPX4 ubiquitination and degradation	(91)
Oxyresveratrol	MDA-MB-231	↑ROS, Fe^{2+}, Lipid ROS, MDA ↓GPX4	Ferroptosis through suppression of the EGFR/PI3K/AKT/GPX4 signalling axis	(92)
Resveratrol	T24 and UM-UC-3	↑ROS, Fe^{2}, Lipid ROS, ↓GPX4, xCT	Induction of ferroptosis	(93)
Resveratrol	H520	↑ROS, MDA, ACSL4, ↓GSH, SOD, SLC7A11, GPX4	Promotion of ferroptosis through SLC7A11-HMMR interaction	(94)
Resveratrol	AML-193 and OCI-AML-3	↑ROS, Fe^{2}, ↓GPX4	Ferroptotic cell death through Hsa-miR-335-5p/NFS1/ GPX4 pathway	(95)
Resveratrol	Melanoma cell lines	↑ROS, Fe^{2+}, Lipid ROS ↓GSH	Enhancement of sulfasalazine-induced ferroptosis	(96)
Resveratrol	PANC1 and BxPC-3	↑ROS, MDA, ↓SLC7A11, GPX4	Increasing cisplatin sensitivity by modulating dihydroorotatede hydrogenase-mediated ferroptosis	(97)
Resveratrol	MKN-45, MKN-1, SNU-5, AGS; gastric cancer xenograft model	↑ROS, Fe^{2}, MDA, ACSL4 ↓FTH1, GSH, GPX4	Induction of autophagy and ferroptosis by inhibiting USP36–SOD2 axis	(98)
Myrislignan	U87 and U251; intracranial xenograft model	↑ROS, MDA ↓SLC7A11, GSH	Ferroptosis via Slug-SLC7A11 pathway	(99)
Curcumin	A549 and H1299; LLC-bearing mice	↑ROS, Fe^{2}, MDA, ACSL4 ↓SLC7A11, GSH, GPX4	Induction of autophagy and ferroptosis	(21)
Curcumin	MNNG/HOS and MG-63	↓NRF2, SLC7A11, HO-1, GPX4	Induction of ferroptosis regulating the NRF2/GPX4 signaling	(28)
Curcumin	HCT-8	↑ROS, Fe^{2}, MDA ↓GSH, SLC7A11, GPX4,	Ferroptosis via PI3K/Akt/mTOR signaling	(100)

Curcumin	HepG2 cells; Hepa1-6 xenograft mouse model	↑ROS, Fe^{2}, MDA, KEAP1 ↓P62, NRF2	Induction of ferroptosis through modulation of the P62-KEAP1-NRF2-signaling pathway	(101)
Curcumin	HepG2 and SMMC7721	↑Fe^{2}, MDA, ACSL4, PTGS2 ↓GSH, GPX4, SLC7A11	Ferroptotic death via upregulation of ACSL4	(102)
Curcumin	MCF-7, MDA-MB-453; Breast cancer xenograft model (BALB/c nude mice)	↑Lipid ROS, Fe^{2+}, ACSL4, SLC1A5 ↓GPX4, FTL	Promotion of SLC1A5-mediated ferroptosis	(103)
Curcumin	MB-MDA-231	↑ROS, Lipid ROS, Fe^{2+}, HO-1 ↓GSH, FHC	Ferroptotic death by increasing HO-1 expression	(104)
Curcumin analogue, EF24	U2os and Saos-2	↑ROS, Fe^{2}, MDA, HO-1 ↓GPX4	Ferroptotic death by increasing HO-1 expression	(105)
Curcumin	FTC-133, and FTC-238; tissue samples	↑ROS, Fe^{2}, MDA, HO-1 ↓GPX4, GSH	Induction of ferroptosis via HO-1 upregulation	(106)
Curcumin	AGS and HGC-27	↑Fe^{2}, MDA, ACSL4, GSH ↓GPX4, SLC7A11	Autophagy-mediated ferroptosis by inhibiting the PI3K/AKT/mTOR signaling pathway	(107)
Curcumin derivative NL01	Anglne and HO8910PM; ovarian cancer xenograft model	↑Lipid ROS, Fe^{2+} ↓GPX4, SLC11A2	Ferroptosis via HCAR1/MCT1 signaling pathway	(108)
Curcumin	LK-2 and H1650 cells; NSCLC tissue samples; xenograft tumor model	↑MDA, LDH, Fe^{2+}, ACSL4, TFR-1 ↓SOD, GSH, GPX4, SLC7A11	Induction of ferroptosis through the DMRT3/SLC7A11 axis	(109)

ACSL4, acyl-CoA synthetase long-chain family member 4; DMRT3, Doublesex and Mab-3 related Transcription Factor 3; FTH1, ferritin heavy chain 1; FTL1, ferritin light chain; GSH, glutathione; GPX4, glutathione peroxidase 4; HCAR1, hydroxycarboxylic acid receptor 1; HO-1, heme oxygenase 1; KEAP1, Kelch-like ECH-associated protein 1; MCT1, monocarboxylate transporter; MDA, malondialdehyde; NRF2, nuclear factor erythroid – 2; PTGS2, prostaglandin-endoperoxide synthase 2; ROS, reactive oxygen species; SLC7A11, solute carrier family 7 member 11; SLC11A2, solute carrier family 11 member 2; TFR-1, transferrin receptor 1

4. Other Phenolic Compounds As Ferroptosis Inducer

4.1. Curcumin

Curcumin is a polyphenolic compound isolated from the rhizomes of *Curcuma longa* and exhibits a broad spectrum of biological activities. Recent literature indicates that curcumin triggers ferroptotic cell death in cancer cells, and that this occurs through a wide range of mechanisms (Table 3). These mechanisms include suppression of the antioxidant system, increased lipid peroxidation, modulation of signaling pathways (PI3K/Akt/mTOR, NRF2), and processes associated with autophagy (21,28). These activities of curcumin reinforce the emerging importance of ferroptosis in anticancer therapy.

A decrease in GSH levels and suppression of GPX4 activity are necessary to trigger ferroptosis. Curcumin administration significantly reduced GSH, SLC7A11, and GPX4 levels in HCT-8 colorectal cancer cells, while increasing intracellular Fe^{2+}, ROS, and lipid peroxidation product levels which supports ferroptotic cell death. Ferroptosis inhibitors such as Ferrostatin-1 can reverse these effects, suggesting that ferroptosis is part of curcumin's antiproliferative effect (100).

In a recent investigation done with liver cancer cells it was found that curcumin triggers the ferroptotic process by suppressing P62-KEAP1-NRF2 signaling (101). In this mechanism, downregulation of NRF2 leads to a decrease in antioxidant response elements (AREs) and thus a weakening of the cellular anti-ferroptosis protective response. Similarly, Jiang et al (2024) demonstrated that curcumin increased lipid peroxidation by increasing ACSL4 levels in hepatocellular carcinoma cells HepG2 and SMMC7721, and weakened antioxidant capacity by lowering intracellular GSH levels

through downregulating the expression of GPX and SLC7A11 (102). In addition to these findings, curcumin and synthetic analogues have been shown to suppress tumorigenesis in breast (103,104), osteosarcoma (105) and follicular thyroid cancer (106) by specifically inducing ferroptosis through the modulation of HO-1 and the inhibition of SLC7A11.

In addition to the mechanisms mentioned above, curcumin initiates the ferroptotic process, particularly in gastric and lung cancer cells, by triggering autophagy activation. Inhibition of the PI3K/Akt/mTOR signaling pathway increases the levels of autophagy markers (ATG5, Beclin-1, LC3B), which, along with the increase in ferroptotic markers, facilitates cell death. This process can be partially inhibited by ferrostatin-1 or other autophagy inhibitors (107,21).

Further studies have revealed that the mechanism by which the curcumin derivative NL01 contributes to ferroptosis is related to lactate metabolism (108). Approximately 13 times more potent than curcumin, NL01 can reduce lactate uptake from the extracellular environment by decreasing HCAR1 (hydroxycarboxylic acid receptor 1)/MCT1 (monocarboxylic acid transporter protein 1) expression, and improve energy metabolism by activating the AMPK/SREBP1 pathway in ovarian cancer cells, thereby reducing glucose uptake and lactate production.

Curcumin's effect on ferroptosis is important because it offers a potential therapeutic target as a cell death pathway other than classical apoptosis/necrosis (109). Ferroptosis is considered an additional death mechanism, particularly in chemotherapy-resistant tumors. The effect of curcumin and its derivatives on this process may have the potential for a synergistic effect in combination therapies. Accumulated evidence shows that curcumin plays a role in cancer not only as a ferroptosis-inducing agent but also as a potent chemosensitizer that enhances the efficacy of chemotherapeutic drugs (110-112). Curcumin weakens the resistance mechanisms developed by tumor cells against chemotherapy by increasing ROS accumulation, causing cell cycle arrest, and disrupting redox balance. In this respect, curcumin stands out as a promising adjuvant strategy that simultaneously enhances chemotherapy efficacy through ferroptosis-based cell death. However, since the bioavailability of the bioactive compound is poor, research continues on solutions such as nanoformulations, drug delivery systems, and derivative development strategies for clinical applications.

5. Mechanistic Insights from Network Pharmacology, Molecular Docking, and Systems Biology Approaches

Recent advances in systems biology and computational pharmacology have significantly expanded our understanding of the way how the plant-derived phenolic compounds regulate ferroptosis in multiple cancer types (113, 114). Evidence from network pharmacology, molecular docking, virtual screening, ADMET profiling, and transcriptomic analyses consistently demonstrate that phenolic compounds modulate ferroptosis through multiple target and multiple pathway mechanisms rather than single-gene regulation.

Ming et al. (2024) demonstrated that curcumin induced dose-dependent ferroptotic cell death in colorectal cancer cells through the regulation of the p53/SLC7A11/GSH/GPX4 signaling axis. This study highlights GPX4 and SLC7A11 as core ferroptosis-related targets using an integrated network pharmacology and molecular docking strategy (113). In parallel, a very recently published study revealed that a newly synthesized curcumin derivative (Compound 4d) strongly binds to the active site of GPX4 in MCF-7 cells, inducing SLC7A11/GPX4 axis-mediated ferroptosis (115). In another study, network pharmacology and molecular docking analyses have shown that curcumin's ferroptosis-inducing activity against esophageal squamous cell carcinoma targets CHEK1 and CDK6 proteins (116). These findings suggest that curcumin is capable of simultaneously targeting multiple nodes within the ferroptosis regulatory network, thereby reinforcing its role as a multi-target ferroptosis modülatör in cancer therapy.

Furthermore, transcriptomic and multidimensional data-driven studies have increasingly highlighting ferroptosis as a key outcome of curcumin-mediated

anticancer activity. Firouzjaei et al (2023) systematically investigated the effect of curcumin on ferroptosis-related gene expression in colorectal cancer using integrated *in silico* analyses and *in vitro* validation, revealing significant transcriptional modulation of genes involved in iron metabolism, lipid metabolism, and antioxidant defense, including MYC, IL1-ß Caveolin 1 and SLC1A5 (117). Li et al. (2020) demonstrated that curcumin treatment in breast cancer cells elicits a ferroptosis-associated gene expression signature, prominently characterized by the upregulation of HMOX1/HO-1, linking oxidative stress responses, iron metabolism, and lipid peroxidation to ferroptotic cell death (118). Consistent with these findings, EF24, a synthetic curcumin analog, was shown to induce ferroptosis in osteosarcoma cells through transcriptional activation of HMOX1, further supporting HO-1 as a recurrent ferroptosis-associated molecular feature of curcumin-based compounds rather than a single direct target (105). In colorectal cancer, transcriptome-guided pathway analyses revealed that combined treatment with curcumin and Andrographis activates ferroptosis-related gene networks through coordinated suppression of antioxidant defense mechanisms, including GPX4 and ferroptosis suppressor protein-1 (FSP1), highlighting ferroptosis as an emergent outcome of large-scale transcriptional modulation (119). Moreover, a curcumin synthetic derivative, NL01, was reported to induce ferroptosis in ovarian cancer cells via modulation of the HCAR1/MCT1 signaling axis, a mechanism supported by gene expression changes associated with metabolic reprogramming and redox imbalance (108). These studies underscore the value of transcriptomic approaches in uncovering ferroptosis as a systems-level response to curcumin and its derivatives, revealing consistent ferroptosis-associated gene signatures across different cancer types and compound variants.

In another study employing molecular docking approaches, hydroxytyrosol, a phenolic compound derived from olives, was shown to exhibit strong binding affinities toward several key ferroptosis-related proteins, including NRF2, NAD(P)H quinone oxidoreductase 1 (NQO1), PTGS2, AKR1C3, and thioredoxin reductase 1 (TrxR1), in colorectal cancer cells (120). These targets are critically involved in redox regulation, lipid peroxidation, and antioxidant defense, underscoring the potential role of hydroxytyrosol in modulating ferroptosis-associated pathways. Similarly, Hong et al. (2021) applied virtual screening and molecular docking strategies to evaluate the therapeutic potential of GA in colorectal cancer. Their analyses revealed that GA displays high binding affinity toward several prognostically relevant proteins, including GPX4, TP53, TFRC, and AURKA, all of which are implicated in ferroptosis regulation and cancer progression. Beyond these predicted static interactions, the study suggested that GA actively contributes to ferroptosis induction by perturbing iron metabolism and disrupting ROS homeostasis, thereby reinforcing the functional relevance of the docking-based predictions (58). Similarly, oxyresveratrol emerged as a novel ferroptosis inducer in breast cancer by targeting the EGFR/PI3K/AKT/GPX4 signaling axis, with molecular docking analyses confirming stable binding to GPX4 and upstream signaling proteins (121).

Flavonoids constitute a prominent class of phenolic ferroptosis modulators with diverse molecular targets. 4,4′-Dimethoxychalcone was reported to induce ferroptosis in cancer cells by synergistically activating the Keap1/NRF2/HMOX1 pathway while simultaneously inhibiting ferrochelatase (FECH), thereby increasing intracellular labile iron levels and promoting lipid peroxidation. These findings were supported by molecular docking and mechanistic pathway analyses, illustrating how iron metabolism and antioxidant signaling converge in ferroptosis execution (122). Consistently, baicalin induced ferroptosis in osteosarcoma cells via a novel NRF2/xCT/GPX4 regulatory axis, where inhibition of cystine uptake and GPX4 activity disrupted redox homeostasis (123). Comparable mechanisms were observed for nobiletin, which triggered ferroptosis in melanoma cells through a GSK3β-mediated Keap1/NRF2/HO-1 signaling cascade, reinforcing the central role of NRF2-dependent antioxidant responses in ferroptosis resistance (124). Similarly, luteolin was demonstrated to trigger ferroptosis in clear cell renal cell carcinoma by promoting

HO-1-dependent increases in the labile iron pool and lipid peroxidation, thereby linking flavonoid-mediated iron dysregulation to ferroptotic cell death (125). Finally, hesperetin was identified via network pharmacology and docking analyses to promote bladder cancer cell death through modulation of the PI3K/AKT pathway, indirectly sensitizing cells to ferroptosis-associated oxidative stress (89).

Consequently, these findings demonstrate that phenolic compounds regulate ferroptosis through integrated redox modulation, iron metabolism dysregulation, and signaling pathway interference, as revealed by multi-layered computational and experimental approaches. The convergence of network pharmacology, molecular docking, ADMET analysis, and systems-level validation highlights phenolic compounds as promising multi-target agents for ferroptosis-based cancer therapy and provides a robust framework for future translational and clinical investigations.

6. Phenolic Compound Integrated Nanomaterials as Ferroptosis-Inducing Platforms for Cancer Treatment

Despite the potent regulatory effects of phenolic compounds on ferroptosis, their clinical translation of phenolic compounds in cancer therapy is often limited by pharmacokinetic barriers such as poor aqueous solubility, rapid metabolism, restricted tissue penetration, insufficient systemic distribution and low bioavailability (126). To overcome these limitations, recent studies have focused on integrating phenolic compounds into nanostructured delivery systems, which markedly improve their stability, tumor accumulation, and therapeutic efficacy while enabling ferroptosis-based anticancer strategies. Nanocarrier systems improve intracellular delivery of phenolics, provide controlled-release profiles, and contribute to overcoming multiple drug-resistance mechanisms. Moreover, tumor microenvironmental features such as acidic pH, elevated ROS levels, and abnormal vasculature facilitate both passive (EPR effect) and active targeting of nanoparticles, thereby enhancing the selectivity of ferroptosis-based therapies. These nano-enabled platforms include metal-polyphenol networks, polymeric nanoparticles, lipid-based nanocarriers, biomimetic systems, and inorganic nanocomposites (127).

Among these approaches, metal-phenolic coordinated nanomaterials have emerged as particularly effective ferroptosis inducers due to their intrinsic iron content and redox activity (Table 4). Metal-polyphenol coordination assemblies formed through supramolecular interactions between Fe^{2+}/Fe^{3+} ions and phenolic ligands generate stable nanostructures capable of catalyzing Fenton reactions and amplifying lipid peroxidation. Yu et al. (2022) developed a Fe(II)–polyphenol coordinated nanomedicine that combined photoacoustic imaging guidance with mild hyperthermia, thereby enhancing iron-catalyzed lipid peroxidation and inducing ferroptotic cell death in breast cancer models. The nanoformulation exhibited potent anticancer efficacy by inducing ROS production and inhibiting the expression of GPX4 in both *in vitro* and *in vivo* settings. (128). Similarly, self-assembled Fe-phenolic acid networks were shown to synergize with ferroptosis pathways, resulting in significant tumor suppression through iron-dependent ROS accumulation and GPX4 inactivation (129). Furthermore, Qing et al. (2025) reported a supramolecular nanocomposite (bm–Cur–NC) formed via the coordination of bisdemethylcurcumin with Cu(II) exhibiting high aqueous stability and mitochondrial affinity. Specifically, this nanomedical product represents the first system capable of depleting intracellular glutathione (GSH) through three synergistic mechanisms: suppression of GSH biosynthesis via SLC7A11 downregulation, Cu(II)-mediated GSH redox depletion, and Michael addition reactions with a polyphenolic framework. The resulting redox imbalance leads to lipid peroxidation and mitochondrial dysfunction, triggering ferroptosis in drug-resistant cancer cells. bm–Cur–NC demonstrated strong antitumor activity both *in vitro* and *in vivo*, with ferroptosis identified as the dominant mode of cell death, and exhibited broad cytotoxic activity in multiple drug-resistant cancer models (130). In line with this polyphenol-metal coordination strategy, Wang et al. (2024) developed an EGCG-based supramolecular nanocomplex using Fe(III) instead of Cu(II) as the catalytic metal center. In contrast to the Cu-mediated GSH depletion dominant mechanism reported by Qing et al., the FeE@PEG nanocomplex primarily generates excess hydroxyl radicals (•OH) using H_2O_2-sensitive cleavage and Fe(III)-driven Fenton reactions. Simultaneously, EGCG enhances

Table 4. Nanomaterials integrated with phenolic compounds that trigger ferroptosis in cancer treatment.

Phenolic compound	Nanomaterial structure	Nanosystem	Cancer model	Ferroptosis-related mechanism	Reference
Gallic acid	Fe(II)-polyphenol coordinated nanoparticles co-loaded with Sorafenib	Fe-GA@BSA-SRF	Breast cancer cells and xenograft breast cancer model	Fe(II)-catalyzed Fenton reaction, lipid peroxidation, hyperthermia-enhanced ferroptosis	(128)
Rosmarinic acid	Self-assembled Fe-phenolic acid network	Fe-RA	Hepatoma-22 (H22) cells and xenograft tumor model	Iron overload, ROS amplification, GPX4 suppression	(129)
Curcumin	Polyphenol-metal supramolecular nanocomplex	bm–Cur–NC	Cisplatin-resistant HCC (HepG2/DDP) cells; HCC mouse model	Activation of ferroptosis via iron-dependent lipid peroxidation	(130)
Catechins (green tea)	Self-assembled metal-phenolic nanocomplex	FeE@PEG	SKOV3 ovarian cancer cells and xenograft mouse model	Tumor-specific ferroptosis via iron redox cycling and ROS generation	(131)
Curcumin	Cancer cell membrane-camouflaged nanoparticles	MSN-CUR@CM	SGC7901 and MGC803 gastric cancer cells; mouse xenograft tumor model	Lipid ROS accumulation, iron dysregulation, ferroptosis induction	(132)
Curcumin	Curcumin – polydopamine nanoparticles	Cur–PDA NPs	PC-12 cells	Iron chelation and redox modulation (ferroptosis regulation)	(133)
Resveratrol	Nanoliposomes co-loaded with rapamycin	Rapa/Res liposomes	HCT116 colorectal cancer cells; CRC mouse model	Lipid peroxidation, antioxidant system inhibition, apoptosis–ferroptosis crosstalk	(134)
Resveratrol	Biomimetic nano-delivery system	RSV-NPs@RBCm	HT29 and HCT116 CRC cells; CRC mouse model	Iron metabolism modulation, ferroptosis induction	(29)
Gallic acid	Iron oxide nanoparticles	IONP–GA/PAA	glioblastoma (U87MG and U373MG); neuroblastoma (IMR32); fibrosarcoma (HT1080)	Iron overload, ROS-mediated lipid peroxidation	(135)
Apigenin	Fe_2O_3/Fe_3O_4@$mSiO_2$ nanocomposites	API-Fe2O3/Fe3O4@mSiO2-	A549 lung cancer cells	Iron accumulation, oxidative stress, ferroptotic cell death	(136)
Apigenin	Iron–apigenin nanocomplex	FeAPG	4T1, MDA-MB-231 breast cancer cells; xenograft tumor model	Photothermal-enhanced ferroptosis and immune activation	(137)
Hesperetin	Targeted nanocomposites	HFPN	4T1, MDA-MB-231 and BT-549 breast cancer cells; subcutaneous tumor model	AURKA targeting, ferroptosis induction, radiosensitization	(138)
Gallic acid	Ultrasound-responsive nanoparticles	GA-Fe@BSA@PTX	B16F10 melanoma cells	Iron accumulation, oxidative stress, ultimately leading to mitochondrial damage, lipid peroxidation, and apoptosis	(139)

ferroptotic stress by promoting H_2O_2 production via auto-oxidation and depleting intracellular GSH, leading to significant lipid peroxidation and ferroptosis in chemotherapy-resistant ovarian cancer models (131). These findings highlight how metal selection critically determines the ferroptotic pathway activated by polyphenol-based nanomedical drugs.

Polymeric (e.g., PLGA, chitosan, PEG-modified systems) and hybrid nanocarriers incorporating phenolic compounds further enhance ferroptosis-mediated anticancer effects by improving intracellular delivery and controlled release. Curcumin-loaded nanoparticles camouflaged with cancer cell membranes represent a biomimetic polymer-based system that enhances tumor targeting and immune evasion while triggering ferroptosis in gastric cancer via excessive lipid peroxidation and iron dysregulation (132). In contrast, curcumin-polydopamine nanoparticles have been reported to chelate iron and modulate oxidative stress, highlighting that the ferroptotic outcome of phenolic

nanoformulations strongly depends on nanocarrier composition and iron availability (133).

Lipid-based nanocarriers, particularly nanoliposomes, have also been successfully employed to co-deliver phenolic compounds and synergistic agents. Nanoliposomal encapsulation of resveratrol in combination with rapamycin significantly enhanced both apoptotic and ferroptotic cell death in colorectal cancer by promoting lipid ROS accumulation and impairing antioxidant defenses (134). Biomimetic resveratrol-loaded nano-delivery systems have further demonstrated tumor-specific ferroptosis induction through modulation of iron metabolism and membrane lipid peroxidation (29).

In addition to organic nanocarriers, inorganic and magnetic nanocomposites incorporating GA provide multifunctional ferroptosis-based therapeutic platforms. Iron oxide nanoparticles and Fe-based nanocomposites inherently promote ferroptosis through iron overload and ROS generation (135). Apigenin-loaded $Fe_2O_3/Fe_3O_4@mSiO_2$ magnetic nanocomposites significantly enhanced intracellular iron accumulation and oxidative stress, leading to ferroptotic cell death in lung cancer cells (136). Moreover, multifunctional iron-apigenin nanocomplexes integrating photothermal therapy have been shown to amplify ferroptosis while simultaneously activating antitumor immune responses in triple-negative breast cancer (137).

These studies demonstrate that phenolic compound-integrated nanomaterials not only overcome the pharmacokinetic limitations of free phenolics but also actively participate in ferroptosis induction through iron delivery, redox modulation, and lipid peroxidation amplification. The rational design of nanocarrier composition (metal-coordinated, polymeric, lipid-based, or inorganic) plays a decisive role in dictating ferroptotic sensitivity and therapeutic outcomes, highlighting the promise of nanotechnology-enabled phenolic compounds as next-generation anticancer agents.

Beyond polyphenol-metal redox nanocomplexes, emerging nanotherapy platforms incorporate additional physical or procedural triggers to further learn ferroptotic cell destruction. Guo et al. developed a hesperetin-based nanocomposite that enhances radiotherapy in triple-negative breast cancer by inducing AURKA-dependent ferroptosis (138). In parallel, Wang et al. designed an ultrasound-resistant nanocatalyst capable of simultaneously activating ferroptosis and apoptosis, leading to effective suppression of metastatic uveal melanoma (139). These approaches highlight the expanding design of ferroptosis-inducing nanomedical applications that integrate redox regulation with radiotherapy or sonodynamic activation.

7. Future Perspective

Future studies should focus on improving the translational potential of ferroptosis-targeting strategies by addressing key challenges such as bioavailability, pharmacokinetics, and tissue-specific delivery of ferroptosis modulators. In addition, the identification of reliable ferroptosis-related biomarkers will be critical for patient stratification and therapeutic monitoring in clinical settings. Combining ferroptosis-modulating agents with conventional therapies, such as chemotherapy or radiotherapy, may also represent a promising approach to enhance treatment efficacy and overcome therapeutic resistance, ultimately facilitating the transition of ferroptosis-based interventions from preclinical research to clinical application.

8. Conclusion

This review comprehensively examines the regulatory effects of plant-derived phenolic compounds on ferroptosis by integrating molecular mechanisms, preclinical anticancer evidence, in silico and system-level network pharmacology analyses, nanotechnological delivery strategies, and clinical translation considerations. Collectively, these interconnected layers form a unified framework explaining how phenolic compounds can modulate ferroptosis in a context-dependent manner, exhibiting stimulatory or inhibitory effects depending on cellular redox status, iron metabolism, and disease context, thereby providing high therapeutic selectivity. Within this framework, the phenolic-ferroptosis axis emerges as an innovative anticancer strategy with high potential for overcoming drug resistance, reducing off-target toxicity, and supporting the development of

personalized therapeutic approaches. However, safe and effective clinical translation of this information will require rigorously designed, mechanism-oriented, and large-scale clinical trials.

Conflict of interest: The authors declare no conflict of interest.

Funding: None

Ethics approval: Not applicable

Author Contributions: T.S was responsible for the conceptualization, literature search, formal analysis, and writing of the original draft and final version of this manuscript.

References

1. Sung H, Ferlay J, Siegel RL, Laversanne M, Soerjomataram I, Jemal A, Bray F. Global Cancer Statistics 2020: GLOBOCAN Estimates of Incidence and Mortality Worldwide for 36 Cancers in 185 Countries. CA Cancer J Clin. 2021;71(3):209-249. https://doi.org/10.3322/caac.21660
2. Zafar A, Khatoon S, Khan MJ, Abu J, Naeem A. Advancements and limitations in traditional anti-cancer therapies: a comprehensive review of surgery, chemotherapy, radiation therapy, and hormonal therapy. Discov Oncol. 2025;16(1):607. https://doi.org/10.1007/s12672.025.02198-8
3. Li J, Hu J, Yang Y, Zhang H, Liu Y, Fang Y, Qu L, Lin A, Luo P, Jiang A, Wang L. Drug resistance in cancer: Molecular mechanisms and emerging treatment strategies. Mol Biomed. 2025;6(1):111. https://doi.org/10.1186/s43556.025.00352-w
4. Fu YC, Liang SB, Luo M, Wang XP. Intratumoral heterogeneity and drug resistance in cancer. Cancer Cell Int. 2025;25(1):103. https://doi.org/10.1186/s12935.025.03734-w
5. Hassannia B, Vandenabeele P, Vanden Berghe T. Targeting ferroptosis to iron out cancer. Cancer Cell. 2019;35(6):830-849. https://doi.org/10.1016/j.ccell.2019.04.002
6. Dixon SJ, Lemberg KM, Lamprecht MR, Skouta R, Zaitsev EM, Gleason CE, Patel DN, Bauer AJ, Cantley AM, Yang WS, Morrison B 3rd, Stockwell BR. Ferroptosis: an iron-dependent form of nonapoptotic cell death. Cell. 2012;149(5):1060-1072. https://doi.org/10.1016/j.cell.2012.03.042
7. Stockwell BR, Friedmann Angeli JP, Bayir H, Bush AI, Conrad M, Dixon SJ, Fulda S, Gascón S, Hatzios SK, Kagan VE, Noel K, Jiang X, Linkermann A, Murphy ME, Overholtzer M, Oyagi A, Pagnussat GC, Park J, Ran Q, Rosenfeld CS, Salnikow K, Tang D, Torti FM, Torti SV, Toyokuni S, Woerpel KA, Zhang DD. Ferroptosis: A regulated cell death nexus linking metabolism, redox biology, and disease. Cell. 2017;171(2):273-285. https://doi.org/10.1016/j.cell.2017.09.021
8. Conrad M, Pratt DA. The chemical basis of ferroptosis. Nat Chem Biol. 2019;15(12):1137-1147. https://doi.org/10.1038/s41589.019.0408-1
9. Yang WS, SriRamaratnam R, Welsch ME, Shimada K, Skouta R, Viswanathan VS, Cheah JH, Clemons PA, Shamji AF, Clish CB, Brown LM, Girotti AW, Cornish VW, Schreiber SL, Stockwell BR. Regulation of ferroptotic cancer cell death by GPX4. Cell. 2014;156(1-2):317-331. https://doi.org/10.1016/j.cell.2013.12.010
10. Li J, Cao F, Yin HL, Huang ZJ, Lin ZT, Mao N, Sun B, Wang G. Ferroptosis: past, present and future. Cell Death Dis. 2020;11(2):88. https://doi.org/10.1038/s41419.020.2298-2
11. Pandey KB, Rizvi SI. Plant polyphenols as dietary antioxidants in human health and disease. Oxid Med Cell Longev. 2009;2(5):270-278. https://doi.org/10.4161/oxim.2.5.9498
12. Seca AML, Pinto DCGA. Plant Secondary Metabolites as Anticancer Agents: Successes in Clinical Trials and Therapeutic Application. Int J Mol Sci. 2018;19(1):263. https://doi.org/10.3390/ijms19010263
13. Hashim GM, Shahgolzari M, Hefferon K, Yavari A, Venkataraman S. Plant-Derived Anti-Cancer Therapeutics and Biopharmaceuticals. Bioengineering. 2025; 12(1):7. https://doi.org/10.3390/bioengineering12010007
14. Manach C, Scalbert A, Morand C, Rémésy C, Jiménez L. Polyphenols: food sources and bioavailability. Am J Clin Nutr. 2004 May;79(5):727-747. https://doi.org/10.1093/ajcn/79.5.727
15. Crozier A, Jaganath IB, Clifford MN. Dietary phenolics: chemistry, bioavailability and effects on health. Nat Prod Rep. 2009;26(8):1001-43. https://doi.org/10.1039/b802662a
16. Eghbaliferiz S, Iranshahi M. Prooxidant activity of polyphenols, flavonoids, anthocyanins and carotenoids: Updated review of mechanisms and catalyzing metals. Phytother Res. 2016;30(9):1379-91. https://doi.org/10.1002/ptr.5643
17. Sui X, Wang J, Zhao Z, Liu B, Liu M, Liu M, Shi C, Feng X, Fu Y, Shi D, Li S, Qi Q, Xian M, Zhao G. Phenolic compounds induce ferroptosis-like death by promoting hydroxyl radical generation in the Fenton reaction. Commun Biol. 2024;7(1):199. https://doi.org/10.1038/s42003.024.05903-5
18. Kruk J, Aboul-Enein BH, Duchnik E, Marchlewicz M. Antioxidative properties of phenolic compounds and their effect on oxidative stress induced by severe physical exercise. J Physiol Sci. 2022 Aug 5;72(1):19. https://doi.org/10.1186/s12576.022.00845-1
19. Günther M, Dabare S, Fuchs J, Gunesch S, Hofmann J, Decker M, Culmsee C. Flavonoid–phenolic acid hybrids are potent inhibitors of ferroptosis via attenuation of mitochondrial impairment. Antioxidants. 2024; 13(1):44. https://doi.org/10.3390/antiox13010044
20. Zhao J-W, Zhao W-Y and Yu Z. Correction: Food-derived compounds targeting ferroptosis for cancer therapy: from effects to mechanisms. Front. Oncol. 2025;15:1644727. https://doi.org/10.3389/fonc.2025.164.4727
21. Tang X, Ding H, Liang M, Chen X, Yan Y, Wan N, Chen Q, Zhang J, Cao J. Curcumin induces ferroptosis in non-small-cell lung cancer via activating autophagy. Thorac Cancer. 2021;12(8):1219-1230. https://doi.org/10.1111/1759-7714.13904
22. Hynes MJ, Coinceanainn MO. Investigation of the release of iron from ferritin by naturally occurring antioxidants. J Inorg Biochem. 2002;90(1-2):18-21. https://doi.org/10.1016/s0162-0134(02)00383-5
23. Qin X, Zhang J, Wang B, Xu G, Yang X, Zou Z, Yu C. Ferritinophagy is involved in the zinc oxide nanoparticles-induced ferroptosis of vascular endothelial cells. Autophagy. 2021;17(12):4266-4285. https://doi.org/10.1080/15548.627.2021.1911016
24. Kose T, Sharp PA, Latunde-Dada GO. Phenolic acids rescue iron-induced damage in murine pancreatic cells and tissues. Molecules. 2023; 28(10):4084. https://doi.org/10.3390/molecules28104084
25. Chen L, Lin W, Zhang H, Geng S, Le Z, Wan F, Huang Q, Chen H, Liu X, Lu JJ, Kong L. TRIB3 promotes malignancy of head

and neck squamous cell carcinoma via inhibiting ferroptosis. Cell Death Dis. 2024;15(3):178. https://doi.org/10.1038/s41419.024.06472-5

26. Dodson M, Castro-Portuguez R, Zhang DD. NRF2 plays a critical role in mitigating lipid peroxidation and ferroptosis. Redox Biol. 2019;23:101107. 101107. https://doi.org/10.1016/j.redox.2019.101107
27. Yang JH, Choi MH, Na CS, Cho SS, Kim JH, Ku SK, Cho IJ, Shin HJ, Ki SH. Bamboo Stems (Phyllostachys nigra variety henosis) containing polyphenol mixtures activate Nrf2 and attenuate phenylhydrazine-induced oxidative stress and liver injury. Nutrients. 2019;11(1):114. https://doi.org/10.3390/nu11010114
28. Yuan C, Fan R, Zhu K, Wang Y, Xie W, Liang Y. Curcumin induces ferroptosis and apoptosis in osteosarcoma cells by regulating Nrf2/GPX4 signaling pathway. Exp Biol Med (Maywood). 2023;248(23):2183-2197. https://doi.org/10.1177/153.537.02231220670
29. Zhang Z, Ji Y, Hu N, Yu Q, Zhang X, Li J, Wu F, Xu H, Tang Q, Li X. Ferroptosis-induced anticancer effect of resveratrol with a biomimetic nano-delivery system in colorectal cancer treatment. Asian J Pharm Sci. 2022;17(5):751-766. https://doi.org/10.1016/j.ajps.2022.07.006
30. An S, Hu M. Quercetin Promotes TFEB Nuclear translocation and activates lysosomal degradation of ferritin to induce ferroptosis in breast cancer cells. Comput Intell Neurosci. 2022;2022:5299218. https://doi.org/10.1155/2022/5299218
31. Ding L, Dang S, Sun M, Zhou D, Sun Y, Li E, Peng S, Li J, Li G. Quercetin induces ferroptosis in gastric cancer cells by targeting SLC1A5 and regulating the p-Camk2/p-DRP1 and NRF2/GPX4 Axes. Free Radic Biol Med. 2024;213:150-163. https://doi.org/10.1016/j.freeradbiomed.2024.01.002
32. Wang S, Wang R, Hu D, Zhang C, Cao P, Huang J, Wang B. Epigallocatechin gallate modulates ferroptosis through downregulation of tsRNA-13502 in non-small cell lung cancer. Cancer Cell Int. 2024;24(1):200. https://doi.org/10.1186/s12935.024.03391-5
33. Liu Y, Fu X, Li J, Guo J, Zhao Z, Zheng J. Gallic acid alleviates ferroptosis by negatively regulating APOC3 and improves nerve function deficit caused by traumatic brain injury. Sci Rep. 2025;15(1):7815. https://doi.org/10.1038/s41598.025.92383-0
34. Wu L, Lv L, Xiang Y, Yi D, Liang Q, Ji M, Deng Z, Qin L, Ren L, Liang Z, He J. Rosmarinic acid protects against acetaminophen-induced hepatotoxicity by suppressing ferroptosis and oxidative stress through Nrf2/HO-1 activation in mice. Mar Drugs. 2025; 23(7):287. https://doi.org/10.3390/md23070287
35. Li LY, Wang Q, Deng L, Lin Z, Lin JJ, Wang XY, Shen TY, Zheng YH, Lin W, Li PJ, Fu XQ, Lin ZL. Chlorogenic acid alleviates hypoxic-ischemic brain injury in neonatal mice. Neural Regen Res. 2023;18(3):568-576. https://doi.org/10.4103/1673-5374.350203
36. Zhang N, Wang Z, Li G, Zhang M, Liu Q, Cai C, Shang Y, Zhu H, An H, Ren S. A carrier-free metal-phenolic network with enhanced ferroptosis-immunotherapy for overcoming tumor resistance and metastasis. Chem.Eng.J. 2024;488: 150780. https://doi.org/10.1016/j.cej.2024.150780
37. Jakobušić Brala C, Karković Marković A, Kugić A, Torić J, Barbarić M. Combination chemotherapy with selected polyphenols in preclinical and clinical studies-an update overview. Molecules. 2023;28(9):3746. https://doi.org/10.3390/molecules28093746
38. Zhang X, Ma Y, Wan J, Yuan J, Wang D, Wang W, Sun X and Meng Q. Biomimetic nanomaterials triggered ferroptosis for cancer theranostics. Front. Chem.2021; 9:768248. https://doi.org/10.3389/fchem.2021.768248
39. Farzipour S, Zefrei FJ, Bahadorikhalili S, Alvandi M, Salari A, Shaghaghi Z. Nanotechnology utilizing ferroptosis ınducers in cancer treatment. Anticancer Agents Med Chem.2024;24(8):571-589. https://doi.org/10.2174/011.871.5206278.427.231215111526
40. Gao M, Yi J, Zhu J, Minikes AM, Monian P, Thompson CB, Jiang X. Role of mitochondria in ferroptosis. Mol Cell. 2019;73(2):354-363.e3. https://doi.org/10.1016/j.molcel.2018.10.042
41. Chen X, Yu C, Kang R, Tang D. Iron metabolism in ferroptosis. Front Cell Dev Biol. 2020;8:590226. https://doi.org/10.3389/fcell.2020.590226
42. Ru Q, Li Y, Chen L, Wu Y, Min J, Wang F. Iron homeostasis and ferroptosis in human diseases: mechanisms and therapeutic prospects. Signal Transduct Target Ther. 2024;9(1):271. https://doi.org/10.1038/s41392.024.01969-z
43. Artusi I, Rubin M, Cravin G, Cozza G. Ferroptosis in Human Diseases: Fundamental Roles and Emerging Therapeutic Perspectives. Antioxidants. 2025; 14(12):1411. https://doi.org/10.3390/antiox14121411
44. Salnikow K. Role of iron in cancer. Semin Cancer Biol. 2021;76:189-194. https://doi.org/10.1016/j.semcancer.2021.04.001
45. Kagan VE, Mao G, Qu F, Angeli JP, Doll S, Croix CS, Dar HH, Liu B, Tyurin VA, Ritov VB, Kapralov AA, Amoscato AA, Jiang J, Anthonymuthu T, Mohammadyani D, Yang Q, Proneth B, Klein-Seetharaman J, Watkins S, Bahar I, Greenberger J, Mallampalli RK, Stockwell BR, Tyurina YY, Conrad M, Bayır H. Oxidized arachidonic and adrenic PEs navigate cells to ferroptosis. Nat Chem Biol. 2017;13(1):81-90. https://doi.org/10.1038/nchembio.2238
46. Tang D, Chen X, Kang R, Kroemer G. Ferroptosis: molecular mechanisms and health implications. Cell Res. 2021;31(2):107-125. https://doi.org/10.1038/s41422.020.00441-1
47. Rochette L, Dogon G, Rigal E, Zeller M, Cottin Y, Vergely C. Lipid Peroxidation and Iron Metabolism: Two Corner Stones in the Homeostasis Control of Ferroptosis. Int. J. Mol. Sci. 2023;24(1):449. https://doi.org/10.3390/ijms24010449
48. Ayala A, Muñoz MF, Argüelles S. Lipid peroxidation: production, metabolism, and signaling mechanisms of malondialdehyde and 4-hydroxy-2-nonenal. Oxid Med Cell Longev. 2014;2014:360438. https://doi.org/10.1155/2014/36043
49. Doll S, Proneth B, Tyurina YY, Panzilius E, Kobayashi S, Ingold I, Irmler M, Beckers J, Aichler M, Walch A, Prokisch H, Trümbach D, Mao G, Qu F, Bayir H, Füllekrug J, Scheel CH, Wurst W, Schick JA, Kagan VE, Angeli JP, Conrad M. ACSL4 dictates ferroptosis sensitivity by shaping cellular lipid composition. Nat Chem Biol. 2017;13(1):91-98. https://doi.org/10.1038/nchembio.2239
50. Dixon SJ, Patel DN, Welsch M, Skouta R, Lee ED, Hayano M, Thomas AG, Gleason CE, Tatonetti NP, Slusher BS, Stockwell BR. Pharmacological inhibition of cystine-glutamate exchange induces endoplasmic reticulum stress and ferroptosis. Elife. 2014;3:e02523. https://doi.org/10.7554/eLife.02523
51. Ursini F, Maiorino M. Lipid peroxidation and ferroptosis: The role of GSH and GPx4. Free Radic Biol Med. 2020;152:175-185. https://doi.org/10.1016/j.freeradbiomed.2020.02.027
52. Mashima R, Okuyama T. The role of lipoxygenases in pathophysiology; new insights and future perspectives. Redox Biol. 2015;6:297-310. https://doi.org/10.1016/j.redox.2015.08.006

53. Chu B, Kon N, Chen D, Li T, Liu T, Jiang L, Song S, Tavana O, Gu W. ALOX12 is required for p53-mediated tumour suppression through a distinct ferroptosis pathway. Nat Cell Biol. 2019;21(5):579-591. https://doi.org/10.1038/s41556.019.0305-6
54. Zhang XD, Liu ZY, Wang MS, Guo YX, Wang XK, Luo K, Huang S, Li RF. Mechanisms and regulations of ferroptosis. Front Immunol. 2023;14:1269451. https://doi.org/10.3389/fimmu.2023.126.9451
55. Yan R, Lin B, Jin W, Tang L, Hu S, Cai R. NRF2, a Superstar of Ferroptosis. Antioxidants (Basel). 2023;12(9):1739. https://doi.org/10.3390/antiox12091739
56. Liu Y, Wang Y, Liu J, Kang R, Tang D. Interplay between MTOR and GPX4 signaling modulates autophagy-dependent ferroptotic cancer cell death. Cancer Gene Ther. 2021;28(1-2):55-63. https://doi.org/10.1038/s41417.020.0182-y
57. Xie J, Wang H, Xie W, Liu Y, Chen Y. Gallic acid promotes ferroptosis in hepatocellular carcinoma via inactivating Wnt/β-catenin signaling pathway. Naunyn Schmiedebergs Arch Pharmacol. 2024;397(4):2437-2445. https://doi.org/10.1007/s00210.023.02770-5
58. Hong Z, Tang P, Liu B, Ran C, Yuan C, Zhang Y, Lu Y, Duan X, Yang Y, Wu H. Ferroptosis-related Genes for Overall Survival Prediction in Patients with Colorectal Cancer can be Inhibited by Gallic acid. Int J Biol Sci. 2021;17(4):942-956. https://doi.org/10.7150/ijbs.57164
59. Tang HM, Cheung PCK. Gallic Acid Triggers Iron-Dependent Cell Death with Apoptotic, Ferroptotic, and Necroptotic Features. Toxins. 2019; 11(9):492. https://doi.org/10.3390/toxins11090492
60. Chen X, Cui H, Qin L, Liu R, Fang F, Wang Z. Soybean Lecithin-Gallic Acid Complex Sensitizes Lung Cancer Cells to Radiation Through Ferroptosis Regulated by Nrf2/SLC7A11/GPX4 Pathway. Nutrients. 2025;17(7):1262. https://doi.org/10.3390/nu17071262
61. Zou C, Xu H, Hu F, Yu Y, Liu L, Wang X, Zhang Z, Zou H, Liu J, Huang H and Lai S. Gallic acid attenuates diabetic cardiomyopathy by inhibiting ferroptosis and protecting mitochondria via the TSPO/FTMT pathway. Front. Pharmacol. 2025;16:1661144. https://doi.org/10.3389/fphar.2025.166.1144
62. Zhang Q, Shi Y, Zhang X, Liang S, Xu H, Quan W, Zhong C, Ding Y. The mechanisms and therapeutic applications of phenolic acids in vascular cognitive impairment: A comprehensive review, Curr Mol Pharmacol. 2025;18(1):32-47. https://doi.org/10.1016/j.cmp.2025.09.002
63. Zhao Y, Wang C, Yang T, Wang H, Zhao S, Sun N, Chen Y, Zhang H, Fan H. Chlorogenic Acid Alleviates Chronic Stress-Induced Duodenal Ferroptosis via the Inhibition of the IL-6/JAK2/STAT3 Signaling Pathway in Rats. J Agric Food Chem. 2022;70(14):4353-4361. https://doi.org/10.1021/acs.jafc.2c01196
64. Wu L, Chen HY, Zhang JT, Yang RY, Wang ZB, Xue PS, Peng W, Li KX, Gao WH, Zeng PH. Chlorogenic acid induces hepatocellular carcinoma cell ferroptosis via PTGS2/AKR1C3/GPX4 axis-mediated reprogramming of arachidonic acid metabolism. World J Gastrointest Oncol 2025; 17(3): 98844. https://doi.org/10.4251/wjgo.v17.i3.98844
65. Hitl M, Kladar N, Gavarić N, Božin B. Rosmarinic Acid-Human Pharmacokinetics and Health Benefits. Planta Med. 2021;87(4):273-282. https://doi.org/10.1055/a-1301-8648
66. Huang JY, Hsu TW, Chen YR, Kao SH. Rosmarinic Acid Potentiates Cytotoxicity of Cisplatin against Colorectal Cancer Cells by Enhancing Apoptotic and Ferroptosis. Life (Basel). 2024;14(8):1017. https://doi.org/10.3390/life14081017
67. Xie C, Chan L, Pang Y, Shang Y, Wang W, Zhao L. Rosmarinic acid promotes mitochondrial fission and induces ferroptosis in triple-negative breast cancer cells. Naunyn Schmiedebergs Arch Pharmacol. 2025;398:10461-10475. https://doi.org/10.1007/s00210.025.03927-0
68. Tang J, Zhang J, Chen H, Wang Z, Wu L, Xue P, Yang R, Peng W, Zeng P. Rosmarinic acid induces ferroptosis in colon cancer: insights from AKR1C3/PTGS2 pathway and mitochondrial dysfunction. 3 Biotech. 2025;15(11):374. https://doi.org/10.1007/s13205.025.04551-8
69. Liu L, Weng J, Yue L, Qin Y, Yu J, Li Y, Li S, Wu J, Yang Y, Tang Z, Xu H. Rosmarinic acid suppresses ferroptosis and confers neuroprotection in cerebral ischemia-reperfusion via direct KEAP1 inhibition and NRF2 activation. Free Radic Biol Med. 2026;242:237-249. https://doi.org/10.1016/j.freeradbiomed.2025.10.291
70. Wu L, Lv L, Xiang Y, Yi D, Liang Q, Ji M, Deng Z, Qin L, Ren L, Liang Z, He J. Rosmarinic Acid Protects Against Acetaminophen-Induced Hepatotoxicity by Suppressing Ferroptosis and Oxidative Stress Through Nrf2/HO-1 Activation in Mice. Mar Drugs. 2025;23(7):287. https://doi.org/10.3390/md23070287
71. Qiao O, Zhang L, Han L, Wang X, Li Z, Bao F, Hao H, Hou Y, Duan X, Li N, Gong Y. Rosmarinic acid plus deferasirox inhibits ferroptosis to alleviate crush syndrome-related AKI via Nrf2/Keap1 pathway. Phytomedicine. 2024;129:155700. https://doi.org/10.1016/j.phymed.2024.155700
72. Cao Y, Zhang H, Tang J, Wang R. Ferulic Acid Mitigates Growth and Invasion of Esophageal Squamous Cell Carcinoma through Inducing Ferroptotic Cell Death. Dis Markers. 2022;2022:4607966. https://doi.org/10.1155/2022/4607966
73. Tang X, Liu J, Yao S, Zheng J, Gong X, Xiao B. Ferulic acid alleviates alveolar epithelial barrier dysfunction in sepsis-induced acute lung injury by activating the Nrf2/HO-1 pathway and inhibiting ferroptosis. Pharm Biol. 2022;60(1):2286-2294. https://doi.org/10.1080/13880.209.2022.2147549
74. Consoli V, Fallica AN, Virzì NF, Salerno L, Intagliata S, Sorrenti V, Greish K, Giuffrida A, Vanella L, Pittalà V. Synthesis and in Vitro Evaluation of CAPE Derivatives as Ferroptosis Inducers in Triple Negative Breast Cancer. ACS Med Chem Lett. 2024;15(5):706-713. https://doi.org/10.1021/acsmedchemlett.4c00099
75. Khanam S, Hong YJ, Kim Y, Choi EH, Han I. Enhancing Ferroptosis in Lung Adenocarcinoma Cells via the Synergistic Action of Nonthermal Biocompatible Plasma and a Bioactive Phenolic Compound. Biomolecules. 2025;15(5):691. https://doi.org/10.3390/biom15050691
76. Dias MC, Pinto DCGA, Silva AMS. Plant Flavonoids: Chemical Characteristics and Biological Activity. Molecules. 2021;26(17):5377. https://doi.org/10.3390/molecules26175377
77. Kumar S, Pandey AK. Chemistry and biological activities of flavonoids: an overview. ScientificWorldJournal. 2013;2013:162750. https://doi.org/10.1155/2013/162750
78. Aggarwal D, Chaudhary M, Mandotra SK, Tuli HS, Chauhan R, Joshi NC, Kaur D, Dufossé L, Chauhan A. Anti-inflammatory potential of quercetin: From chemistry and mechanistic insight to nanoformulations. Curr Res Pharmacol Drug Discov. 2025;8:100217. https://doi.org/10.1016/j.crphar.2025.100217
79. Zhu YW, Liu CL, Li XM, Shang Y. Quercetin induces ferroptosis by inactivating mTOR/S6KP70 pathway in oral squamous

cell carcinoma. Toxicol Mech Methods. 2024;34(6):669-675. https://doi.org/10.1080/15376.516.2024.2325989

80. Wang ZX, Ma J, Li XY, Wu Y, Shi H, Chen Y, Lu G, Shen HM, Lu GD, Zhou J. Quercetin induces p53-independent cancer cell death through lysosome activation by the transcription factor EB and reactive oxygen species-dependent ferroptosis. Br J Pharmacol. 2021;178(5):1133-1148. https://doi.org/10.1111/bph.15350
81. Li X, Zhu Q, Ma M, Guo H. Quercetin inhibits the progression of endometrial HEC-1-A cells by regulating ferroptosis-a preliminary study. Eur J Med Res. 2022;27(1):292. https://doi.org/10.1186/s40001.022.00934-2
82. Zheng Y, Li L, Chen H, Zheng Y, Tan X, Zhang G, Jiang R, Yu H, Lin S, Wei Y, Wang Y, Zhang R, Liu Z, Wu J. Luteolin exhibits synergistic therapeutic efficacy with erastin to induce ferroptosis in colon cancer cells through the HIC1-mediated inhibition of GPX4 expression. Free Radic Biol Med. 2023;208:530-544. https://doi.org/10.1016/j.freeradbiomed.2023.09.014
83. Cao Q, Ding S, Zheng X, Li H, Yu L, Zhu Y, Jiang D, Ruan S. Luteolin Induces GPX4-dependent Ferroptosis and Enhances Immune Activation in Colon Cancer. Phytomedicine. 2025;146:157117. https://doi.org/10.1016/j.phymed.2025.157117
84. Fu W, Xu L, Chen Y, Zhang Z, Chen S, Li Q, You X. Luteolin induces ferroptosis in prostate cancer cells by promoting TFEB nuclear translocation and increasing ferritinophagy. Prostate. 2024;84(3):223-236. https://doi.org/10.1002/pros.24642
85. Han S, Lin F, Qi Y, Liu C, Zhou L, Xia Y, Chen K, Xing J, Liu Z, Yu W, Zhang Y, Zhou X, Rao T, Cheng F. HO-1 Contributes to Luteolin-Triggered Ferroptosis in Clear Cell Renal Cell Carcinoma via Increasing the Labile Iron Pool and Promoting Lipid Peroxidation. Oxid Med Cell Longev. 2022;2022:3846217. https://doi.org/10.1155/2022/3846217
86. Liu H, Yang J, Wang L, Meng S, Tang X, Liu C, Wang Y. Luteolin inhibits glioblastoma by regulating ROS levels via the NFE2L2/x-CT/GPX4 signalling axis. Tianjin Medical Journal, 2025, 53(7): 673-678. https://doi.org/10.11958/20250608
87. Li Y, Bai X. Naringenin induces ferroptosis in osteosarcoma cells through the STAT3-MGST2 signaling pathway. J Bone Oncol. 2024;50:100657. https://doi.org/10.1016/j.jbo.2024.100657
88. Li YZ, Deng J, Zhang XD, Li DY, Su LX, Li S, Pan JM, Lu L, Ya JQ, Yang N, Zhou J, Yang LH. Naringenin enhances the efficacy of ferroptosis inducers by attenuating aerobic glycolysis by activating the AMPK-PGC1α signalling axis in liver cancer. Heliyon. 2024;10(11):e32288. https://doi.org/10.1016/j.heliyon.2024.e32288
89. Lv Y, Liu Z, Deng L, Xia S, Mu Q, Xiao B, Xiu Y, Liu Z. Hesperetin promotes bladder cancer cells death via the PI3K/AKT pathway by network pharmacology and molecular docking. Sci Rep. 2024;14(1):1009. https://doi.org/10.1038/s41598.023.50476-8
90. Peng L, Hu X-Z, Liu Z-Q, Liu W-K, Huang Q and Wen Y. Therapeutic potential of resveratrol through ferroptosis modulation: insights and future directions in disease therapeutics. Front Pharmacol. 2024; 15:1473939. https://doi.org/10.3389/fphar.2024.147.3939
91. Zhang E, Wang Y, Zhang H, Li X, Su Y, Cui J, Xu R, Mao X, Sang M, Lin Z, Zhou X. Resveratrol induces ferroptosis in triple-negative breast cancer through NEDD4L-mediated GPX4 ubiquitination and degradation. Free Radic Biol Med. 2025;235:231-247. https://doi.org/10.1016/j.freeradbiomed.2025.04.052
92. Xiang L, Li Q, Guan Z, Wang G, Yu X, Zhang X, Zhang G, Hu J, Yang X, Li M, Bao X, Wang Y, Wang D. Oxyresveratrol as a novel ferroptosis inducer exhibits anticancer activity against breast cancer via the EGFR/PI3K/AKT/GPX4 signalling axis. Front Pharmacol. 2025;15:1527286. https://doi.org/10.3389/fphar.2024.152.7286
93. Chen X, Lu JL, Li H, Liu GY, Li TT, Xiao KH, Ye HS, Li S, Chen X, Liu J. Resveratrol Induces Oxidative Stress and Downregulates GPX4 and xCT to Activate the Ferroptosis Pathway for Anti-Bladder Cancer Organoids. Journal of Cancer. 2025;16(8): 2613-2625. doi: https://doi.org/10.7150/jca.109350
94. Shan G, Minchao K, Jizhao W, Rui Z, Guangjian Z, Jin Z, Meihe L. Resveratrol improves the cytotoxic effect of CD8 +T cells in the tumor microenvironment by regulating HMMR/Ferroptosis in lung squamous cell carcinoma. J Pharm Biomed Anal. 2023;229:115346. https://doi.org/10.1016/j.jpba.2023.115346
95. Liu J, Gao W, Sheng Y, Sun J, Wen D. Resveratrol drives ferroptosis of acute myeloid leukemia cells through Hsa-miR-335-5p/NFS1/GPX4 pathway in a ROS-dependent manner. Cell Mol Biol (Noisy-le-grand). 2023;69(7):131-137. https://doi.org/10.14715/cmb/2023.69.7.21
96. Yamada T, Iwasawa T, Shimizu Y, Kato K. Resveratrol enhances sulfasalazine-induced ferroptosis by promoting iron ion accumulation and lipid peroxidation in cancer cells. Anticancer Res. 2025;45(8):3231-3244 https://doi.org/10.21873/anticanres.17685
97. Zheng Y, Lu S, Li T. Resveratrol increases cisplatin sensitivity in pancreatic cancer cells by modulating dihydroorotatede hydrogenase-mediated ferroptosis. Food Science, 2025;46(9):189-205. https://doi.org/10.7506/spkx1002-6630.202.41118-136
98. Zhao X, Lu S, Yan M, Zhu ZG, Dong F, Yan C. Resveratrol targets mitochondrial USP36–SOD2 to induce autophagy-ferroptosis and inhibit gastric cancer progression. Gastric Cancer. 2025;28:1067–1084. https://doi.org/10.1007/s10120.025.01645-3
99. Zhou Y, Qian W, Li X, Wei W. NF-κB Inhibitor Myrislignan Induces Ferroptosis of Glioblastoma Cells via Regulating Epithelial-Mesenchymal Transformation in a Slug-Dependent Manner. Oxid Med Cell Longev. 2023;2023:7098313. https://doi.org/10.1155/2023/7098313
100. Chen M, Tan AH, Li J. Curcumin represses colorectal cancer cell proliferation by triggering ferroptosis via PI3K/Akt/mTOR signaling. Nutr Cancer. 2023;75(2):726-733. https://doi.org/10.1080/01635.581.2022.2139398
101. Deng J, Wu Z, Ning S, Chang X, Liu J, Yu Y, Zhang M, Zhang L. Curcumin induces ferroptosis in hepatocellular carcinoma by regulating the P62-KEAP1-NRF2-signaling pathway. BMC Cancer. 2025. https://doi.org/10.1186/s12885.025.15307-1
102. Jiang Y, Hui D, Pan Z, Yu Y, Liu L, Yu X, Wu C, Sun M. Curcumin promotes ferroptosis in hepatocellular carcinoma via upregulation of ACSL4. J Cancer Res Clin Oncol. 2024;150(9):429. https://doi.org/10.1007/s00432.024.05878-0
103. Cao X, Li Y, Wang Y, Yu T, Zhu C, Zhang X, Guan J. Curcumin suppresses tumorigenesis by ferroptosis in breast cancer. PLoS One. 2022;17(1):e0261370. https://doi.org/10.1371/journal.pone.0261370
104. Consoli V, Sorrenti V, Pittalà V, Greish K, D'Amico AG, Romeo G, Intagliata S, Salerno L, Vanella L. Heme Oxygenase Modulation Drives Ferroptosis in TNBC Cells. Int J Mol Sci. 2022;23(10):5709. https://doi.org/10.3390/ijms23105709
105. Lin H, Chen X, Zhang C, Yang T, Deng Z, Song Y, Huang L, Li F, Li Q, Lin S, Jin D. EF24 induces ferroptosis in osteosarcoma cells through HMOX1. Biomed Pharmacother. 2021;136:111202. https://doi.org/10.1016/j.biopha.2020.111202

106. Chen H, Li Z, Xu J, Zhang N, Chen J, Wang G, Zhao Y. Curcumin Induces Ferroptosis in Follicular Thyroid Cancer by Upregulating HO-1 Expression. Oxid Med Cell Longev. 2023;2023:6896790. https://doi.org/10.1155/2023/6896790
107. Zheng, Xin, Jun Liu, Wei Hu, Bin Jiang, Xin Zhou, Min Zhang, and Ming Song. Curcumin induces autophagy-mediated ferroptosis by targeting the PI3K/AKT/MTOR signaling pathway in gastric cancer. Turk J Gastroenterol. 2024;35(8):625-633. https://www.turkjgastroenterol.org/index.php/tjg/article/view/4141
108. Shi M, Zhang MJ, Yu Y, Ou R, Wang Y, Li H, Ge RS. Curcumin derivative NL01 induces ferroptosis in ovarian cancer cells via HCAR1/MCT1 signaling. Cell Signal. 2023;109:110791. https://doi.org/10.1016/j.cellsig.2023.110791
109. Xu B, Zhou L, Zhang Q. Curcumin inhibits the progression of non-small cell lung cancer by regulating DMRT3/SLC7A11 axis. Mol Biotechnol. 2025;67(5):1880-1892. https://doi.org/10.1007/s12033.024.01166-x
110. Li G, Fang S, Shao X, Li Y, Tong Q, Kong B, Chen L, Wang Y, Yang J, Yu H, Xie X, Zhang J. Curcumin reverses NNMT-induced 5-Fluorouracil resistance via increasing ROS and cell cycle arrest in colorectal cancer cells. Biomolecules. 2021;11(9):1295. https://doi.org/10.3390/biom11091295
111. Feng T, Zhou Y, Mao X, Rui X, Cai L. Curcumol enhances the sensitivity of gastric cancer to cisplatin resistance by inducing ferroptosis through the P62/KEAP1/NRF2 pathway. Integr Cancer Ther. 2024;23:153.473.54241294043. https://doi.org/10.1177/153.473.54241294043
112. Xu B, Zhu WJ, Peng YJ, Cheng SD. Curcumin reverses the sunitinib resistance in clear cell renal cell carcinoma (ccRCC) through the induction of ferroptosis via the ADAMTS18 gene. Transl Cancer Res. 2021;10(7):3158-3167. https://doi.org/10.21037/tcr-21-227
113. Ming T, Lei J, Peng Y, Wang M, Liang Y, Tang S, Tao Q, Wang M, Tang X, He Z, Liu X, Xu H. Curcumin suppresses colorectal cancer by induction of ferroptosis via regulation of p53 and solute carrier family 7 member 11/glutathione/glutathione peroxidase 4 signaling axis. Phytother Res. 2024;38(8):3954-3972. https://doi.org/10.1002/ptr.8258
114. Mokhtari Tabar MM, Ghasemian A, Kouhpayeh A, Behmard E. Computational discovery of novel GPX4 inhibitors from herbal sources as potential ferroptosis inducers in cancer therapy. Arch Biochem Biophys. 2025;764:110231. https://doi.org/10.1016/j.abb.2024.110231
115. Wu Z, Zhang G, Shang Y, Huang J, Liu Y, Zhou H, Wang T. New curcumin derivative induces ferroptosis in MCF-7 cells through activating SLC7A11/GPX4 axis. Bioorg Med Chem.2025;121:118078. https://doi.org/10.1016/j.bmc.2025.118078.
116. Wang J, Zhang Z, Li Q, Hu Z, Chen Y, Chen H, Cai W, Du Q, Zhang P, Xiong D, Ye S. Network pharmacology and molecular docking reveal the mechanisms of curcumin activity against esophageal squamous cell carcinoma. Front. Pharmacol.2024;15:1282361. https://doi.org/10.3389/fphar.2024.128.2361
117. Firouzjaei AA, Aghaee-Bakhtiari SH, Tafti A, Sharifi K, Abadi MHJN, Rezaei S, Mohammadi-Yeganeh S. Impact of curcumin on ferroptosis-related genes in colorectal cancer: Insights from in-silico and in-vitro studies. Cell Biochem Funct. 2023;41(8):1488-1502. https://doi.org/10.1002/cbf.3889
118. Li R, Zhang J, Zhou Y, Gao Q, Wang R, Fu Y, Zheng L, Yu H. Transcriptome Investigation and In Vitro Verification of Curcumin-Induced HO-1 as a Feature of Ferroptosis in Breast Cancer Cells. Oxid Med Cell Longev. 2020;2020:3469840. https://doi.org/10.1155/2020/3469840
119. Miyazaki K, Xu C, Shimada M, Goel A. Curcumin and Andrographis Exhibit Anti-Tumor Effects in Colorectal Cancer via Activation of Ferroptosis and Dual Suppression of Glutathione Peroxidase-4 and Ferroptosis Suppressor Protein-1. Pharmaceuticals (Basel). 2023;16(3):383. https://doi.org/10.3390/ph16030383
120. Li W, Li Y, Lin F, Guo H, Zhou H, Li H, Su H, Wang T. Hydroxytyrosol induced ferroptosis through Nrf2 signaling pathway in colorectal cancer cells. Sci Rep. 2025;15(1):21271. https://doi.org/10.1038/s41598.025.04415-4
121. Xiang L, Li Q, Guan Z, Wang G, Yu X, Zhang X, Zhang G, Hu J, Yang X, Li M, Bao X, Wang Y, Wang D. Oxyresveratrol as a novel ferroptosis inducer exhibits anticancer activity against breast cancer via the EGFR/PI3K/AKT/GPX4 signalling axis. Front. Pharmacol.2025;15:1527286. https://doi.org/10.3389/fphar.2024.152.7286
122. Yang C, Wang T, Zhao Y, Meng X, Ding W, Wang Q, Liu C, Deng H. Flavonoid 4,4'-dimethoxychalcone induced ferroptosis in cancer cells by synergistically activating Keap1/Nrf2/HMOX1 pathway and inhibiting FECH. Free Radic Biol Med. 2022;188:14-23. https://doi.org/10.1016/j.freeradbiomed.2022.06.010
123. Wen RJ, Dong X, Zhuang HW, Pang FX, Ding SC, Li N, Mai YX, Zhou ST, Wang JY, Zhang JF. Baicalin induces ferroptosis in osteosarcomas through a novel Nrf2/xCT/GPX4 regulatory axis. Phytomedicine. 2023;116:154881. https://doi.org/10.1016/j.phymed.2023.154881
124. Feng S, Zhou Y, Huang H, Lin Y, Zeng Y, Han S, Huang K, Liu Q, Zhu W, Yuan Z, Liang B. Nobiletin Induces Ferroptosis in Human Skin Melanoma Cells Through the GSK3β-Mediated Keap1/Nrf2/HO-1 Signalling Pathway. Front Genet. 2022;13:865073. https://doi.org/10.3389/fgene.2022.865073
125. Han S, Lin F, Qi Y, Liu C, Zhou L, Xia Y, Chen K, Xing J, Liu Z, Yu W, Zhang Y, Zhou X, Rao T, Cheng F. HO-1 Contributes to Luteolin-Triggered Ferroptosis in Clear Cell Renal Cell Carcinoma via Increasing the Labile Iron Pool and Promoting Lipid Peroxidation. Oxid Med Cell Longev. 2022;2022:3846217. https://doi.org/10.1155/2022/3846217
126. Niu L, Li Z, Fan W, Zhong X, Peng M, Liu Z. Nano-Strategies for Enhancing the Bioavailability of Tea Polyphenols: Preparation, Applications, and Challenges. Foods. 2022;11(3):387. https://doi.org/10.3390/foods11030387
127. Jia W, Zhou L, Li L, Zhou P, Shen Z. Nano-based drug delivery of polyphenolic compounds for cancer treatment: Progress, opportunities, and challenges. Pharmaceuticals (Basel). 2023;16(1):101. https://doi.org/10.3390/ph16010101
128. Yu X, Shang T, Zheng G, Yang H, Li Y, Cai Y, Xie G, Yang B. Metal-polyphenol-coordinated nanomedicines for Fe(II) catalyzed photoacoustic-imaging guided mild hyperthermia-assisted ferroustherapy against breast cancer. Chin Chem Lett. 2022;33(4):1895-1900. https://doi.org/10.1016/j.cclet.2021.10.021
129. Chen Y, Yang X, Li H, Wu X, Wu W, Chen J, Wu A, Wang X. Self-Assembled Fe-Phenolic Acid Network Synergizes with Ferroptosis to Enhance Tumor Nanotherapy. Small. 2024;20(36):e2402073. https://doi.org/10.1002/smll.202402073
130. Qin Y, Fan J, Zhang Y, Yang W, Cao J, Liu B, He Q. Natural Polyphenol–Metal Supramolecular Nanocomplex for Ferroptosis Activation in Chemoresistant Hepatocellular Carcinoma. Aggregate. 2025;6. https://doi.org/10.1002/agt2.70149
131. Wang M, Yu A, Han W, Chen J, Lu C, Tu X. Self-assembled metal-phenolic nanocomplexes comprised of green tea catechin for

tumor-specific ferroptosis. Mater Today Bio. 2024;26:101040. https://doi.org/10.1016/j.mtbio.2024.101040

132. Fan Y, Zhang X, Zhao J, Chen S, Liang J. Cancer cell membrane-camouflaged curcumin nanoparticles trigger ferroptosis for accurate gastric cancer therapy. Eur J Pharm Biopharm. 2024;204:114509. https://doi.org/10.1016/j.ejpb.2024.114509
133. Lei L, Yuan J, Yang Q, Tu Q, Yu H, Chu L, Tang L, Zhang C. Curcumin-polydopamine nanoparticles alleviate ferroptosis by iron chelation and inhibition of oxidative stress damage. RSC Adv. 2024;14(21):14934-14941. https://doi.org/10.1039/d4ra02336f
134. Jia M, Tan X, Yuan Z, Zhu W, Yan P. Nanoliposomes encapsulated rapamycin/resveratrol to induce apoptosis and ferroptosis for enhanced colorectal cancer therapy. J Pharm Sci. 2024;113:2565–74. https://doi.org/10.1016/j.xphs.2024.05.015
135. Fernández-Acosta R, Iriarte-Mesa C, Alvarez-Alminaque D, Hassannia B, Wiernicki B, Díaz-García AM, Vandenabeele P, Vanden Berghe T, Pardo Andreu GL. Novel iron oxide nanoparticles induce ferroptosis in a panel of cancer cell lines. Molecules. 2022; 27(13):3970. https://doi.org/10.3390/molecules27133970
136. Liu R, Rong G, Liu Y, Huang W, He D, Lu R. Delivery of apigenin-loaded magnetic Fe2O3/Fe3O4@mSiO2 nanocomposites to A549 cells and their antitumor mechanism. Mater Sci Eng C Mater Biol Appl. 2021;120:111719. https://doi.org/10.1016/j.msec.2020.111719
137. Chen R, Jiang Z, Cheng Y, Ye J, Li S, Xu Y, Ye Z, Shi Y, Ding J, Zhao Y, Zheng H, Wu F, Lin G, Xie C, Yao Q, Kou L. Multifunctional iron-apigenin nanocomplex conducting photothermal therapy and triggering augmented immune response for triple negative breast cancer. Int J Pharm. 2024;655:124016. https://doi.org/10.1016/j.ijpharm.2024.124016
138. Guo Y, Wang H, Wang X, Chen K, Feng L. Enhancing radiotherapy in triple-negative breast cancer with hesperetin-induced ferroptosis via AURKA targeting nanocomposites. J Nanobiotechnology. 2024;22(1):744. https://doi.org/10.1186/s12951.024.02987-3
139. Wang Q, He J, Qi Y, Ye Y, Ye J, Zhou M. Ultrasound-enhanced nano catalyst with ferroptosis-apoptosis combined anticancer strategy for metastatic uveal melanoma. Biomaterials. 2024;305:122458. https://doi.org/10.1016/j.biomaterials.2023.122458

Cite this article: Sahin T. Regulatory Effects of Plant-Derived Phenolic Compounds on Ferroptosis: A Novel Paradigm in Cancer Therapy. Pharmedicine J. 2026;3(1): 1-26. DOI: 10.62482/pmj.53

RESEARCH IN PHARMACY AND MEDICINE
PHARMEDICINE JOURNAL

2026; 3(1):27-36. doi: 10.62482/pmj.39

Original Article

Micellar Pseudo-Models for Biological Membranes: Spectrophotometric Analysis of Micellar Binding of Antiviral (Oseltamivir Phosphate) and Anticoagulant (Enoxaparin Sodium)

Seher Guclu[1,2], Sinem Gokturk[1]✉

[1] Marmara University, Faculty of Pharmacy, Department of Basic Pharmaceutical Sciences, General Chemistry Division, Istanbul, Türkiye
[2] Marmara University, Institute of Health Sciences, Pharmaceutical Basic Sciences, General Chemistry Msc Program, Istanbul, Türkiye

✉**Corresponding Author:** Sinem Gokturk (**E-mail:** sgokturk@marmara.edu.tr)

Received: 2025.10.07; **Revised:** 2025.11.06 **Accepted:** 2025.12.28 **Published:** 2026.02.28

Abstract

Introduction: The micellar environment formed by the aggregation of surfactants at a specific concentration, known as the critical micelle concentration (CMC), behaves like a simple biological system and is thus considered a pseudo-model of a biological system. Owing to these properties, which define them as mimetic systems, the microscopic environment created by surfactant micelles is similar to phospholipid membranes, allowing micelles to serve as models for biological membrane systems. Therefore, data on the binding of drugs to micelles is important as it can elucidate the drug's mechanism of action. Due to these interesting and unique physicochemical properties, surfactant micelles are widely used as a simple pseudo-model even for highly complex biomembranes. Therefore, this study aims to investigate the interactions of the antiviral drug Oseltamivir phosphate (OP) and the anticoagulant drug Enoxaparin sodium (ES) with different micellar systems.

Methods: The interactions of ES and OP with anionic, cationic, and nonionic surfactants were examined by the spectrophotometric method (UV-Vis), and their binding constants to micelles were calculated. Tween 20 (nonionic), sodium dodecyl sulfate (SDS) (anionic), and cetyltrimethylammonium bromide (CTAB) (cationic)-surfactants frequently used in pharmaceutical applications as models for mimetic systems-were selected for this study.

Results: The results of this study are expected to provide information about the behaviour of OP and ES in micellar systems that model biological membranes, as well as offer insight into the effectiveness of surfactants used in the improvement of drug formulations.

Conclusions: Given the importance of micellar systems in drug development, these results also offer practical insights for selecting the right pharmaceutical additives to create novel dissolving media for various applications.

Keywords: Drug-membrane interaction, enoxaparin sodium, oseltamivir phosphate, spectrophotometry (UV-Vis), surfactant micelles

1. Introduction

Effectively developed drug delivery systems are crucial for the production of pharmaceutical products that are both safe and effective. The strategic use of surfactants, or surface-active agents, which are amphiphilic molecules with both hydrophilic (loving water) and lipophilic (loving oil) regions, is at the fundamental basis of many of these formulations. They serve a role in drug formulation for processes including solubilization, emulsification, wetting, and improving bioavailability because of their special structure, which lowers surface and interfacial tension. Surfactants are frequently used to stabilize suspensions and emulsions, change the kinetics of drug release, and dissolve poorly water-soluble drugs. However, in a formulation, a drug rarely exists in isolation; it interacts chemically and physically with all excipients, including surfactants (1-7).

The resulting drug-surfactant interaction is a complex phenomenon that dictates the final properties, stability, and therapeutic performance of the pharmaceutical product. These interactions can manifest in various ways, from the partitioning of drug molecules into surfactant micelles to the formation of specific drug-surfactant complexes at interfaces or in bulk solution. Understanding the nature and magnitude of these interactions is crucial for drug development, as even a slight change in the surfactant-to-drug ratio or environmental conditions (e.g., pH, temperature) can significantly alter the drug's thermodynamic activity, solubility, and ultimately, its absorption profile in the body. Therefore, for ensuring the quality, effectiveness, and reproducibility of the pharmaceutical dosage forms, analytical studies and accurate data publishing relating to drug-surfactant physicochemical behaviour are still crucial. Furthermore, the significance of surfactants in the pharmaceutical industry is increased by the restricted water solubility of many active pharmaceutical ingredients (APIs). This is particularly important since a lot of biological activity takes place in the hydrophobic core of membranes or on their surfaces. Surfactants are active in a wide range of environments, including body fluids, bacterial cell surfaces, and animal cell membranes. Furthermore, surfactant micelles can form compartments with distinct properties (hydrophobic and hydrophilic), enabling the selective solubilization and transport of various substances within these compartments. This property makes them suitable for controlled drug transport and release (1,2).

Studies of the physical characteristics of molecules binding to membranes are simplified by surfactant micelles' amphiphilic nature, which enables the use of simple models that mimic biological membrane systems. Accordingly, the physicochemical interaction of a drug and a micelle is considered an approach to modelling the drug's interactions with biological surfaces (1,7-10).

This helps in understanding the more complex issue associated with drug transport across the cell membrane. Estimating the amount of drugs incorporated into membranes can be made possible by determining their binding constants, which relate to the basic molecular interaction between the drug and biological tissues. Based on this information, this study investigated the interactions of nonionic Tween 20, anionic sodium dodecyl sulfate (SDS), and cationic cetyl trimethylammonium bromide (CTAB) surfactant micelles-which were selected as mimetic models with different molecular structures and hydrophobic characteristics-with ES and OP. The present study attempted to identify how ES and OP interact with the examples of mimetic systems include anionic, nonionic, and cationic micelles of surfactants.

OP is an antiviral medication that inhibits the the ability of influenza virus to replicate within body cells by preventing the virus from chemically binding to its host. OP is an antiviral inhibitor that effectively and selectively inhibits the influenza virus's neuraminidase. The IUPAC name of OP is (3R,4R,5S) ethyl-4-acetamido-5-amino-3-(1-ethylpropoxy) phosphate carboxylate of cyclohexene (11). ES is the sodium salt of a heparin possessing a low molecular mass. ES is an anticoagulant that reduces the formation of blood clots. It is used to treat or prevent deep vein thrombosis (DVT), a kind of blood clot that can cause pulmonary embolism. The IUPAC name of ES is 6-[5-acetamido-4,6-dihydroxy-2-(sulfooxymethyl) oxan-3-yl]oxy-3-[5-(6-carboxy-4,5-dihydroxy-3-sulfooxyoxan-2-yl)oxy-6-(hydroxymethyl)-3-(sulfoamino)-4-sulfooxyoxan-2-yl]oxy-4-hydroxy-5-sulfooxyoxane-2-carboxylic acid (12-14).

The interactions were evaluated quantitatively and qualitatively using spectrophotometric

measurements. Based on absorbance and wavelength variations, the Benesi-Hildebrand Equation (15) was applied to determine the binding constants of both drugs to the micelles.

2. Methods

2.1. Materials

OP and ES were supplied by Atabay Kimya Company (Istanbul, Turkey). The chemical structures of surfactant micelles are given in Table 1.

Table 1. The molecular structures and CMC values of SDS, CTAB and Tween 20.

Surfactant	Molecular structure	CMC (mmol/L)
SDS $C_{12}H_{25}SO_4Na$	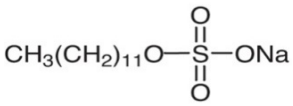	8.00
CTAB $C_{19}H_{42}BrN$	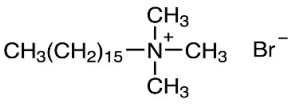	0.92
Tween 20 $C_{58}H_{113}O_{26}$	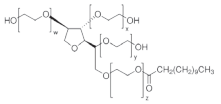	0.05

The SDS, CTAB, and Tween 20 used were obtained from Sigma Co. Doubly distilled, high-purity water was used to prepare the solutions. Fig 1 shows the molecular structures of OP and ES.

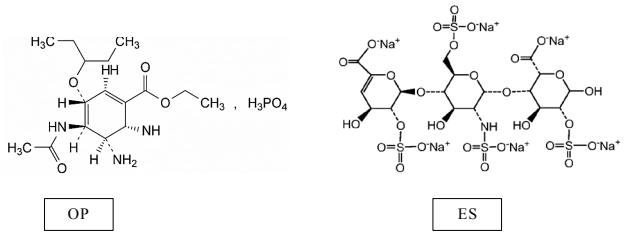

Figure 1. Molecular structures of OP and EP.

2.2. Method

The UV spectra of the fixed concentration of drugs (with and without surfactants) were recorded using a computer-connected Shimadzu UV-2100S double-beam UV-visible spectrophotometer. The instrument utilized a water-jacketed thermostatic cell holder and a matched pair of 1.0 cm path length cuvettes. All measurements were repeated at least three times, and the maximum wavelength (λ_{max}) showed excellent repeatability of ±0.1 nm. The spectrophotometric values reported here represent the mean of at least three measurements performed at 298 K. The relative Standard Deviation (SD) was consistently ≤ 1.1%.

2.3. Quantifying Binding Degree of Drugs using the Modified Benesi-Hildebrand Equation (KB)

The binding constant (K_B) was calculated to quantify the interaction (binding degree) of the drugs OP and ES with the surfactant micelles of SDS, CTAB and Tween 20. The K_B value that describes how a substance (likely a drug or molecule), interacts with micelles is calculated using the pseudophase model. The pseudophase model treats micelles and the surrounding water as distinct compartments or "pseudophases" where the drug molecule can reside. The equilibrium for drug binding to a micelle is represented as:

Drug (D) + Micelle (M) ⇆ D. M

An improved comparison of this interaction degree was obtained using a modified variation of the Benesi-Hildebrand equation (1), which is applicable at high surfactant concentrations (14).

$$\frac{1}{\Delta A} = \frac{1}{\Delta \varepsilon} + \frac{1}{K_B \left[C_M\right](\Delta \varepsilon)} \quad (1)$$

In this equation, $[C_M]$ is the concentrations of the drug and the micelle, where $[C_M]$ equals the total surfactant concentration minus the CMC (C_M= total surfactant concentration – CMC. The terms A and A_0 denote the drug absorbance in the presence and absence of surfactants ($\Delta A = A - A_0$), and $\Delta\epsilon$ is the difference in molar extinction coefficients ($\varepsilon_M - \varepsilon_0$) in the presence and absence of micelles. ε_M is the molar absorption coefficient of drugs when it is completely bound to the micelles. A linear plot of the of 1 /(ΔA) against $1/[C_M]$ confirms that this model and equation are applicable for determining K_B and ε_M. The linearity of the $1/\Delta A$ versus $1/[C_M]$ plot also confirmed that OP and ES binds to the micelles to form a 1:1 complex (8-10).

In this study, the CMC was determined by monitoring the change in the absorption spectrum upon the

interaction of OP and ES, which is indicative of micelle formation. Notably, the CMC values for ionic surfactants in the presence of fixed drug concentrations differed from their CMCs in pure water. However, no such change in the CMC was observed for the non-ionic surfactant, Tween 20.

3. Results

3.1. Micellar binding of OP

OP is a new ester prodrug and neuraminidase inhibitor used to treat influenza types A and B. Since oseltamivir's hydrophobic group causes poor oral absorption, the drug was developed as a phosphate salt to enable oral administration. OP is the salt form of oseltamivir, a small-molecule antiviral prodrug. Its ionization primarily depends on its basic functional group (the amine) and its acidic counterion (the phosphate). The active metabolite, oseltamivir carboxylate, also has a carboxylic acid group with an approximate pKa of 4.3, which significantly affects its properties. The pKa ≅ 7.9 is the most cited value for the amine group of the parent drug itself. In our experimental conditions, the medium pH is above 4.3, resulting in the existence of more stable OP cations. Depending on the concentration range, OP can be easily identified in pharmaceutical formulations at wavelengths of 208.5, 217, and 215 nm. OP, a cationic drug (chemical structure shown in Figure 1), exhibits the maximum absorption band at 209 nm. The absorption spectra for OP within the Lambert-Beer law's linear concentration range in an aqueous medium are plotted in Fig 2.

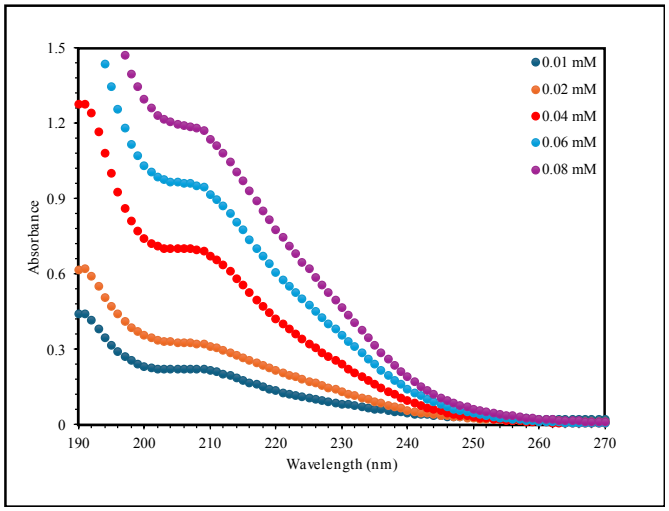

Figure 2. UV-Vis absorption spectra of OP in an aqueous medium at 298 K.

The change in absorbance of a fixed concentration (0.04 mM) of OP at 209 nm was monitored in the present study to analyse how OP interacts with varying concentrations of SDS, CTAB, and Tween 20 (both below and above their CMCs) at 298 K. Figures 3, 4, and 5 show the associated absorption spectra of OP in the presence and absence of CTAB, SDS, and Tween 20 micelles, respectively, to compare their impact on spectral behaviour of OP. In the presence of nonionic surfactant Tween 20, there was no spectral interaction observed with OP below the CMC. Conversely, when the surfactant concentration exceeded the CMC, all studied surfactants caused a progressive increase in absorbance. The only weak interaction observed was between OP and CTAB micelles, due to the electrostatic repulsion.

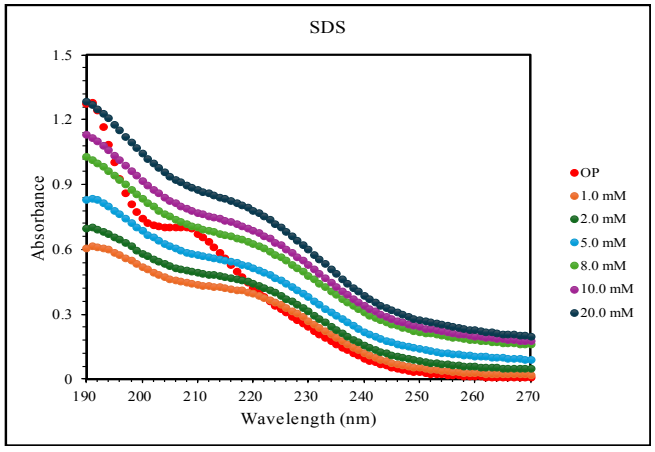

Figure 3. Absorption spectra of OP in various concentrations of SDS at 298 K.

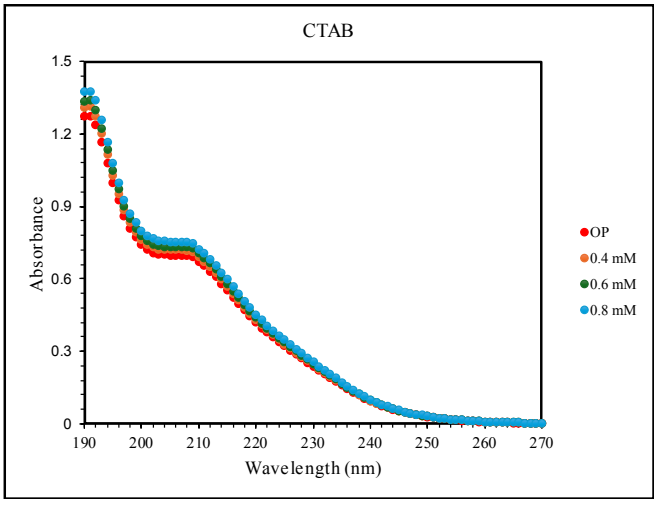

Figure 4. Absorption spectra of OP in various concentrations of CTAB at 298 K.

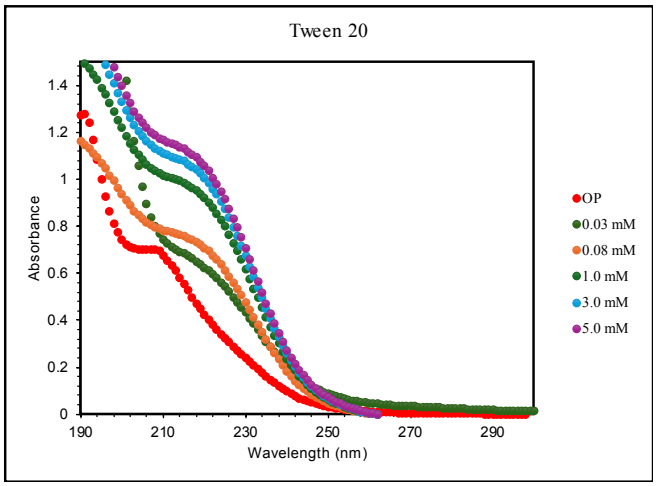

Figure 5. Absorption spectra of OP in various concentrations of Tween 20 at 298 K.

The variation of absorbance values of OP in the presence of Tween 20, CTAB, and SDS was illustrated in Figures 6 and 7. As shown in Fig 7, OP's absorbance dropped sharply as the SDS concentration increased up to 1.0 mM, although its spectral characteristics remained unchanged. This initial decrease in absorbance is evidence that a complex is forming between the OP and SDS molecules. The onset of micelle formation was detected by monitoring changes in the absorption spectrum of OP; this spectral shift served as the basis for determining the CMC in this study (9,16).

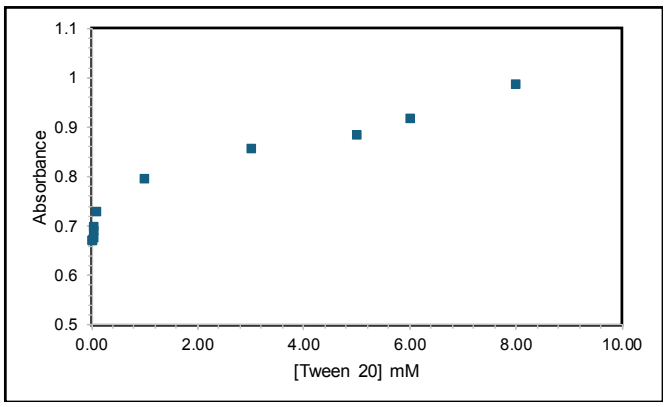

Figure 6. The absorbance change of 0.04 mM OP with the concentrations of Tween 20 at 298 K

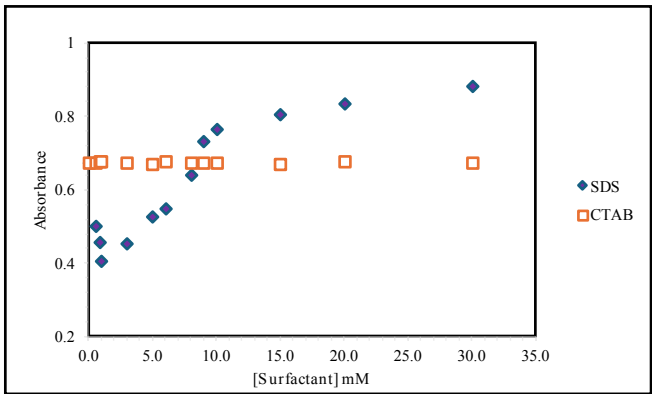

Figure 7. The absorbance changes of 0.04 mM OP with the concentrations of SDS and CTAB at 298 K.

The highly linear plots ($R^2 > 0.99$) of $1/\Delta A$ vs $1/C_M$ for all experiments confirmed that OP binds to the micelles in a 1:1 complex (Fig 8a and 8b). Binding constants (K_B) were calculated using equation (1) and are summarized in Table 2 along with their associated errors and correlation coefficients. Since OP and CTAB did not interact, it was not possible to calculate the binding constant. Overall, the spectral data showed that the affinity of the drug-micelle interaction varied among the surfactants, following the order: Tween 20 > SDS > CTAB.

Table 2. The CMC and calculated binding constants (KB) for the interaction of OP and ES with SDS, CTAB and Tween 20 micelles using UV-vis spectroscopy at 298 K.

	OP			ES		
Surfactant	**K_B (M^{-1})**	**CMC (mM)**	**CMC^{0*} (mM)**	**K_B (M^{-1})**	**CMC (mM)**	**CMC^{0*} (mM)**
Tween 20	1459.70	0.05	0.05	2034.71	0.05	0.05
SDS	89.08	1.0	8.0	-	-	8.0
CTAB	-	-	0.92	215.51	0.8	0.92

*Error limit in KB values is ± 5%. The correlation coefficients (R2) are 0.9988, 0.9987 for OP in the presence of SDS and Tween 20, respectively and 0.9938, 0.9958, for ES, in the presence of Tween 20 and CTAB, respectively. CMC0 values that are consistent with the literature obtained by conductometric measurement in water (17).

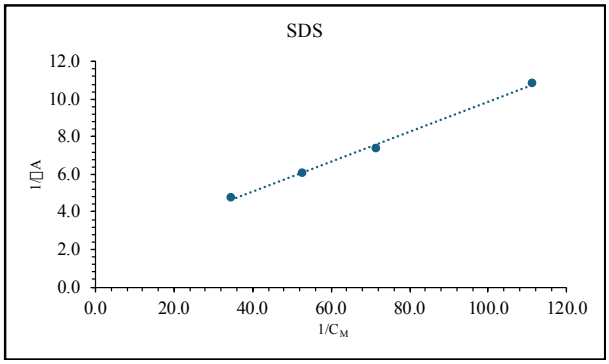

Figure 8a. Linearized Benesi-Hildebrand plot for the binding of OP (0.04 mM) to SDS micelles.

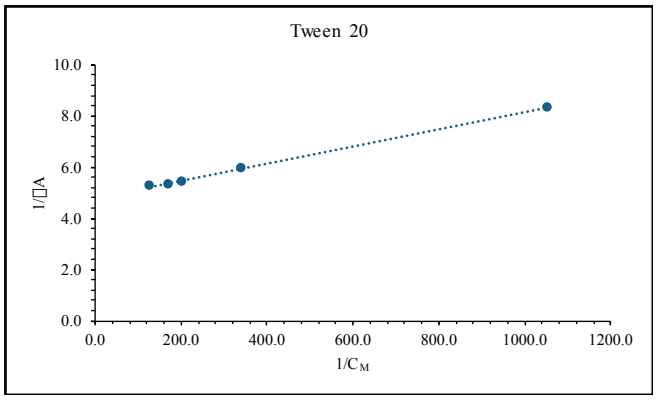

Figure 8b. Linearized Benesi-Hildebrand plot for the binding of OP (0.04 mM) to Tween 20 micelles.

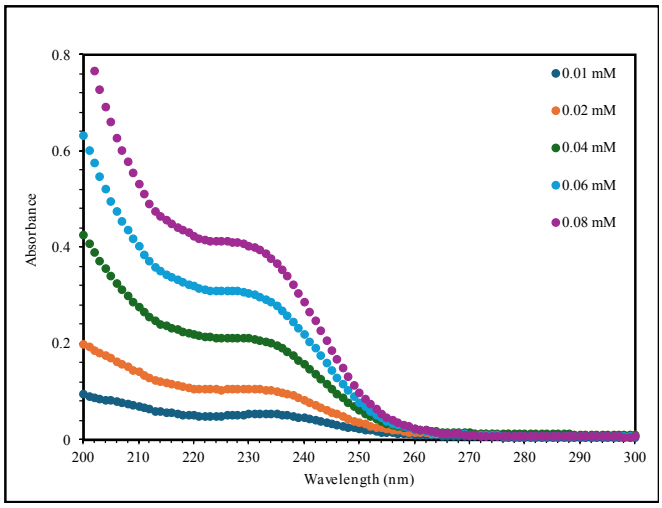

Figure 9. UV-Vis absorption spectra of ES in an aqueous medium at 298 K.

3.2. Micellar binding of ES

ES, chemically a white crystalline powder, exhibits practical solubility in water and free solubility in 0.1 N HCl. Clinically, it is preferred over unfractionated heparin due to its enhanced bioavailability and extended half-life, which enable a reduction in the frequency of subcutaneous administration (12-14). Due to its polymeric structure as a complex mixture of sulfated polysaccharide chains, it does not have a single, defined pKa value, but rather a distribution of values corresponding to its numerous functional groups. Enoxaparin is a strong polyacid, meaning it is highly ionized under almost all physiological conditions. Since ES is a polyanionic molecule, its activity is dependent on its high negative charge density, derived from functional groups that have very low pKa values. These groups are extremely acidic and are essentially fully ionized (as $R\text{-}OSO_3^-$) in aqueous solution across the entire physiological pH range. In our experimental conditions, the medium pH is approximately 5-6, resulting in the existence of more stable ES anions. Within the proper concentration range of the Lambert-Beer Law, the anionic drug ES, the molecular structure of which was shown in Fig 1, was examined in an aqueous medium. The maximum absorption of ES occurs at 230 nm, and the ES spectra of absorption are shown in Fig 9.

The interaction of a fixed concentration (0.04 mM) of the drug ES with SDS, CTAB, and Tween 20 at 298 K was studied by monitoring the change in the absorbance of ES at 230 nm with a wide range of surfactant concentrations both below and above their CMCs. The absorption spectra (Figures 10, 11, and 12) were used to compare the influence of surfactants on the spectral behaviour of ES. Below the CMC, no spectral interaction was observed between ES and the nonionic surfactant Tween 20. However, as the surfactant concentration exceeded the CMC, all three surfactants contributed to a gradual rise in ES absorbance, except for SDS, which showed a small increase. An exception was the weak interaction with SDS micelles, evidenced by a minimal change in absorbance and attributed to electrostatic repulsion. In contrast, a sharp initial drop in the absorbance of ES was seen with CTAB up to 0.8 mM (Fig 13), indicating the formation of an ES-CTAB complex without altering the spectral shape. The change in the absorption spectrum of ES was also used as the basis for determining the CMCs of the surfactants. The overall variation in ES's absorbance with each surfactant is detailed in Figures 13 and 14.

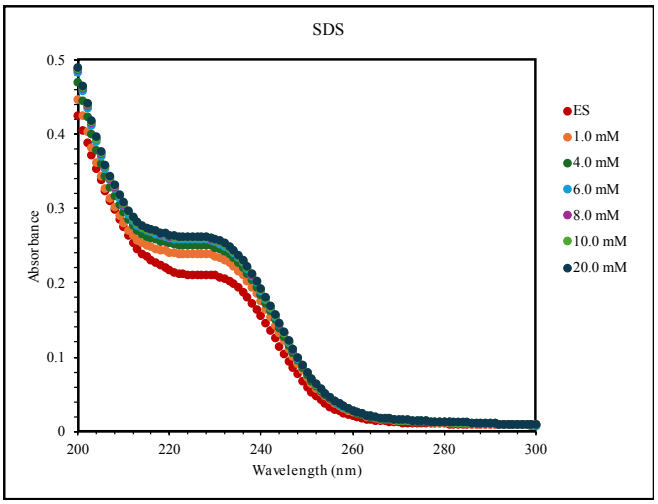

Figure 10. Absorption spectra of ES in various concentrations of SDS at 298 K.

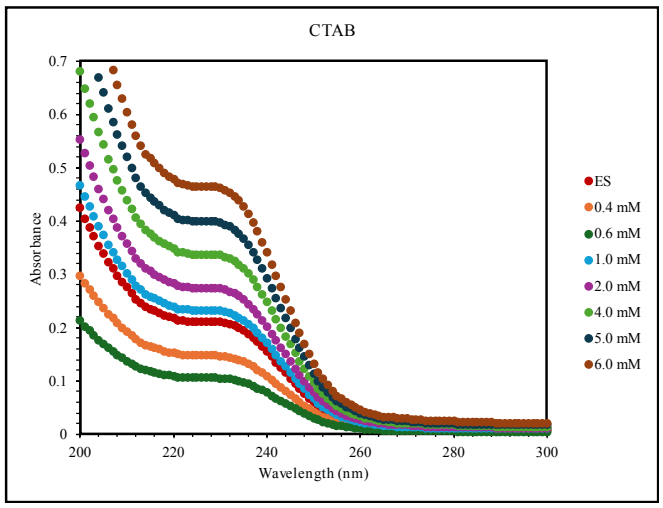

Figure 11. Absorption spectra of ES in various concentrations of CTAB at 298 K.

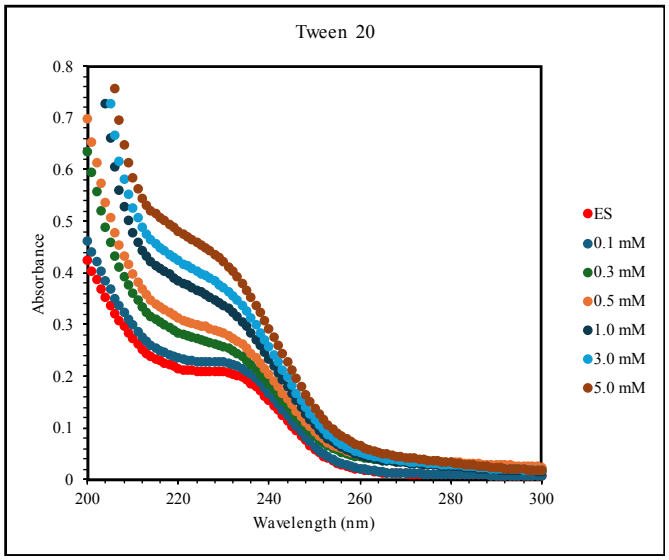

Figure 12. Absorption spectra of ES in various concentrations of Tween 20 at 298 K.

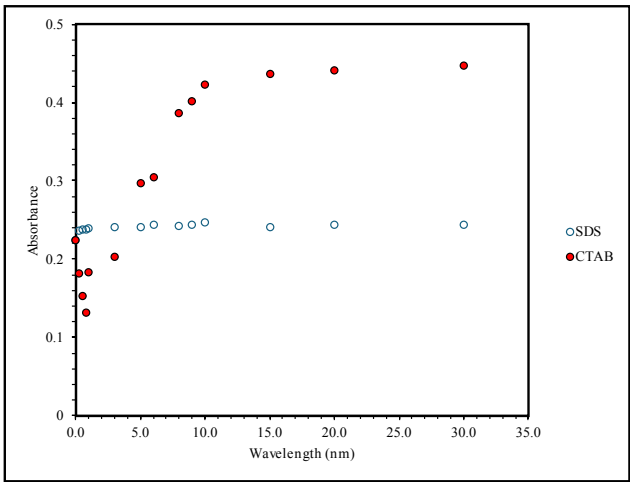

Figure 13. The absorbance changes of 0.04 mM ES with the concentrations of SDS and CTAB at 298 K.

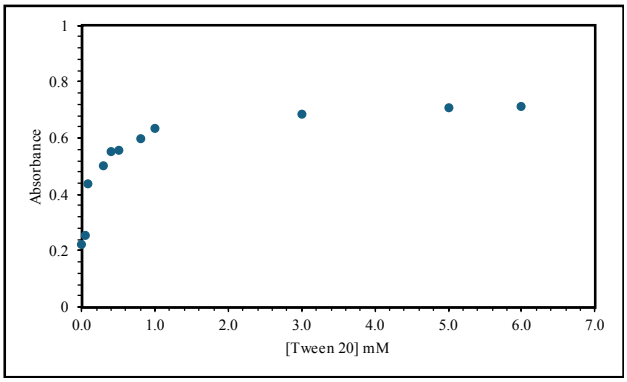

Figure 14. The absorbance changes of 0.04 mM ES with the concentrations of Tween 20 at 298 K.

Based on the highly linear plots ($R^2 > 0.999$) shown in Fig 15a and 15b, the binding of ES to the micelles occurs through a 1:1 complex. The calculated binding constants (K_B) (Table 2) showed that Tween 20 exhibited the strongest affinity, followed by CTAB. Conversely, the lack of interaction between ES and SDS due to the electrostatic repulsion meant its binding constant could not be determined, placing the overall affinity order at Tween 20 > CTAB > SDS.

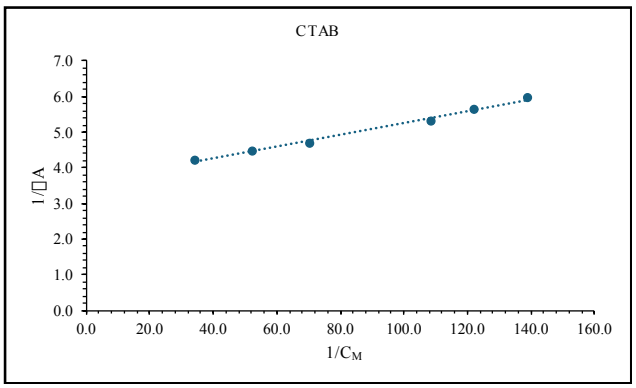

Figure 15a. Linearized Benesi-Hildebrand plot for the binding of ES (0.04 mM) to CTAB micelles.

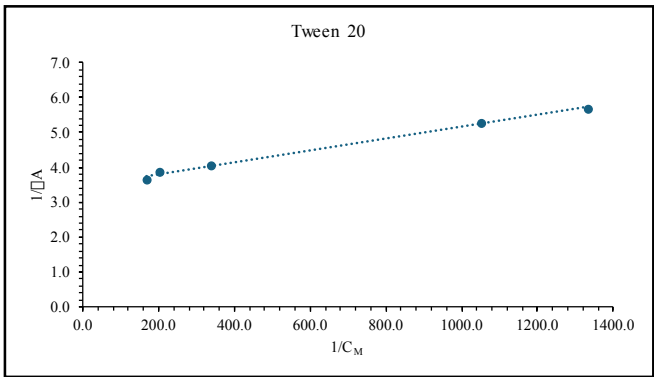

Figure 15b. Linearized Benesi-Hildebrand plot for the binding of ES (0.04 mM) to Tween 20 micelles.

4. Discussion

In the present study, to understand the *in vivo* behaviour of OP and ES, their interaction with different types of micelles was investigated. The results provide valuable information about the character and properties of the binding of the drugs to these structures, which serve as models for various biological components. Fig 16 illustrates the similarities between micelles and biological membranes, which are often referred to as mimetic systems. It can be clearly seen that there is a fundamental similarity between a spherical micelle and a flat lipid bilayer (biological membrane). Both systems self-assemble due to the hydrophobic effect, orienting their hydrophilic head groups toward the water and sequestering their hydrophobic tails away from the aqueous environment. This structural analogy allows micelles to function as mimetic systems for studying drug-membrane interactions and also acting as effective drug carriers.

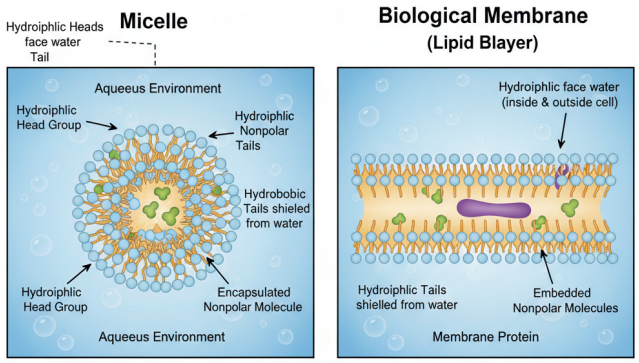

Figure 16. Micelles as mimetic drug delivery systems

In the present study, the observed spectral changes and increased absorbance above the CMC indicate that OP and ES successfully bind to the Tween 20, CTAB, and SDS micelles. Conversely, no binding was detected between the cationic OP and the cationic surfactant CTAB in the same way as anionic ES and anionic SDS. This lack of interaction may be attributed to electrostatic repulsion and inadequate hydrophobic attraction. It was hypothesized that the strongest interaction would occur between oppositely charged drugs and surfactants, given the presence of both electrostatic attraction and hydrophobic forces. This expectation aligns with the observed lack of interaction between ES-SDS and OP-CTAB micelles. Despite this, both ES and OP were found to bind more strongly to the nonionic micelles than to the ionic CTAB or SDS micelles. The superior binding strength is likely due to the nonionic micelles' aqueous polyoxyethylene oxide mantle, which provides a more accommodating environment for drugs compared to the anionic or cationic sites of ionic micelles. The observed variance in the binding constant is mainly a result of the distinctive micellar environments. Specifically, there is a correlation between the local polarity around the micelle and the ethylene oxide (EO) residues of nonionic surfactants, such that a decrease in polarity leads to an increase in the binding constant. The structure of a micelle is characterized by three zones: a nonpolar core of hydrocarbon tails, a Stern layer of head groups, and the diffuse Gouy–Chapman layer containing the majority of counterions. The binding location of the drug molecule is determined by the nature of both the drug and the micelle, resulting in localization within either the nonpolar core or the micelle–water interface. The fact that the maximum absorbance wavelengths of ES and OP don't significantly change upon the addition of surfactants indicates that both drugs are binding at the micelle-water interface (18-20). In this study, we also found that the presence of ES and OP consistently lowered the CMC for ionic surfactants. In case of SDS and CTAB micellar solutions, the addition of both ES and OP exhibited a neutral salt effect, effectively reducing the electrostatic repulsion among the charged head groups. Specifically, when added to ionic micelle solutions, ES and OP acted as a neutral salt, which reduced the electrostatic repulsion between the charged head groups

The chemical mechanisms driving the drug-micelle interactions are governed by a competition between electrostatic forces and hydrophobic partitioning, mediated by the structure of the micelle. In conclusion, the study of the binding affinity of ES and OP with structurally different surfactants (CTAB, SDS, and Tween 20) leads to the following points:

I. The Role of Electrostatic Repulsion

The most definitive mechanism observed is electrostatic repulsion, which prevents strong binding between identically charged components. The anionic drug (ES) exhibited no detectable binding with the anionic surfactant (SDS). The cationic drug (OP) exhibited no detectable binding with the cationic surfactant (CTAB). This lack of interaction confirms that simple electrostatic repulsion, combined with insufficient hydrophobic drive, governs when binding cannot occur.

II. The Superiority of Nonionic Binding

Despite the hypothesis that opposite charges should yield the strongest binding (due to electrostatic attraction), both the anionic (ES) and cationic (OP) drugs bound more strongly to the nonionic surfactant (Tween 20) than to the oppositely charged ionic micelles. The nonionic micelle's structure, specifically its aqueous polyoxyethylene oxide mantle, provides a highly accommodating environment for the drug molecules. This environment is chemically superior for partitioning compared to the more rigidly defined anionic or cationic surfaces of the ionic micelles. A decrease in the local polarity around the nonionic micelle's ethylene oxide (EO) residues directly correlates with an increase in the binding constant, indicating that the partitioning is highly dependent on localized polarity changes within the interface.

III. Binding Location

The exact location of drug incorporation is critical to the mechanism. The micelle structure is characterized by a nonpolar core, a Stern layer (head groups), and a diffuse Gouy–Chapman layer (counterions). The fact that the maximum absorbance wavelengths of ES and OP do not significantly change upon surfactant addition indicates that the drugs are not penetrating deep into the nonpolar core. Instead, both drugs are binding at the micelle-water interface, where they are influenced by both the hydrophobic tails and the surrounding aqueous environment.

5. Conclusion

This study employed spectrophotometric analysis to model the binding behaviour of antiviral (OP) and anticoagulant (ES) drugs with anionic (SDS), cationic (CTAB), and non-ionic (Tween 20) surfactant micelles, thereby simulating drug-membrane interactions at a molecular level. The overall strength of the drug-micelle interaction was found to be greater in nonionic micelles of Tween 20 than in ionic ones. This binding trend directly correlates with the hydrophobic character of the surfactants, i.e., the lower the CMC, the higher the hydrophobicity, confirming that hydrophobic interaction is crucial for the micellar binding, particularly as it enhances the binding constant (K_B) values of OP and ES in ionic and nonionic systems depending on the chemical structure of drugs. Given the importance of micellar systems in drug development, these results also offer practical insights for selecting the right pharmaceutical additives to create novel dissolving media for various applications. Furthermore, by modelling drug-membrane interactions, this study enhances understanding of the behaviour of ES and OP within biological organisms.

Conflicts of interest: The authors declare no conflicts of interest related to this work.

Funding: None

Ethics approval: Not applicable

Acknowledgment: The authors wish to express their gratitude to Atabay Kimya Sanayi ve Ticaret A.Ş. for generously providing the ES and OP drugs.

Author contributions: Study conception and design: Gokturk S and Guclu S; Data collection: Guclu S; Data analysis: Gokturk S; Manuscript draft preparation: Gokturk S; Writing – review & editing: Gokturk S and Guclu S. All authors reviewed the results and approved the final version of the manuscript.

References

1. Pokhrel DR, Sah MK, Gautam B, Basak HK, Bhattarai A, Chatterjee A. A recent overview of surfactant–drug interactions and their importance. *RSC Adv*. 2023;13:17685-17704. https://doi.org/10.1039/D3RA02883F.
2. Hou L, Wu B, Han Y, Qi H. Synergistic effects of an amphiphilic drug (propranolol hydrochloride) with cationic surfactants in an aqueous medium: A physicochemical study. J Mol Liq. 2024; 408:125327. https://doi.org/10.1016/j.molliq.2024.125327.
3. Hanif S, Usman M, Hussain A, Rasool N, Khan A, Jamal MA, Elgorban AM, Ali Rana U. Spectroscopic study of benzothiophene partitioning in sodium dodecyl sulfate and cetyl trimethyl ammonium bromide micellar media. J Surfact Deterg. 2016;19(5):1033-41. https://doi.org/10.1007/s11743.016.1852-5.
4. Elworthy PH, Florence AT, Macfarlene CB. Solubilization by surface-active agents. New York: Chapman and Hall Ltd; 1968.
5. Urmila S, De R, Das B. Interactions between loaded drugs and surfactant molecules in micellar drug delivery systems: A critical review. J Mol Liq. 2023;121906. https://doi.org/10.1016/j.molliq.2023.121906.
6. Agatić ZF, Tepavčević V, Puača G, Poša M. Interaction of drug molecules with surfactants below (Benesi-Hildebrand equation) and above the critical micelle concentration (Kawamura equation). Int J Pharm. 2024;665:124675. https://doi.org/10.1016/j.ijpharm.2024.124675.
7. Gokturk S, Toprak C. Solubilization of Insoluble and Poorly-Water Soluble Drugs in Micellar Systems. Pharmedicine J. 2024;1(2):74-84. https://doi.org/10.62482/pmj.9.
8. Gokturk S, Caliskan E, Talman RY, Var U. A study on solubilization of poorly soluble drugs by cyclodextrins and micelles: complexation and binding characteristics of sulfamethoxazole and trimethoprim. Sci. World J. 2012;2012:718791. https://doi.org/10.1100/2012/718791.
9. Gokturk S, Aslan S. Study on binding properties of poorly soluble drug trimethoprim in anionic micellar solutions. J Dispers Sci Technol. 2014;35(1):84-92. https://doi.org/10.1080/01932.691.2013.775583.
10. Gokturk S, Tamer ZB. Interactions and solubilization of poorly soluble drugs in aerosol-OT micelles. J Surfact Deterg. 2018 Sep;21(5):889-98. https://doi.org/10.1002/jsde.12192.
11. Bano T, Yadav G, Dudhe R. Development and validation of Oseltamivir Phosphate API by UV-Spectrophotometer. Glob J Pharmacol. 2013;7(3):294-297.
12. Prasanthi C, Gundala A. Development and validation of UV spectrometric method for quantitative determination of Enoxaparin Sodium in bulk and injectable. World J Pharm Res. 2017;6(16):1517-1523.
13. Hofmann T. Clinical application of enoxaparin. Expert Rev Cardiovasc Ther. 2004;2(3):321–7. https://doi.org/10.1586/14779072.2.3.321.
14. Iqbal Z, Cohen M. Enoxaparin: a pharmacologic and clinical review. Expert Opin Pharmacother. 2011;12(7):1157-1170. https://doi.org/10.1517/14656.566.2011.570261.
15. Benesi HA, Hildebrand JH. A spectrophotometric investigation of the interaction of iodine with aromatic hydrocarbons. J Am Chem Soc. 1949;71(8):2703-2707. https://doi.org/10.1021/ja01176a030.
16. Erdinc N, Gokturk S, Tuncay M. Interaction of epirubicin HCl with surfactants: effect of NaCl and glucose. J Pharm Sci. 2004;93(6):1566-1576. https://doi.org/10.1002/jps.20056.
17. Rosen MJ. Surfactants and interfacial phenomena. 2nd ed. New York: John Wiley & Sons; 1989.
18. Gokturk S, Var U. Effect of pharmaceutically important cosolvents on the interaction of promethazine and trifluopromazine hydrochloride with sodium dodecyl sulfate micelles. J Dispers Sci Technol. 2012;33(4):527-535. https://doi.org/10.1080/01932.691.2011.574934.
19. **Čudina O, Brborić J, Janković I, Karljiković-Rajić K, Vladimirov S. Study of valsartan interaction with micelles as a model system for biomembranes. Colloids** Surf B Biointerfaces. 2008;65(1):80-84. https://doi.org/10.1016/j.colsurfb.2008.03.002.
20. Enache M, Volanschi E. Spectral studies on the molecular interaction of anticancer drug mitoxantrone with CTAB micelles. J Pharm Sci. 2011;100(2):558-65. https://doi.org/10.1002/jps.22289.

Cite this article: Guclu S, Gokturk S. Micellar Pseudo-Models for Biological Membranes: Spectrophotometric Analysis of Micellar Binding of Antiviral (Oseltamivir Phosphate) and Anticoagulant (Enoxaparin Sodium). Pharmedicine J. 2026;3(1):27-36. DOI: 10.62482/pmj.39

RESEARCH IN PHARMACY AND MEDICINE
PHARMEDICINE JOURNAL

2026; 3(1):37-44. doi: 10.62482/pmj.41

Original Article

Therapeutic Properties of Alpha Lipoic Acid and Quercetin on Methotrexate-Induced Oxidative Stress in Rat Liver

Seyma Savas[1], Esin Ak[2], Sarfraz Ahmad[3], Sehkar Oktay[4]

[1] Marmara University, Institute of Health Sciences, Istanbul, Türkiye
[2] Marmara University, Faculty of Dentistry, Department of Basic Medical Sciences, Histology and Embryology, Istanbul, Türkiye
[3] Gynecologic Oncology Program, AdventHealth Cancer Institute, Orlando, USA
[4] Marmara University, Faculty of Dentistry, Department of Basic Medical Sciences, Biochemistry, Istanbul, Türkiye

✉**Corresponding Author:** Seyma Savas (**E-mail:** seyma.savas@gmail.com)

Received: 2025.10.28; **Revised:** 2026.01.20 **Accepted:** 2026.01.22 **Published:** 2026.02.28

Abstract

Introduction: Methotrexate (MTX), is a widely used drug however it can cause tissue toxicity; but the concurrent use of antioxidants may help reduce this damage. This study investigates the therapeutic properties of alpha-lipoic acid (α-LA) and Quercetin (Que) on MTX-induced oxidative stress in the rat liver.

Methods: The experimental groups were designed as: C: Control, MT: MTX-given group (20 mg/kg, i.p. single dose), MT+α-LA: MTX+α-LA given group (20 mg/kg, i.p. for 5 days), and MT+Q: MTX+Que given group (20 mg/kg, i.p. for 5 days). Liver tissues were analyzed using biochemical, histopathological, and electrophoretic mobility shift assays.

Results: There was a significant increase in lipid peroxidation (LPO) and nitric oxide levels (NO) and a decrease in glutathione (GSH) levels, superoxide dismutase (SOD), catalase (CAT), and glutathione-S-transferase activities in the MT group compared to the control. MTX caused a significant increase in alkaline phosphatase (ALP) and sialic acid (SA) levels and decreased boron level and tissue factor activity. Biochemical results related to hepatotoxicity were also correlated with the histological examinations. Administration of α-LA and Que regulated LPO, GSH, ALP, SA, and boron levels, as well as SOD and CAT activities. Besides, Que was found to be more effective at restoring these values to normal levels.

Conclusions: The results suggest that α-LA and, in particular, Que may help alleviate MTX-induced liver damage.

Keywords: Alpha lipoic acid, methotrexate, oxidative stress, rat; quercetin;

1. Introduction

Methotrexate (MTX), a folate antimetabolite, is widely utilized in the treatment of various immune-mediated and neoplastic disorders (1). It is clinically employed to manage chronic inflammatory diseases, such as rheumatoid arthritis and psoriasis, and the treatment of certain malignancies, including osteosarcoma (2). The primary mechanism of MTX in oncology is the inhibition of dihydrofolate reductase, which blocks the intracellular production of reduced tetrahydrofolate (3). This suppression limits the synthesis of thymidylate and certain amino acids, thereby inhibiting DNA synthesis and cell proliferation. Additionally, MTX inhibits thymidylate synthase, an enzyme essential for the formation of deoxythymidine monophosphate (dTMP). The disruption of these pathways by MTX impairs the synthesis of DNA, RNA, and ATP, ultimately halting cellular replication (4).

Folate deficiency induced by MTX impacts mitochondrial function because mitochondria require folate for various processes and results in cellular dysfunction that increases the generation of reactive oxygen species (ROS) due to impaired antioxidant defense mechanisms and mitochondrial dysfunction. Besides, MTX inhibits the deamination pathway of adenosine and adenosine monophosphate. Thus, increased extracellular adenosine levels result from low-dose MTX's anti-inflammatory and immunosuppressant effects (3,4). Moreover, MTX causes various toxicological side effects, such as teratogenicity, infertility, and neurotoxicity by forming ROS that damage cell components. Depletion of folate, which causes disturbances in the metabolism of purine and pyrimidine bases, is thought to cause liver damage (5).

Alpha lipoic acid (α-LA), or thioctic acid, is produced in the mitochondria in all prokaryotic and eukaryotic cells. It is mainly found in the heart, kidney, and liver in animal tissues; it is also found in tomatoes, spinach, and broccoli in plants, thus, it can be used as a food supplement. Dihydrolipoic acid, the reduced form of α-LA, repairs functional parts of the cell, such as proteins and lipids, protects DNA from damage in oxidative reactions, and acts as a cofactor for various enzymes in the antioxidant defense system and as a chelating agent for heavy metals (6). Alpha-LA is indicated for the amelioration of complications of several neurological disorders, including diabetic neuropathy and Alzheimer's disease (7).

Quercetin (Que), the most abundant flavonoid in the Mediterranean diet, is found in many seeds, vegetables, and fruits. Que prevents cell death and oxidative damage by scavenging oxygen radicals and chelating metal ions to protect against lipid peroxidation. In addition to its therapeutic activities, Que stimulates mitochondrial biogenesis and inhibits lipid peroxidation (8).

The liver is an organ that performs various tasks in maintaining life. It has many vital functions, such as detoxification, defence against infections, control of energy sources, and production of some proteins. Since MTX is primarily metabolized in the liver by enzymes like dihydrofolate reductase and glutamate hydrolase, the metabolic products of MTX can be toxic to hepatocytes, leading to liver injury. While several studies have examined the effects of antioxidants in conjunction with MTX therapy, there is a relative lack of comparative studies evaluating the differences in their protective effects. Therefore, this study examines the potential protective and therapeutic role of α-LA and Que on MTX-induced liver damage in rats.

2. Methods

2.1. Drugs and Chemicals

MTX (50 mg/5 mL) was obtained from Koçak Farma Pharmaceutical and Chemical Co. (Istanbul, Turkey), and α-lipoic acid (Catalog Number: 1077-28-7) and quercetin (Catalog Number:117-39-5) were obtained from Sigma-Aldrich Chemical Company (St. Louis, MO, USA). All other chemicals and solvents used were of best available analytical grades.

2.2. Animals and Ethics Statement

Approval of the study was granted by the Marmara University Animal Care and Use Committee (71.2015.mar). Adult male Wistar albino rats (200-250 g) were purchased from Aziz Sancar Experimental Medicine Research Institute, Istanbul University, Istanbul, Turkiye.

This study used four animal groups, six rats for each group as follows: i) C: the control group, received only physiological saline, ii) intraperitoneal (i.p.) MT: injected MTX (20 mg/kg body weight, i.p. single dose), iii) MT+ α-LA: injected α-LA (20 mg/kg body weight, i.p. for five days) after MTX (20 mg/kg body weight i.p. injection), and iv) MT+Q: injected Que (20 mg/kg body weight i.p. for five days) after MTX (20 mg/kg body weight i.p. injection). On day 6th, rats were sacrificed under anesthesia, liver tissues were resected and divided into two parts – the left half of the liver tissues were taken for histopathological analysis, and the right half of the tissues were taken and stored at – 20°C until the day of the experiment for biochemical analyses.

2.3. Biochemical Analysis

Liver homogenates [10% (w/v)] were prepared with physiological saline (0.9% g NaCl) solution for the biochemical analysis. Total protein level and the parameters investigate oxidative stress; lipid peroxidation (LPO) and nitric oxide (NO), antioxidant parameters; glutathione (GSH), superoxide dismutase (SOD), catalase (CAT), glutathione-S-transferase (GST), and structural and functional parameters; alkaline phosphatase (ALP), sialic acid (SA), boron and tissue factor (TF) were measured spectrophotometrically, also electrophoretic mobility shift assays were done in the liver according to the methods described previously (9).

2.4. Histopathologic Analysis

For light microscopic investigation, liver tissue samples taken from the experimental animals were fixed in 10% neutral buffered formaldehyde at room temperature. The tissues were dehydrated by ascending alcohol series (70%, 90%, 96%, and 100%), cleared in toluene, kept in paraffin in an oven at 60°C, and embedded in paraffin blocks at room temperature. Following the staining of the approximately 5 µm thick paraffin section with hematoxylin and eosin (H&E), they were examined and photographed with a microscope (ZEISS-Axio Scope A, Göttingen, Germany) attached camera (ZEISS Axiocam 105 color, Göttingen, Germany). For histopathological analysis, each section was evaluated by the following criteria: i) vacuolization of hepatocytes and pyknotic nucleus, ii) vascular congestion and dilatation of sinusoids, and iii) activation of the Kupffer cells and inflammatory cell infiltration. Each criterion was scored using the semiquantitative scale as follows: 0 (none), 1 (mild), 2 (moderate), and 3 (severe).

2.5. Statistical Analysis

GraphPad Prism 9.0 (GraphPad Software, San Diego, CA, USA) program was used for statistical analysis. The one-way ANOVA method and Tukey test were used to compare the mean of more than two groups and to interpret the differences between subgroups in the variables with a difference. P value <0.05 was considered significant.

3. Results

3.1. Effects of MTX, α-LA, and Que administration on hepatic oxidative stress markers

The effects of MTX, α-LA, and Que on hepatic ROS generation were investigated by evaluating the levels of LPO and NO (Table 1). Administration of MTX significantly elevated LPO and NO levels than group C ($p<0.01$). Both α-LA and Que reduced LPO levels compared to the ($p<0.01$). Administration of α-LA decreased the NO level significantly compared to the MT group ($p<0.05$). Although a slight decrease was observed in NO level after Que administration to the MT group, the result was insignificant ($p>0.05$).

Table 1. Comparison of LPO and NO values in liver tissues between the experimental groups.

Experimental Groups (n=6)	LPO (nmoL MDA/mg protein)	NO (nmoL MDA/mg protein)
C	5.94±0.57	15.34±2.04
MT	10.31±0.56**	21.34±1.8**
MT+α	7.17±1.48$^{\alpha\alpha}$	19.05±1.18$^{\alpha}$
MT+Q	6.3±1.76$^{\alpha\alpha}$	19.72±0.68

n: number of animals. Values are given as mean ± standard deviation. LPO: Lipid peroxidation, NO: Nitric oxide, C: Control group, MT; Methotrexate group, MT+α-LA: Alpha lipoic acid given methotrexate group, MT+Q: Quercetin given methotrexate group. **$p<0.01$ compared to the group C, $^{\alpha}p<0.05$, $^{\alpha\alpha}p<0.01$ compared to the MT group.

3.2. Effects of MTX, α-LA, and Que on hepatic antioxidant markers

As shown in Table 2, the GSH level and activities of SOD, CAT, and GST were decreased significantly in the MT group than the group C ($p<0.05$). GSH level and, SOD and CAT activities increased significantly in the MT+α-LA group compared to the MT group ($p<0.05$). Besides, Que was also effective in elevating hepatic GSH levels and SOD and CAT activities compared to the MT group ($p<0.05$) (Table 2). Neither α-LA nor Que changed GST activity ($p>0.05$).

Table 2. Comparison of GSH, SOD, CAT, and GST values in liver tissues between the experimental groups.

Experimental Groups (n=6)	GSH (mg/g protein)	SOD (U/mg protein)	CAT (U/mg protein)	GST (U/g protein)
C	4.03±0.16	1.14±0.39	92.62±2.97	94.42±7.7
MT	2.06±0.65**	0.63±0.16*	77.06±6.53**	78.38±8.31*
MT+α	3.04±0.41α	1.10±0.23αα	84.76±3.14α	80.88±6.38
MT+Q	3.16±0.64α	1.11±0.25αα	85.88±3.82α	85.86±4.53

n: number of animals. Values are given as mean ± standard deviation. GSH: Glutathione, SOD: Superoxide dismutase, CAT: Catalase, GST: Glutathione-S-transferase, C: Control group, MT; Methotrexate group, MT+α-LA: Alpha lipoic acid given methotrexate group, MT+Q: Quercetin given methotrexate group. *p<0.05, **p<0.01 compared to the group C, αp<0.05 compared to the MT group.

3.3. Effects of MTX, α-LA, and Que on Hepatic Structural and Functional Markers

The effect of MTX, α-LA, and Que administration on ALP, SA, and boron values and TF activities in liver tissue is shown in Table 3. MTX caused an increase in ALP and SA levels compared to the group C ($p<0.05$). Que decreased ALP and SA levels significantly compared to the MT group ($p<0.05$); however, the decrease with α-LA administration was insignificant. Hepatic boron levels reduced significantly in the MT group, and Que elevated the results significantly ($p<0.05$). Prolonging the time in TF activity means that the activity decreases. TF activity of the MT group reduced significantly than group C ($p<0.05$).

Table 3. Comparison of ALP, SA, Boron and TF values in liver tissues between the experimental groups.

Experimental Groups (n=6)	ALP (U/mg protein)	SA (mg/g protein)	Boron (ppm)	TF activity (second)
C	261.5±16.84	6.06±0.42	2.79±0.48	74.83±7.46
MT	300.8±19.73*	7.23±0.43**	1.32±0.74**	85.83±3.06*
MT+α	281.2±11.75	6.28±0.9	2.2±0.56	78.33±10.07
MT+Q	273±8.36α	6.04±1.11α	2.4±0.62α	85.0±5.72

n: number of animals. Values are given as mean ± standard deviation. ALP: Alkaline phosphatase, SA: Sialic acid, TF: Tissue factor, C: Control group, MT; Methotrexate group, MT+α-LA: Alpha lipoic acid given methotrexate group, MT+Q: Quercetin given methotrexate group. *p<0.05, **p<0.01 compared to the group C, αp<0.05 compared to the MT group.

3.4. SDS-polyacrylamide Gel Electrophoresis Results

The liver samples analyzed through SDS-PAGE showed protein bands at the same position for all samples, with molecular weights ranging from 21 to 136 kD. When assessed through the Image J program, some unsignificant differences in the densities of the protein bands were detected in the electrophoretic examination of the groups. The MT group showed an increase in the band density of the protein with a molecular weight of 117, 110, 84, 78, 38, and 24 kD than those of the group C, and a decrease was observed in these bands in the MT+α-LA and MT+Q groups compared to the MT group (Fig. 1).

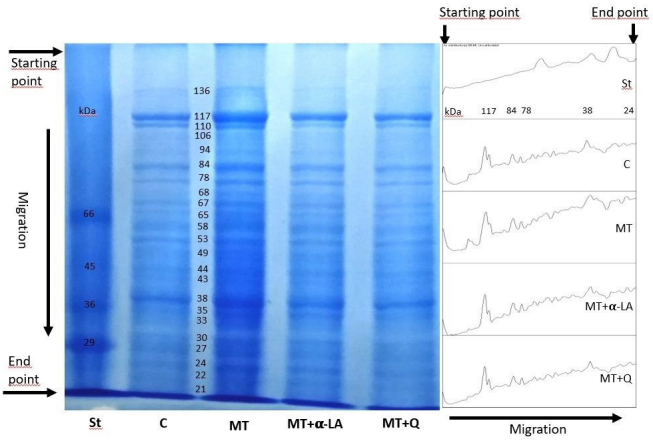

Figure 1. SDS-PAGE patterns of liver tissue protein of the groups. St: Standard protein mixture (bovine albumin:66 kD; egg albumin: 45 kD; glyceraldehyde-3-phosphate: rabbit muscle, 36 kD and bovine carbonic anhydrase: 29 kD); MW: Molecular weight: C: Control group, MT; Methotrexate group, MT+α-LA: Alpha lipoic acid given methotrexate group, MT+Q: Quercetin given methotrexate group.

3.5. Histological Results

A normal morphology of liver parenchyma with regular hepatocytes and sinusoids was seen in the group C (Fig. 2A). In the MT group, severe degeneration of hepatocytes with cytoplasmic vacuolization and pyknotic nucleus, sinusoidal dilatation and congestion, inflammatory cell infiltration, and increased activated Kupffer cells were observed (Fig. 2B). On the other hand, all

these histological alterations were decreased in the liver parenchyma of the MT+α-LA and MT+Q groups compared to the MT group (Figure 2C, D). The histopathologic score of the MT group was significantly higher than the C group ($p<0.01$). On the other hand, the histopathological scores of the MT+α-LA and MT+Q groups were significantly lower compared to the MT group ($p<0.01$). There was no statistically significant difference between the histopathological score of the MT+α-LA group and the MT+Q group (Fig. 2E).

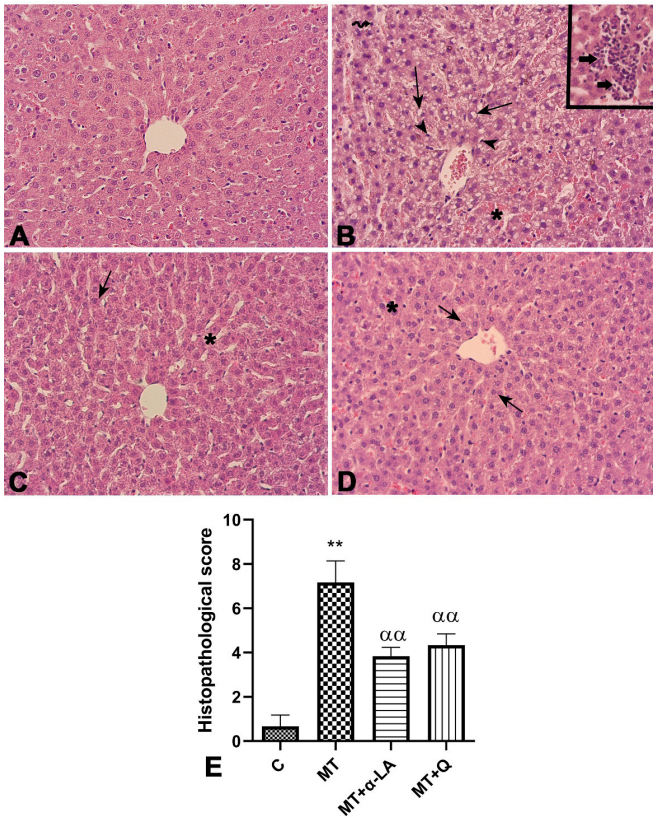

Figure 2. Representative light micrographs (A-D) and the graph of the histopathologic score (E) of the liver in the experimental groups. A: Normal liver parenchyma with hepatocytes and sinusoids was seen in the control group. B: Degenerated hepatocytes with cytoplasmic vacuolization (arrows), pyknotic nucleus (broken arrow), marked sinusoidal dilatation and congestion (asterisk), and Kupffer cells (arrowheads), and inflammatory cells (thick arrow-inset) were seen in the MT group. C: Besides hepatocytes with normal morphology (arrows) in many areas, degenerated hepatocytes and mild sinusoidal dilatation (asterisk) were observed in the MT+α-LA group. D: Besides hepatocytes with normal morphology (arrows) in many areas, degenerated hepatocytes and mild sinusoidal congestion (asterisk) were observed in the MT+Q group. Original magnification: x200, H&E stain. E: **$p<0.01$ compared to the C group, αα$p<0.001$ compared to the MT group. C: Control group, MT; Methotrexate group, MT+α-LA: Alpha lipoic acid given methotrexate group, MT+Q: Quercetin given methotrexate group

4. Discussion

Chemotherapeutic drugs show their anticancer effects by disrupting tumor cells' structures or metabolic pathways. However, they cannot be used selectively against cancer cells and can cause potentially serious side effects at therapeutic doses. The group of antimetabolites, including the frequently used MTX, is also among the treatments that cause serious side effects (2,10). MTX can cause a wide variety of toxicological effects, biochemical dysfunctions, and severe changes in enzyme levels and cellular structures-functions. It is known that MTX is converted to 7-hydroxymethotrexate in the liver, its extracellular metabolite, and stored as its polyglutamated form. However, long-term use of MTX can cause the accumulation of MTX polyglutamates, which MTX hepatotoxicity (2).

According to peer-reviewed studies conducted to understand the MTX-related liver toxicity, it is thought to develop due to oxidative stress (11). Excessive free radicals resulting from oxidative stress overwhelm the body's defence system and disrupt metabolism, and the reason behind the damage is the loss of antioxidant molecules. This situation can result in increased production of reactive substances, such as MDA (a reactive substance of LPO), and NO (a gas-formed free radical in the cell), resulting in hepatotoxicity and tissue damage. Mitochondrial dysfunction and concomitant ROS generation have been proven to mediate autophagic cell death (5).

MTX also can reduce the antioxidant levels, which in turn lowers the effectiveness of the body's natural defense system against ROS. GSH plays a crucial role in maintaining cell integrity, while SOD, CAT, and GST are antioxidants that are effective in detoxification. These antioxidants are essential for protecting the cell against oxidative stress. According to previous studies (5,12,13), MTX administration causes elevated MDA and NO levels. Besides, it was determined that GSH levels and antioxidant enzymes, such as SOD and CAT decreased significantly following MTX intoxication

(14). In a related study (15), GST and CAT activities in the MTX-induced damage group were found to be decreased. It was concluded that MTX administration triggers ROS production, thereby increasing oxidants and reducing antioxidants (16). Consistent with previous findings, our study showed that LPO levels (an indicator of ROS generation) increased significantly in the MTX-treated group compared to Group C; conversely, GSH levels, as well as CAT, GST, and SOD activities, were significantly reduced. According to these results, MTX-induced damage appears to occur through two primary mechanisms: direct cellular toxicity and increased ROS production. Furthermore, MTX inhibits several antioxidant enzymes, thereby elevating LPO levels and exacerbating oxidative stress.

ALP is a vital enzyme in the calcification process; its expression is linked to inflammation, and abnormal levels of ALP may indicate tissue damage (17). SA is a part of the cell structure and plays a crucial role in functioning biological systems. Also, SA determines the inflammatory state and tissue destruction (18). Boron is an important trace element for the body because it regulates biological processes and metabolism. It affects brain functions and skeletal health and regulates the immune system (19). TF is one of the regulators of thrombosis, an initiator of the coagulation cascade in the body. In case of organ damage, TF quickly stops bleeding to prevent excessive blood loss and ensures hemostasis (9). To our knowledge, this is the first study that attempts to investigate both α-LA and Que treatment on MTX-induced tissue damage on boron level and TF activity of the liver tissue in rats. Exposing MTX caused an increase in ALP and SA levels and decreased boron levels and TF activity in the liver, which is a sign of structural and functional changes in the liver tissue caused by MTX administration. Elevated liver ALP levels may be a sign of disrupted normal functions, and the increase in liver SA levels may be a response to tissue self-protection against damage caused by MTX administration. Also, this increase may be due to SA's protective effect in reducing damage by creating a negative charge on cell membranes. Decreased boron levels are also another sign of damage in liver tissue. Boron, which functions as an antioxidant in the organism, may have decreased due to the reduced activities of the other antioxidant enzymes in the tissue. Prolonged TF activity may indicate that the body is delayed in repairing the injury. The electrophoretic examination shows that MTX caused a boost in the band density of the proteins with a molecular weight of 117, 110, 84, 78, 38, and 24 kD compared to the control. The structural and functional proteins in the liver maintain the proper and regular functioning of the tissue. Any disruption or change in the arrangement of these proteins may cause dysfunction or insufficiency of the liver.

Our altered biochemical results related to hepatotoxicity were also correlated with the histological examinations. Both α-LA and Que efficiently neutralized the structural and functional changes resulting from the MTX application; Que, in particular, brought the parameters to a controlled level. Our results suggest that both α-LA and Que treatment on MTX had positive effects on the liver, especially since Que was more effective in neutralizing damage and using substances with antioxidant properties to prevent tissue damage caused by MTX. Alpha LA helps to form cellular antioxidants by making them reusable by regenerating (20). According to previous studies, α-LA treatment to MTX administration elevates SOD activity and GSH levels and reduces MDA levels, and also reverses the decreased antioxidant parameters (21,22). Besides, α-LA has beneficial effects on fatty liver disease patients by reducing ALP levels were reported (23). The antioxidant capacity of α-LA in the inflammatory process by reducing SA levels in plasma was also pointed out (24). In our study, we found that α-LA administration to MT significantly decreased MDA and NO levels, and decreased GSH levels, SOD and CAT activities, compared to the MT group.

The protective effects of Que have been documented in various models of chemically-induced hepatotoxicity (25). For instance, Que administration was shown to normalize elevated MDA and depleted GSH levels in ethanol-induced injury (26). Similarly, Similarly, in MTX-administered rats, Que acted as a therapeutic agent

by reversing MTX-induced lipid peroxidation and restoring SOD activity (27). While most studies, such as those involving lipopolysaccharide/D-galactosamine-induced injury, report an increase in GSH levels following Que treatment (28), contrasting results have been observed in other models. In chlorpyrifos-induced testicular damage, for example, Que was found to decrease previously elevated antioxidant enzymes and ALP levels (29). This reduction in ALP levels suggests that Que possesses membrane-stabilizing activity (30). Consistent with these findings, our research demonstrated that Que administration to MTX-treated rats significantly reduced MDA, ALP, and SA levels while elevating GSH content and the activities of SOD and CAT.

The experimental study demonstrated that MTX induced oxidative stress in rat liver tissue, leading to increased generation of ROS and a significant reduction in antioxidant levels. Both α-LA and Que were effective in reducing oxidative stress and protecting tissue against damage, and thus, they may be promising drugs for preventing MTX-induced liver damage.

5. Conclusion

We experimentally demonstrated that oxidative damage caused by MTX administration could be biochemically reversed by α-LA and Que administration in liver tissue. Que was more effective in normalizing the investigated biochemical and functional parameters, although both α-LA and Que are hepatoprotective agents for oxidative stress. The present study, however, is limited by the absence of parameters in the blood, as the sample amount was insufficient for determining parameters.

Conflict of interest

The authors declare that there are no conflicts of interest associated with this research.

Funding

This work was thankfully supported by the Marmara University Scientific Research Projects Commission (Project No: TYL-2022-10429).

Ethics approval

Ethical approval for this study was obtained from the Marmara University Animal Care and Use Committee (71.2015.mar)

Author Contributions

Conception/Design of Study – Ş.S, E.A., S.A., Ş.O..; Data Acquisition– Ş.S, Ş.O. ; Data Analysis/Interpretation – Ş.S, E.A., Ş.O.; Drafting Manuscript – Ş.S, E.A., S.A., Ş.O; Critical Revision of Manuscript – E.A., S.A., Ş.O.; Final Approval and Accountability – Ş.S, E.A., S.A., Ş.O.

References

1. Woolf R, Smith C. Methotrexate. In: Wakelin SH, Maibach HI, Archer CB, editors. Handbook of Systemic Drug Treatment in Dermatology. 3rd ed. London: CRC Press; 2023. p.195. https://doi.org/10.1201/978.100.3016786
2. Chen C, Liu YH, Cheng SB, Wu SL, Zhai XJ. The hepatoprotective effects of XCHD and MgIG against methotrexate-induced liver injury and inflammation in rats through suppressing the activation of AIM2 inflammasomes. Pathol Res Pract 2020;216:152875. https://doi.org/10.1016/j.prp.2020.152875
3. Alqarni AM, Zeidler MP. How does methotrexate work? Biochem Soc Trans 2020;48(2):559-567. https://doi.org/10.1042/bst20190803
4. Cronstein BN, Aune TM. Methotrexate and its mechanisms of action in inflammatory arthritis. Nat Rev Rheumatol 2020;16:145-154. https://doi.org/10.1038/s41584.020.0373-9
5. Ahmed ZSO, Hussein S, Ghandour RA, Azouz AA, El-Sakhawy MA. Evaluation of the effect of methotrexate on the hippocampus, cerebellum, liver, and kidneys of adult male albino rat: Histopathological, immunohistochemical and biochemical studies. Acta Histochem 2021;123:151682. https://doi.org/10.1016/j.acthis.2021.151682
6. Esposito C, Garzarella EU, Santarcangelo C, Di Minno A, Dacrema M, Sacchi R, Piccinocchi G, Piccinocchi R, Daglia M. Safety and efficacy of alpha-lipoic acid oral supplementation in the reduction of pain with unknown etiology: A monocentric, randomized, double-blind, placebo-controlled clinical trial. Biomed Pharmacother 2021;144:34649217. https://doi.org/10.1016/j.biopha.2021.112308
7. Cheng Y, Yang X, Tang W, Fu Q, Li H, Liang B. Alpha-lipoic acid inhibits sodium arsenite-mediated autophagic death of rat insulinoma cells. Hum Exp Toxicol 2023;42:096.032.71221149196. https://doi.org/10.1177/096.032.71221149196
8. Sánchez-González PD, López-Hernández FJ, Dueñas M, Prieto M, Sánchez-López E, Thomale J, Ruiz-Ortega M, López-Novoa JM, Morales AI. Differential effect of quercetin on cisplatin-induced toxicity in kidney and tumor tissues. Food Chem Toxicol 2017;107:226-236. https://doi.org/10.1016/j.fct.2017.06.047
9. Elik G, Oktay S, Turkyilmaz IB, Alev-Tuzuner B, Magaji UF, Sacan O, Yanardag R, Yarat A. Dermatoprotective effect of Moringa oleifera leaf extract on sodium valproate-induced skin damage in rats. Drug Chem Toxicol 2024; 47(6):1257-1266. https://doi.org/10.1080/01480.545.2024.2369586

10. Eldridge S, Guo L, Hamre J. A comparative review of chemotherapy-induced peripheral neuropathy in in vivo and in vitro models. Toxicol Pathol 2020;48(1):190-201. https://doi.org/10.1177/019.262.3319861937
11. Yang Z, Mo J, Li W, Zhao Z, Mei S. Methotrexate polyglutamates. Expert Rev Clin Pharmacol 2024;17(11):1025-1037. https://doi.org/10.1080/17512.433.2024.2416674
12. Kalantar M, Kalantari H, Goudarzi M, Khorsandi L, Bakhit S, Kalantar H. Crocin ameliorates methotrexate-induced liver injury via inhibition of oxidative stress and inflammation in rats. Pharmacol Rep 2019;71(4):746-752. https://doi.org/10.1016/j.pharep.2019.04.004
13. Mehrzadi S, Fatemi I, Malayeri AR, Khodadadi A, Mohammadi F, Mansouri E, Rashno M, Goudarzi M. Ellagic acid mitigates sodium arsenite-induced renal and hepatic toxicity in male Wistar rats. Pharmacol Rep 2018;70:712-719. https://doi.org/10.1016/j.pharep.2018.02.007
14. Arpag H, Gül M, Aydemir Y, Atilla N, Yiğitcan B, Cakir T, Polat C, Þehirli Ö, Sayan M. Protective effects of alpha-lipoic acid on methotrexate-induced oxidative lung injury in rats. J Invest Surg 2017;31(2):107-113. https://doi.org/10.1080/08941.939.2017.1296513
15. Khalifa MMA, Bakr AG, Osman AT. Protective effects of phloridzin against methotrexate-induced liver toxicity in rats. Biomed Pharmacother 2017;95:529-535. https://doi.org/10.1016/j.biopha.2017.08.121
16. Safaei F, Mehrzadi S, Khadem Haghighian H, Hosseinzadeh A, Nesari A, Dolatshahi M, Esmaeilizadeh M, Goudarzi M. Protective effects of gallic acid against methotrexate-induced toxicity in rats. Acta Chir Belg 2018;118:152-160. https://doi.org/10.1080/00015.458.2017.1394672
17. Haarhaus M, Brandenburg V, Kalantar-Zadeh K, Stenvinkel P, Magnusson P. Alkaline phosphatase: A novel treatment target for cardiovascular disease in CKD. Nat Rev Nephrol 2017;13:429-442. https://doi.org/10.1038/nrneph.2017.60
18. Volkhina IV, Butolin EG. Clinical and diagnostic significance of sialic acids determination in biological material. Biochem Mosc Suppl B: Biomed Chem 2022;16:165-174. https://doi.org/10.1134/s199.075.082203012x
19. Kabu M, Akosman MS. Biological effects of boron. In: Whitacre D, editor Rev Environ Contam Toxicol 2013;225:57-75. https://doi.org/10.1007/978-1-4614-6470-9_2
20. Armagan I, Bayram D, Candan IA, Yigit A, Celik E, Armagan HH, Uğuz AC. Effects of pentoxifylline and alpha lipoic acid on methotrexate-induced damage in liver and kidney of rats. Environ Toxicol Pharmacol 2015;39(3):1122-1131. https://doi.org/10.1016/j.etap.2015.04.003
21. Hasan RRA, Algareeb AI. Hepatoprotective effects of alpha-lipoic acid, vitamin C alone, or in combination on methotrexate-induced liver injury. Mustansiriya Med J 2022;21(1):41-47. https://doi.org/10.4103/mj.mj_23_21
22. Pınar N, Çakırca G, Özgür T, Kaplan M. The protective effects of alpha lipoic acid on methotrexate induced testis injury in rats. Biomed Pharmacother 2018;97:1486-1492. https://doi.org/10.1016/j.biopha.2017.11.078
23. Amirkhizi F, Hosseinpour-Arjmand S, Ebrahimi-Mameghani M. The effect of alpha-lipoic acid on liver function and metabolic markers in obese patients with non-alcoholic fatty liver disease: A double-blind randomized controlled trial. Iran Red Crescent Med J 2018;20(3):e67615. https://doi.org/10.1111/jcpt.12784
24. Yildirim C, Yucetas SC, Kaya M, Öziç C, Kaya I, Bilgin B, Balioğlu M, Karapehlivan M, Akın T, Topçu B. Investigation of the effects of alpha lipoic acid application on total antioxidant and oxidant status, paraoxonase, and total sialic acid levels in laminectomized rabbits. Kafkas Univ Vet Fak Derg 2014;20(1):115-120. https://doi.org/10.9775/kvfd.2013.9601
25. Sharma A, Parikh M, Shah H, Gandhi T. Modulation of Nrf2 by quercetin in doxorubicin-treated rats. Heliyon 2020;6(4):e03803. https://doi.org/10.1016/j.heliyon.2020.e03803
26. Chen X. Protective effects of quercetin on liver injury induced by ethanol. Pharmacogn Mag 2010;6(22):135-141. https://doi.org/10.4103/0973-1296.62900
27. Yuksel Y, Yuksel R, Yagmurca M, Haltas H, Erdamar H, Toktas M, Ozcan O. Effects of quercetin on methotrexate-induced nephrotoxicity in rats. Hum Exp Toxicol 2017;36(1):51-61. https://doi.org/10.1177/096.032.7116637414
28. Peng Z, Gong X, Yang Y, Huang L, Zhang Q, Zhang P, Wan R, Zhang B. Hepatoprotective effect of quercetin against LPS/ d-GalN induced acute liver injury in mice by inhibiting the IKK/NF-κB and MAPK signal pathways. Int Immunopharmacol 2017;52:281-289. https://doi.org/10.1016/j.intimp.2017.09.022
29. 29. Kalender Y, Kaya S, Durak D, Uzun FG, Demir F. Protective effects of catechin and quercetin on antioxidant status, lipid peroxidation and testis-histoarchitecture induced by chlorpyrifos in male rats. Environ Toxicol Pharmacol 2012;33(2):141-148. https://doi.org/10.1016/j.etap.2011.12.008
30. Gelen V, Sengul E, Gedikli S, Gür C, Özkanlar S. Therapeutic effect of quercetin on renal function and tissue damage in the obesity induced rats. Biomed Pharmacother. 2017;89:524-528. https://doi.org/10.1016/j.biopha.2017.02.057

Cite this article: Savas S, Ak E, Ahmad S, Oktay S. Therapeutic Properties of Alpha Lipoic Acid and Quercetin on Methotrexate-Induced Oxidative Stress in Rat Liver. Pharmedicine J. 2026;3(1): 37-44. DOI: 10.62482/pmj.41

RESEARCH IN PHARMACY AND MEDICINE
PHARMEDICINE JOURNAL

2026; 3(1):45-60. doi: 10.62482/pmj.40

Original Article

Integrative Analysis of Molecular Interactions and Repurposable Drugs in Primary Biliary Cholangitis

Duygu Sari-Ak[1], Nazli Helvaci-Kurt[2], Fatih Con[3], Alev Kural[3]

[1] University of Health Sciences, Hamidiye International School of Medicine, Department of Medical Biology, Istanbul, Türkiye
[2] University of Health Sciences, Hamidiye International School of Medicine, Department of Medical Biology, Istanbul, Türkiye
[3] University of Health Sciences, Bakirkoy Dr. Sadi Konuk Training and Research Hospital, Istanbul, Türkiye

Corresponding Author: Duygu Sari Ak (**E-mail:** duygusariak@gmail.com)

Received: 2025.10.10; **Revised:** 2025.12.30 **Accepted:** 2026.01.17 **Published:** 2026.02.28

Abstract

Introduction: Primary Biliary Cholangitis (PBC) is an autoimmune liver disease characterized by chronic destruction of intrahepatic bile ducts, leading to fibrosis and eventual liver failure. Current first-line treatments, including ursodeoxycholic acid (UDCA) and obeticholic acid (OCA), provide insufficient therapeutic benefit for a substantial proportion of patients. Integrative systems-level analyses of multi-omic data enable the identification of potential therapeutic targets and the repurposing of existing drugs.

Methods: A total of 214 human genes associated with PBC were retrieved from NCBI Gene and DisGeNET databases. Protein-protein interaction (PPI) networks were constructed using STRING and subsequently analyzed for hub genes and network clusters using Cytoscape. Pathway enrichment analysis was performed using Reactome, and drug-gene associations were evaluated using the DSigDB database. Selected drug-target interactions were further assessed using experimentally validated binding data from BindingDB and molecular docking results generated by SwissDock.

Results: The network analysis produced 187 nodes which connected through 1,645 edges. Hub gene analysis highlighted TP53, IL6, CXCL8, STAT3, IFNG, JUN, and CDKN1A as central regulators of immune and apoptotic signaling pathways. The Reactome analysis showed that interleukin and TP53-mediated pathways achieved statistical significance at an FDR value of less than 0.05. The FDA has approved six compounds for medical use including Simvastatin and Budesonide and Tocilizumab and N-acetylcysteine and PD98059 and Vorinostat which demonstrate supportive experimental or computational evidence of target engagement.

Conclusions: This integrative network-based framework identified central molecular regulators and repurposable drugs for PBC. Further experimental and clinical studies are required to determine the therapeutic potential of these candidates in autoimmune liver disease.

Keywords: Computational validation, cytokine signaling, drug repurposing, hub genes, primary biliary cholangitis

1. Introduction

Primary Biliary Cholangitis (PBC) is a chronic autoimmune liver disease characterized by the progressive destruction of small intrahepatic bile ducts. This process leads to cholestasis, hepatic inflammation, and, if left untreated, progression to cirrhosis and eventual liver failure. Although PBC can occur at any age, it predominantly affects middle-aged women. Clinically, the disease is diagnosed based on a characteristic triad comprising the presence of antimitochondrial antibodies, elevated liver enzyme levels, and chronic cholestasis (1-3). The etiology of PBC is multifactorial and involves a complex interplay of genetic predisposition, epigenetic modifications, and environmental triggers (4-6). A central immunopathological mechanism is T lymphocyte–mediated destruction of biliary epithelial cells, which disrupts bile duct architecture and initiates progressive fibrotic remodeling of the liver (7-10). Recent omics-based studies have further demonstrated that dysregulation of the Interleukin-6 (IL6)/Signal Transducer and Activator of Transcription 3 (STAT3) axis, interferon gamma (IFNG) signaling, and oxidative stress-related pathways act synergistically to promote immune-mediated biliary injury in PBC (10-16). These findings highlight IL6, IFNG, and C-X-C Motif Chemokine Ligand 8 (CXCL8) as key molecular nodes with therapeutic relevance.

Ursodeoxycholic acid (UDCA) remains the first-line therapy for PBC, while obeticholic acid (OCA) has been evaluated as a second-line option for patients with an inadequate response to UDCA. However, approximately 30-40% of patients fail to achieve sufficient biochemical or clinical improvement with UDCA-based therapy (3,17-21). Notably, the conditional marketing authorization application for OCA was withdrawn by the sponsor in 2024, underscoring ongoing challenges in optimizing second-line treatment strategies (22-24). Despite these advances, a substantial unmet need remains, particularly for therapies that directly target immune-mediated inflammation, fibrotic remodeling, and cytokine-driven signaling pathways implicated in PBC pathogenesis. Most currently available treatments primarily modulate bile acid metabolism or lipid homeostasis and may not adequately address immune and inflammatory mechanisms in all patients. Therefore, complementary therapeutic strategies targeting immune and stress-response pathways may provide additional clinical benefit.

Drug repurposing has emerged as an efficient and cost-effective approach to accelerate therapeutic development for complex and rare diseases such as PBC. By identifying new clinical indications for existing FDA-approved drugs, this strategy reduces development time, cost, and safety-related uncertainty. Drug repurposing is particularly well suited to immune-mediated disorders, where pathway redundancy and compensatory signaling often limit the efficacy of single-target interventions (17,25-29). Network pharmacology integrates systems biology with pharmacological data to identify disease-relevant molecular networks, regulatory hub genes, and candidate drugs capable of modulating multiple interconnected pathways (15,30).

In the present study, we applied a network-based drug repurposing strategy to identify potential therapeutic agents for PBC. Using a curated list of 214 PBC-associated genes obtained from the NCBI Gene and DisGeNET databases (31), we constructed a protein–protein interaction (PPI) network using Search Tool for the Retrieval of Interacting Genes/Proteins (STRING) (32) and visualized it in Cytoscape (33). Topological analysis enabled the identification of highly connected hub genes within the network. These hub genes were subsequently interrogated using the Drug Signature Database (DSigDB) to identify candidate drugs with repurposing potential (34). Tocilizumab, targeting IL6 signaling, and N-acetylcysteine (NAC), associated with IFNG-related oxidative stress pathways, were selected for further computational validation based on their biological relevance and central network positions. Drug–target interaction plausibility was evaluated using experimentally validated binding data from BindingDB (35) and molecular docking simulations performed with SwissDock (36,37).

This integrative framework aims to complement existing bile acid-and metabolism-centered therapies by highlighting immune – and fibrosis-related

molecular targets and clinically accessible drugs with repositioning potential. By bridging network biology with pharmacological validation, this study provides a hypothesis-generating approach to guide future experimental and translational investigations in precision hepatology.

2. Methods

2.1. Gene Selection

Multiple biomedical databases with reliable multi-omic data integration were used to retrieve disease-associated genes for systematic characterization of the PBC genetic landscape.

The NCBI Gene database (https://www.ncbi.nlm.nih.gov/gene) serves as a centralized repository for gene-specific information maintained by the National Center for Biotechnology Information. The research extracted gene entries which received the Medical Subject Heading (MeSH) term "Primary Biliary Cholangitis" annotation. This query enabled the identification of established PBC-associated genes supported by multiple evidence sources, including genome-wide association studies, differential expression analyses, functional experiments, and expert manual curation.

The research team expanded their study by using DisGeNET (https://www.disgenet.org/) to obtain more evidence from structured biomedical knowledge sources which integrates gene-disease associations from UniProt and CTD databases and animal models and high-throughput literature mining. Specifically, we retrieved genes associated with the unique disease identifier Concept Unique Identifier (CUI): C0021446, corresponding to "Primary Biliary Cholangitis". The evaluation of each gene-disease association used DisGeNET evidence scores to determine the most relevant biological targets.

Following data retrieval, all gene symbols were harmonized and standardized to official HGNC (HUGO Gene Nomenclature Committee) gene symbols to ensure interoperability and downstream compatibility. The normalization process solved previous issues that resulted from outdated gene names and platform-dependent aliases and synonyms. Duplicate records between databases were removed using string-matching algorithms in Microsoft Excel, followed by manual verification to ensure data accuracy characterize.

As a result of this rigorous curation pipeline, we assembled a non-redundant list of 214 unique protein-coding genes with established or inferred associations with PBC pathophysiology. The researchers used the selected gene panel to construct interaction networks which revealed crucial molecular hubs that play a role in PBC disease progression. However, it must be emphasized that network-derived drug candidates represent hypothesis-generating outputs rather than proven therapeutic options and therefore require careful evaluation against existing clinical evidence.

2.2. STRING-based PPI Network Construction

To elucidate the molecular interplay among the 214 PBC-associated genes identified in Section 2.1, we constructed a comprehensive PPI network using the STRING database (version 12.0; https://string-db.org). STRING serves as a major repository that integrates experimentally validated and predicted protein interactions derived from multiple evidence sources, including high-throughput experimental data, curated biological databases, text mining of scientific literature, co-expression patterns, and computational predictions.

The HGNC-standardized gene symbols were uploaded to STRING using the following parameters:

I. Organism: Homo sapiens (taxonomy ID: 9606)

II. Minimum interaction score: ≥ 0.40 (medium-confidence threshold suitable for exploratory disease-specific network analyses)

III. Active interaction sources: experimental evidence, curated databases, co-expression, neighborhood, gene fusion, and co-occurrence

IV. Additional interactors: none (analysis restricted to the 214 PBC-associated proteins). Self-interactions were excluded, and the network was treated as undirected to reflect bidirectional functional protein interactions.

STRING generated an interactome including both experimentally verified physical interactions and predicted functional associations. Edge confidence scores were retrieved to permit weighting of interaction strength in subsequent analyses. The resulting network file was exported in tab-separated values (TSV) format containing protein attributes and interaction metrics for downstream visualization and topological evaluation.

The exported file was then imported into Cytoscape version 3.10.0 (Cytoscape Consortium, San Diego, CA, USA) for advanced network visualization and quantitative analysis of key network properties such as node degree, betweenness centrality, and clustering coefficients. This integrative pipeline produced a reproducible PPI network framework that served as the basis for subsequent hub-gene prioritization, module detection, and pathway enrichment analysis.

To address potential interaction noise, a sensitivity analysis was also performed using a higher STRING confidence threshold (0.7), restricted to experimentally validated and curated database interactions. Network topology and hub-rank stability were compared across thresholds to ensure robustness of the identified key regulators. At the higher confidence threshold (0.7), key hub genes including IL6, TP53, STAT3, JUN, and v-rel avian reticuloendotheliosis viral oncogene homolog A (RELA) remained among the highest-ranked nodes, indicating that hub-rank stability was preserved and that the network architecture was not driven by low-confidence interactions. The hub-gene analysis was repeated using a high-confidence STRING threshold (≥ 0.70), restricted to experimental and curated-database interactions. Hub-rank stability was evaluated across thresholds.

2.3. Network Visualization and Hub Gene Identification

The STRING network data were imported into Cytoscape for systems-level analysis of PPI dynamics in PBC using this open-source visualization platform.

We used the NetworkAnalyzer plugin in Cytoscape to calculate different topological metrics for each gene product node in the network which included degree, betweenness centrality and closeness centrality. Node degree represents the number of direct connections a given node has and is used to infer its potential role as a signaling hub. The number of shortest paths that pass through a node determines its betweenness centrality value because it shows how much the node affects information transfer in the network. Closeness centrality, defined as the inverse of the average shortest path length to all other nodes, captures the efficiency of a node's communication and influence across the interactome.

Each of these centrality measures offers complementary insight into the structural and functional hierarchy of the interactome. All calculations were performed under default conditions without node or edge filtering. The network's degree distribution was fitted to a power-law model by log-log linear regression using degree frequency data in Cytoscape's NetworkAnalyzer, yielding an $R^2 = 0.87$, consistent with a scale-free topology characteristic of biological networks.

Genes ranking in the top 10th percentile for node degree were designated as putative hub genes, based on the well-established principle that hubs are frequently critical to network integrity and may serve as master regulators in disease-relevant signaling cascades. This threshold is consistent with prior systems-biology literature, where the top decile of the degree distribution is widely applied to distinguish true regulatory hubs from general high-degree nodes while preserving biological interpretability. These genes were further shortlisted for downstream drug repurposing analysis due to their high potential as pharmacological targets.

The PPI network visualization used prefuse force-directed layout optimization to generate its layout structure while node size and color followed degree centrality for hubness representation.

2.4. Cluster Detection via MCODE

The Molecular Complex Detection (MCODE) plugin in Cytoscape enabled us to find densely connected regions in the protein–protein interaction network. The algorithm identifies clusters of densely

connected nodes which could indicate important biological protein complexes or functional modules.

Default MCODE parameters were applied to ensure reproducibility and consistency with previous studies. The researchers used a degree cutoff of 2 to select nodes with at least two connections and a node score cutoff of 0.2 to exclude low-scoring nodes and a K-core value of 2 to find the central core subgraph and a maximum depth of 100 to define cluster extension distance from seed nodes.

The MCODE algorithm produced clusters which researchers validated through their analysis of literature and pathway database verification from Reactome and KEGG. The dual-step method validated each identified module by showing both statistical significance and biological importance which enabled researchers to determine vital molecular pathways in PBC.

2.5. Pathway Enrichment Using Reactome

To characterize functionally the biological processes associated with PBC, we performed pathway enrichment analysis using the Reactome Pathway Browser (version 86; https://reactome.org). The expert-curated resource Reactome provides detailed mappings of genes and proteins to biological pathways, enabling researchers to study cellular and disease mechanisms at high resolution.

Pathway enrichment analysis was first performed using the full set of 214 PBC-associated genes, in order to avoid hub-driven pathway bias and to capture the broader disease-relevant signaling architecture. In a secondary, hypothesis-focused analysis, we repeated enrichment using the 30 top-degree hub genes to examine whether these highly connected regulators preferentially mapped to cytokine – and interleukin-related pathways.

For both analyses, official gene symbols were used to ensure compatibility with the Reactome database. In the primary analysis, the input gene set consisted of all 214 PBC-associated genes identified in Section 2.1. In the secondary analysis, the input gene set was restricted to the 30 hub genes with the highest node degree centrality in the PPI network.

Results from the full-gene-set enrichment are presented in the main text and figures, whereas hub-only enrichment outputs are provided in Supplementary Fig S1.

The following parameters were applied during analysis: species was set to Homo sapiens; the false discovery rate (FDR) threshold was defined as < 0.05 using the Benjamini–Hochberg correction; the minimum pathway overlap was set to three genes; and the analysis type was over-representation based on the hypergeometric test.

The researchers applied strict criteria to achieve statistical reliability when they chose biological pathways showing substantial gene enrichment patterns. The background gene universe was set to the entire Homo sapiens genome, consistent with the default Reactome over-representation analysis parameters.

Reactome outputs were filtered to retain only statistically significant results (FDR< 0.05). The researchers analyzed different pathways based on FDR values and biological importance through their examination of immune pathways such as interferon signaling and cytokine networks and apoptotic mechanisms and metabolic pathways related to cholestasis and liver damage.

The researchers added annotations to each enriched pathway which included the number of shared genes and FDR values and biological processes related to the results. Multiple signaling pathways were identified that are implicated in PBC pathogenesis and these pathways present potential targets for therapeutic treatments.

The researchers conducted additional analysis of Reactome-enriched pathways to determine their relationship with hub gene connectivity and established drug targets for drug repurposing. The research team selected pathways with multiple druggable hub genes for pharmacological investigation. The integrated network-based analysis model was built through cross-linking Reactome outputs with drug–gene associations for systematic drug repurposing evaluation.

The researchers used drug–gene interaction data to create a mechanistic framework which connected molecular hubs to possible therapeutic approaches.

2.6. Drug-Gene Interaction Analysis

To identify potential therapeutic agents for PBC via drug repurposing, we conducted drug–gene interaction analysis using the DSigDB (Drug Signatures Database) through the Enrichr web-based platform (https://maayanlab.cloud/Enrichr/). DSigDB provides curated associations between genes and drug-induced gene expression signatures, making it a valuable resource for network pharmacology-based drug discovery.

Importantly, DSigDB does not catalogue direct drug–target interaction data, but rather compound-induced gene-expression signatures. Accordingly, DSigDB-derived hits in this study were treated as hypothesis-generating pharmacogenomic leads rather than as confirmed drug-target relationships.

The full list of top-ranked hub genes obtained from protein-protein interaction network analysis was uploaded to Enrichr for enrichment analysis using DSigDB as the target library. The identification of clinically relevant candidates involved selecting FDA-approved drugs with defined molecular targets and mechanisms of action, particularly those with potential relevance to liver disorders, fibrosis, and immunomodulation.

We obtained drug-gene association metadata through manual curation of DrugBank and PubChem databases and primary literature sources for each enriched association. The curated information included drug names and classifications and known indications and target genes and mechanisms of action and current liver and autoimmune disease applications and potential PBC treatment possibilities which we evaluated as high moderate or low based on functional significance and existing scientific evidence.

The output data was organized in Supplementary Table S1 and presented through a bar graph (Fig 4) to show the top candidate drugs based on their combined enrichment score and pharmacological plausibility. The integrative analysis resulted in the selection of multiple FDA-approved drugs for additional validation as potential repurposing candidates in PBC.

Following enrichment analysis, an additional clinical-biological filtering step was applied. Candidate drugs were evaluated according to: (i) biological plausibility based on the enriched immune and fibrotic pathways, (ii) existing evidence in autoimmune or cholestatic liver disease, and (iii) feasibility and known hepatic safety, including reported hepatotoxicity profiles, hepatic metabolism, and cholestasis-related risk. Drugs lacking reasonable translational plausibility were downgraded in repurposing priority and interpreted as exploratory.

2.7. Computational Validation of Drug–target Binding Affinities

The results from DSigDB enrichment analysis (Section 2.6) were validated through BindingDB database and SwissDock molecular docking server binding affinity assessments for drug–gene associations. This dual strategy integrated experimentally measured ligand–target interactions with computational docking simulations to assess the pharmacological relevance of the candidate drug–target pairs identified for PBC.

2.7.1. Binding affinity data retrieval (BindingDB)

Binding affinity values (IC_{50}, K_i, or K_d) were obtained from the BindingDB database (https://www.bindingdb.org/) for drug–target pairs shortlisted in the DSigDB-based analysis. Experimentally validated interactions were available for the following pairs:

PD98059–MAP2K1 (MEK1): IC_{50} = 2.8 μM - inhibition of MAPK phosphorylation by activated MEK1.

- Budesonide–NR3C1: IC_{50} = 0.5–1.6 nM - high-affinity binding to the human glucocorticoid receptor.
- Simvastatin–HMGCR: IC_{50} = 4.3–18 nM - inhibition of microsomal HMG-CoA reductase activity.
- Vorinostat–HDAC1/HDAC2: K_i = 10–50 nM - inhibition of recombinant human histone deacetylases 1 and 2.

For N-acetylcysteine and Tocilizumab, no quantitative BindingDB data were available for their specific PBC-related targets. These interactions were therefore evaluated computationally via molecular docking simulations.

2.7.2. Molecular docking (SwissDock)

Molecular docking simulations were carried out using the SwissDock server (http://www.swissdock.ch) to explore the potential molecular interactions between candidate drugs and their respective targets. The Protein Data Bank (PDB) provided protein structures which underwent preprocessing to eliminate water molecules and heteroatoms before initiating the docking procedure. The PDB ID 1FG9 crystal structure with all available chains received energy minimization and cavity optimization treatment before IFNG docking.

The IFNG–N-acetylcysteine complex underwent SwissDock's Accurate mode analysis with these parameters: Attracting Cavities 2.0 as the method and medium sampling exhaustivity and one Random Initial Condition (RIC) and box center coordinates at 34, – 5, – 19 and box dimensions of 20 × 20 × 20 and buried cavity prioritization. Docking simulations generated multiple clusters, with Cluster 0 – Member 1 showing the highest ranking, characterized by an Attracting Cavities (AC) score of −24.70 (unitless) and a SwissDock/SwissParam–estimated binding free energy (ΔG) of −6.62 kcal/mol, indicating a moderate binding affinity compatible with physiological interactions. The ligand established multiple hydrogen bonds and ionic bonds with surrounding residues inside the binding cavity which indicated a possible weak to moderate regulatory connection.

The researchers started docking Tocilizumab–IL6 receptor (IL6R) but they could not perform structural modeling because the 3D data of the receptor–Fab interface was not available.

Docking simulations were performed for exploratory assessment of structural plausibility only. Because NAC is a small redox-active molecule rather than a classical receptor-binding ligand, the docking results were not intended to imply physiologically relevant affinity.

2.7.2.1. Tocilizumab–IL6R interaction validation (Literature and structural evidence)

The IL6–IL6R–Tocilizumab complex does not have a complete crystal structure which makes small-molecule docking analysis impossible so researchers confirmed Tocilizumab's binding to IL6R through structural analysis and scientific literature.

Tocilizumab functions as a humanized monoclonal antibody which specifically targets both soluble (sIL6R) and membrane-bound (mIL6R) interleukin-6 receptor forms to stop their interaction with gp130 and block JAK/STAT signaling. The PDB contains structural data (IDs: 3L5H, 4CNI) that shows the partial Fab–IL6R binding domains and shows how the antibody physically blocks IL6 from binding to its receptor.

According to kinetic data from biophysical assays, Tocilizumab exhibits subnanomolar affinity for IL6R ($K_d \approx 2–4 \times 10^{-10}$ M) as determined by surface plasmon resonance and competitive binding studies (38,39). The drug achieves its strong IL6 signaling inhibition and clinical effectiveness in autoimmune and inflammatory diseases because of its exceptionally high binding affinity.

The experimental validation and structural characterization results led to the conclusion that Tocilizumab–IL6R interaction was proven experimentally so it was removed from additional computational docking analysis.

Accordingly, tocilizumab was not treated as a computationally docked candidate in this study; rather, its inclusion reflects experimentally established IL6R binding and network/pathway relevance.

2.7.3. Data integration and prioritization

BindingDB and SwissDock results were qualitatively integrated to assess the strength and plausibility of each drug–target interaction. The study defines strong interactions as those which bind to experimentally validated high-affinity targets (IC_{50} or K_i < 100 nM). The docking-derived interactions which showed binding energies of ΔG<-6 kcal/mol were considered as potentially relevant.

The results of both experimental and computational validations are summarized in Table 2. Collectively, the integrated computational validation corroborated the mechanistic plausibility and pharmacological relevance of the proposed repurposed drug candidates in PBC.

3. Results

3.1. PPI Network Topology

Of the 214 genes, 187 were mapped in STRING to known protein interactions, yielding a network with 1,645 edges (Fig. 1). The network displayed features of a scale-free topology typical of biological systems, indicating robustness and modularity. The degree distribution followed a power-law fit ($R^2 = 0.87$), consistent with a scale-free network. The complete STRING-derived protein–protein interaction dataset contains all edge confidence scores and interaction types and is provided in Supplementary Table S2. This network architecture indicated the presence of key hub nodes likely driving the molecular pathogenesis of PBC.

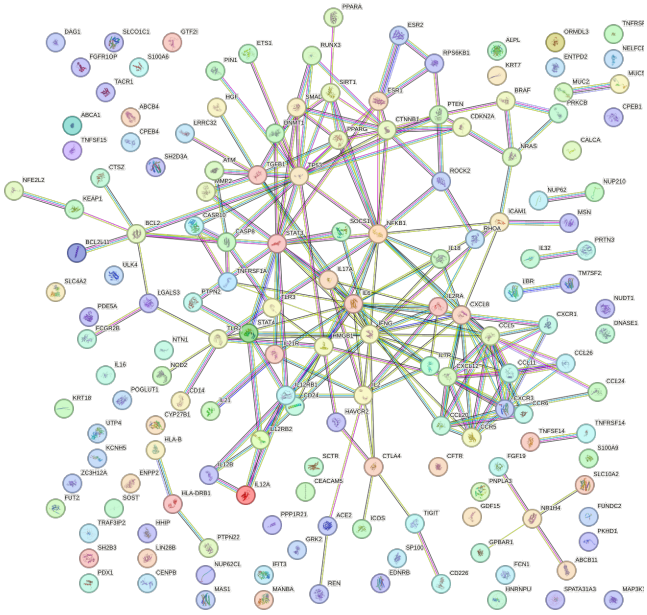

Figure 1. Protein–protein interaction network of 187 PBC-associated genes constructed using STRING (V12.0).The network comprises 187 nodes and 1,645 edges representing known and predicted protein interactions. Each node corresponds to a protein encoded by a gene associated with PBC. Edges indicate functional associations derived from experimental data, curated databases, co-expression patterns, and text mining. Nodes are color-coded by clustering or interaction strength. The network exhibits scale-free topology, characteristic of biological systems, suggesting the presence of functional hubs and modularity.

3.2. Hub Gene Identification

Based on topological analysis of the PPI network, we systematically calculated multiple network metrics using the NetworkAnalyzer plugin in Cytoscape, including node degree, betweenness centrality, and closeness centrality. Node degree was selected as the primary criterion for hub gene selection, given its biological relevance in indicating the number of direct protein interactions. Hub status was defined a priori as the top 10th percentile of nodes ranked by degree centrality, consistent with widely applied network-biology practice.

Genes with the highest degree values were designated as hub genes (Table 1). The top 10 hub genes-TP53, IL6, CXCL8, STAT3, IFNG, JUN, CDKN1A, RELA, FOS, and MYC-exhibited numerous connections to multiple partners, demonstrating their critical function in PBC immunoinflammatory and apoptotic pathways.

Table 1. Top 10 Hub genes identified from the PPI network of PBC-associated genes. Hub status was assigned based on node degree computed via NetworkAnalyzer in Cytoscape. These genes represent key molecular nodes potentially driving PBC pathogenesis.

Gene	Node Degree	Biological Role
TP53	42	Cell cycle control, apoptosis
IL6	39	Cytokine signaling, immune response
CXCL8	34	Chemokine activity, neutrophil recruitment
STAT3	32	Transcription factor, inflammation
IFNG	31	Immune activation, Th1 signaling
JUN	30	AP-1 transcription complex, stress response
CDKN1A	28	Cell cycle arrest (p21)
RELA	26	NF-κB subunit, inflammatory regulation
FOS	25	AP-1 transcription complex
MYC	24	Cell proliferation, metabolism

Abbrevations: **TP53**-Tumor Protein p53; **IL6** – Interleukin-6; **CXCL8**-C-X-C Motif Chemokine Ligand 8 (Interleukin-8); **STAT3**-Signal Transducer and Activator of Transcription 3; **IFNG** – Interferon-Gamma; **CDKN1A**-Cyclin-Dependent Kinase Inhibitor 1A (p21); **RELA** – v-rel avian reticuloendotheliosis viral oncogene homolog A.

These hub genes are widely reported as key regulators of immune signaling, cytokine production, apoptosis, and cell cycle control, all of which are relevant to PBC pathogenesis. Thus,

they were prioritized for downstream enrichment and drug repurposing analysis. Collectively, these hubs support the central involvement of inflammatory signaling and cell fate regulation in PBC.

These genes were selected for downstream enrichment, drug–gene interaction, and binding validation analyses. A sensitivity analysis performed at a STRING confidence score ≥ 0.7, restricted to experimentally validated and curated database interactions, confirmed that IL6, TP53, STAT3, JUN, and RELA remained among the highest-ranked hub genes. This indicates that the centrality of key regulators was stable and not dependent on the chosen interaction confidence threshold.

3.3. Cluster analysis via MCODE

MCODE identified three highly connected modules (clusters) within the STRING-derived PPI network, Table 2. The disease-associated network shows functional modularity through these clusters supporting the involvement of immune-inflammatory, apoptotic, and metabolic pathways in PBC.

Table 2. Functional modules detected by MCODE analysis of The PPI network. Each cluster is characterized by high internal connectivity (MCODE score) and enriched biological functions derived from Reactome annotations and literature evidence.

Cluster No	MCODE Score	No. of Genes	Key Genes	Enriched Function
Cluster 1	6.4	12	TP53, IL6, STAT3, RELA	Cytokine and interleukin signaling
Cluster 2	4.9	9	CDKN1A, FOS, JUN	Cell cycle and apoptosis regulation
Cluster 3	3.2	5	DHCR7, CYP7A1	Metabolic processes and bile acid homeostasis

Abbrevations: TP53-Tumor Protein p53; IL6 – Interleukin-6; CXCL8-C-X-C Motif Chemokine Ligand 8 (Interleukin-8); STAT3-Signal Transducer and Activator of Transcription 3; IFNG – Interferon-Gamma; CDKN1A-Cyclin-Dependent Kinase Inhibitor 1A (p21); RELA – v-rel avian reticuloendotheliosis viral oncogene homolog A; DHCR7-7-dehydrocholesterol reductase; CYP7A1-cytochrome P450 family 7 subfamily A member 1.

Notably, Cluster 1 encompassed several canonical immune and cytokine regulators (TP53, IL6, STAT3, RELA), underscoring the centrality of immune signaling in PBC.

3.4. Reactome Pathway Enrichment

Pathway enrichment analysis was performed using the Reactome database to better understand the biological functions and signaling pathways associated with the PBC-associated gene set (Fig. 2). In the primary analysis based on all 214 PBC-associated genes, we observed significant over-representation of immune-regulatory, cytokine, and TP53-related pathways. A secondary analysis restricted to the 30 top-degree hub genes yielded a qualitatively similar pattern with an even stronger over-representation of interleukin and cytokine signaling (Supplementary Fig 3), indicating that the immune-cytokine signature is not an artefact of hub selection but a core feature of the network.

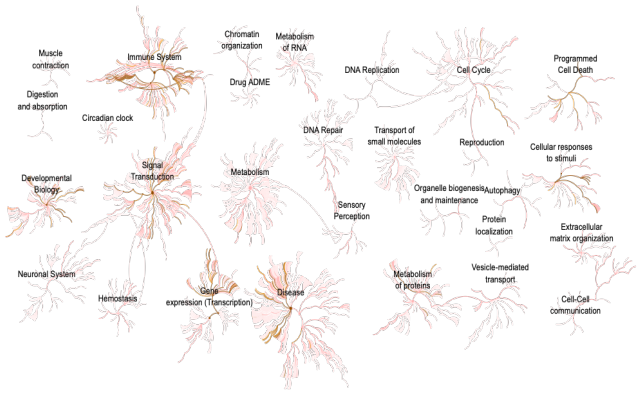

Figure 2. Reactome Pathway Overview. A global map of pathway involvement generated from the input gene list. Highlighted branches represent significantly enriched nodes based on hub gene overlaps.

As shown in Fig 3, the top enriched pathways were predominantly related to immune regulation and cytokine signaling, which are critically implicated in the pathogenesis of PBC.

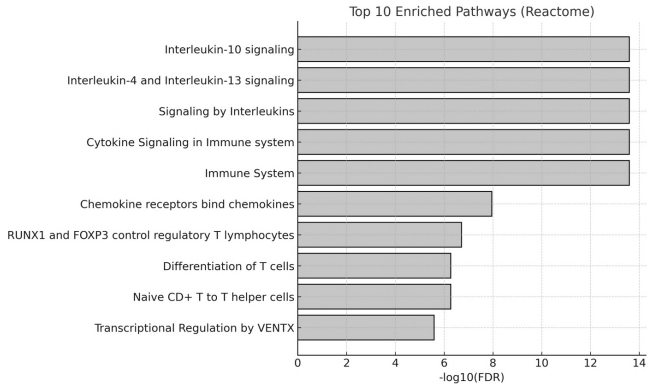

Figure 3. Top 10 enriched biological pathways ıdentified via Reactome analysis. The x-axis represents the – $\log_{10}$ (FDR) values, indicating significance. The top pathways involve interleukin signaling, immune system modulation, and transcriptional regulation-all relevant to the immunopathogenesis of PBC.

These pathways collectively reflect the multifactorial nature of PBC, involving cross-talk between immune activation, apoptotic processes, and metabolic dysregulation.

3.5. Drug-gene Interactions

A drug-gene interaction was performed to (Passive voice shoul be used) explore the therapeutic relevance of the identified hub genes in PBC, analysis using the DSigDB database via the Enrichr platform. The analysis identified FDA-approved drugs and investigational compounds linked to the selected hub genes. The study analyzed compounds that have established mechanisms of action which play a crucial role in both immune system regulation and liver function.

The MEK inhibitor PD98059 which indirectly affects TP53-regulated pathways showed promise as an antifibrotic compound among the most popular hits (Fig 4). The IL-6 receptor blocker Tocilizumab emerged as a mechanistically relevant candidate based on network centrality and pathway involvement; however, current evidence does not establish a therapeutic benefit in PBC, and its relevance remains exploratory. The hepatoprotective antioxidant N-acetylcysteine, linked to IFNG in the enrichment output, also showed therapeutic relevance.

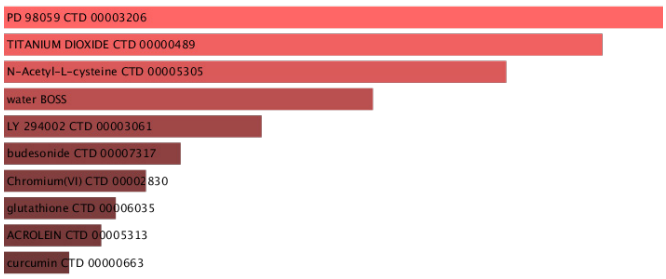

Figure 4. Top drug-gene ınteractions based on Dsigdb analysis. Bar length reflects – $\log_{10}$ (p-value) enrichment. Drugs with relevance to hepatic or immune pathways are emphasized.

Table 3. Summary of top drug–gene interactions identified via DSigDB.

Drug	Pharmacological Target (Direct)	Network/ Pathway Gene Influenced	Drug Class	Indication	Approval	Repurposing Potential
PD98059	MAP2K1 (MEK1)	TP53 (p53 signaling axis)	MEK inhibitor	Preclinical oncology	–	Moderate (antifibrotic)
Tocilizumab	IL6R (Interleukin-6 receptor)	IL6	IL-6 blocker	Rheumatoid arthritis, cytokine storms	FDA	High (immune suppression)
Budesonide	NR3C1 (Glucocorticoid receptor)	CXCL8	Corticosteroid	Crohn's disease, ulcerative colitis	FDA	High (liver inflammation)
NAC	– (Redox modulation / glutathione precursor)	IFNG (hypothesis-supported docking)	Antioxidant	Acetaminophen toxicity	OTC	High (hepatoprotective)
Simvastatin	HMGCR	DHCR7 (cholesterol biosynthesis pathway)	Statin	Hyperlipidemia	FDA	Moderate (antifibrotic)
Vorinostat	HDAC1/HDAC2	CDKN1A (p21 expression)	HDAC inhibitor	T-cell lymphoma	FDA	Experimental (autoimmunity)

Abbrevations: TP53-Tumor Protein p53; IL6 – Interleukin-6; CXCL8-C-X-C Motif Chemokine Ligand 8 (Interleukin-8); IFNG – Interferon-Gamma; CDKN1A-Cyclin-Dependent Kinase Inhibitor 1A (p21); DHCR7-7-dehydrocholesterol reductase; MAP2K1 (MEK1)-Mitogen-Activated Protein Kinase Kinase 1; HDAC-Histone Deacetylase; HMGCR-3-Hydroxy-3-Methylglutaryl-CoA Reductase; NR3C1-Nuclear Receptor Subfamily 3 Group C Member 1.

Overall, these findings point to clinically accessible or repositionable agents that may modulate key pathways involved in PBC pathogenesis. A summary of selected drug-gene interactions is presented in Table 3, while the complete list is provided in Supplementary Table S1.

These interactions were further validated through computational binding and structural analyses.

3.6. Computational Validation of Drug–target Binding Affinities

BindingDB affinity data and SwissDock docking results supported the plausibility of the prioritized drug–target relationships (Table 4). Several pairs showed nanomolar-range inhibitory activity based on reported BindingDB values.

Reported affinities included IC_{50} = 2.8 μM for PD98059–MAP2K1, IC_{50} = 0.5–1.6 nM for Budesonide–NR3C1, IC_{50} = 4–18 nM for Simvastatin–HMGCR, and K_i = 10–50 nM for Vorinostat–HDAC1/2.

The results show that the identified compounds possess high target specificity and their action mechanisms match what science has proven.

The docking simulation of N-acetylcysteine against IFNG produced an AC score of −24.70 and a SwissParam energy of −6.62 kcal/mol suggesting a potential weak-to-moderate interaction. The top-ranked pose localized to a buried pocket within the IFNG structure and formed multiple hydrogen-bond and electrostatic contacts with nearby polar residues, supporting a hypothesis of redox-sensitive cytokine modulation. A binding free energy of approximately −6.6 kcal/mol represents weak–moderate affinity, and therefore the NAC–IFNG interaction should be interpreted as exploratory rather than physiologically meaningful

The researchers did not perform computational docking of tocilizumab with IL-6R because the complete receptor–Fab interface structure is not available, preventing reliable in silico modeling. Instead, tocilizumab was retained based on experimentally confirmed target engagement. Surface plasmon resonance and structural studies have demonstrated sub-nanomolar affinity for IL-6R ($K_d \approx 2–4 \times 10^{-10}$ M). In contrast to NAC, tocilizumab was therefore not docked, and its relevance in this study derives exclusively from these experimentally validated binding data rather than computational prediction. The high-affinity IL-6R blockaded achieved by tocilizumab underlies its established clinical activity in immune-mediated diseases.

Table 4. Summary of experimentally validated and computationally predicted drug–target interactions.

Drug	Target	Experimental Binding (BindingDB/ Literature)	Type of Data	Docking (SwissDock)	Binding Energy (ΔG, kcal/mol)	AC Score (unitless)	Interpretation
PD98059	MAP2K1	IC_{50} = 2.8 μM	Experimental	–	–	–	Moderate inhibitor
Budesonide	NR3C1	IC_{50} = 0.5–1.6 nM	Experimental	–	–	–	Strong GR agonist
Simvastatin	HMGCR	IC_{50} = 4–18 nM	Experimental	–	–	–	Potent enzyme inhibitor
Vorinostat	HDAC1/2	K_i = 10–50 nM	Experimental	–	–	–	Strong epigenetic modulator
NAC	IFNG	–	Docking	Completed	−6.62	−24.70	Potential weak-moderate binding
Tocilizumab	IL6R	$K_d \approx 2–4 \times 10^{-10}$ M	Literature	Not applicable	–	–	Experimentally validated antibody-receptor binding

Overall, integrating experimental affinity evidence with docking results supports the pharmacological feasibility of the proposed repurposed agents in PBC.

4. Discussion

This study employed network-based approaches with computational validation to identify therapeutic targets and drug candidates for PBC, a disease that requires improved treatment options due to suboptimal responses to current therapies. The research integrated multi-omics data mining with PPI network analysis, hub gene prioritization, Reactome pathway enrichment, drug-gene mapping, and binding affinity evaluation using BindingDB and SwissDock to develop a comprehensive systems-level framework linking computational findings to translational relevance.

The identified hub genes-TP53, IL6, CXCL8, STAT3, IFNG, JUN, CDKN1A, RELA, FOS, and MYC-act as key regulatory factors governing immune responses, apoptotic pathways, and cell cycle regulation. The PPI network shows their essential position in PBC disease development because they interact strongly with numerous other proteins. IL6 and STAT3 function as essential components of the IL6/ Janus Kinase (JAK)/ STAT3 signaling pathway which plays a key role in both chronic inflammation and fibrogenesis during autoimmune liver injury. CXCL8 promotes neutrophil recruitment, contributing to liver tissue damage, whereas TP53 and CDKN1A (p21) indicate that dysregulated apoptosis plays a role in cholangiocyte loss. These findings demonstrate that PBC develops through multiple interconnected mechanisms, including immune dysregulation, apoptosis, oxidative damage, and impaired tissue repair. Importantly, the hub genes identified in this study should be interpreted within the biological context of biliary injury. In PBC, cholangiocytes are the primary immune targets, and cytokine pathways such as IL6–STAT3 signaling promote cholangiocyte survival, epithelial–mesenchymal transition, ductular reaction, and peri-portal inflammation. CXCL8-mediated neutrophil recruitment further amplifies biliary injury, while TP53–CDKN1A activation reflects oxidative-stress-induced DNA damage and apoptosis in stressed cholangiocytes. These pathways are also influenced by infiltrating T lymphocytes, macrophages, and Kupffer cells, indicating that the identified hub genes function across multiple cellular compartments rather than within a single-cell population. Therefore, the network signature likely represents a composite of immune-epithelial cross-talk, hepatocyte stress responses, and stromal remodeling rather than a purely hepatocyte-limited process.

Pathway enrichment analysis revealed significant enrichment of interleukin signaling, TP53-regulated transcription, and cytokine-mediated signaling pathways showed significant enrichment which corresponds to the immunopathological features of PBC. The disease progression extends past immune system activation because apoptotic and metabolic pathways show signs of enrichment which indicates that hepatocytes and cholangiocytes experience intrinsic survival challenges and bile acid regulation has become disrupted. The study results confirm previous research which shows that oxidative stress and mitochondrial dysfunction and fibrotic remodeling work together to create PBC pathophysiology. The research findings validate a therapeutic model which treats immune system dysfunction and metabolic problems and apoptosis simultaneously instead of using a single treatment approach. Importantly, a similar pattern of interleukin – and TP53-related pathway enrichment was observed when using either the full 214-gene set or the restricted hub-gene subset, supporting the robustness of the immune–cytokine network signature.

The evaluation of drug–gene interactions showed several drugs which have strong potential for drug repositioning. The IL6 receptor blocker Tocilizumab functions as a central network node blocker with subnanomolar affinity ($K_d \approx 2–4 \times 10^{-10}$ M) according to previous structural and kinetic research. Budesonide functions as a glucocorticoid that undergoes extensive first-pass liver metabolism to produce localized immunosuppression while maintaining low systemic drug levels. SwissDock analysis suggested that N-acetylcysteine may interact with IFNG with an estimated binding free energy of approximately −6.6 kcal/mol which enables it to reduce oxidative stress by regulating redox reactions. The nanomolar inhibitory constants of Simvastatin (HMGCR target) and Vorinostat (HDAC1/2 target) in BindingDB indicate their

potential to regulate fibrosis and epigenetic processes. Collectively, these pharmacological profiles suggest that effective PBC treatment may require therapeutic strategies targeting inflammatory cytokine signaling, oxidative stress, and epigenetic regulatory mechanisms. It should also be emphasized that some immune-targeting agents, including IL-6 pathway inhibitors such as tocilizumab, have previously shown limited clinical benefit in PBC despite mechanistic plausibility. This further highlights the need for rigorous translational validation beyond computational prediction. Since DSigDB reports transcriptomic-signature similarity rather than experimentally verified target binding, enriched drugs such as PD98059 should be viewed as exploratory mechanistic probes. In our interpretation, only compounds with supportive biological plausibility, hepatology-relevant indications, and acceptable liver safety profiles were considered higher-priority repositioning candidates, whereas other DSigDB hits were classified as low-priority or purely exploratory.

In addition to UDCA-based therapy, recent clinical guidelines have incorporated fibrates (such as bezafibrate and fenofibrate) and emerging peroxisome proliferator–activated receptor (PPAR) agonists, including elafibranor, which have shown biochemical efficacy in selected patient populations. Despite these advances, current treatment options do not consistently achieve full biochemical remission in all patients. The conditional marketing authorization application for OCA was withdrawn by the sponsor in 2024 which demonstrates the requirement for new treatment options. The research identified multiple drugs which are FDA-approved and show good liver safety characteristics and can be quickly moved to clinical use. Although IL-6 pathway blockade and antioxidant modulation emerged as mechanistically relevant axes in our analysis, these observations should be regarded as hypothesis-generating. In particular, IL-6 receptor blockade with tocilizumab has not demonstrated consistent clinical benefit in PBC to date, and therefore its role remains uncertain.

This study illustrates how established network-based analyses can support the identification of biologically plausible drug–target relationships in PBC. Nonetheless, certain limitations must be acknowledged. The use of pre-existing gene–disease databases may introduce bias, as these resources are enriched for genes that have already been extensively studied. In addition, STRING and Reactome may not fully capture tissue-specific or dynamic interactions that are particularly relevant to cholangiocytes. The results from docking experiments also require experimental validation through biochemical assays and in vivo studies to verify the predicted binding potential. The NAC–IFNG docking signal was weak and no benchmarking controls were applied; therefore, this finding should be regarded as hypothesis-generating only and does not provide evidence of a true ligand–receptor interaction. Nevertheless, even though hub stability was preserved at higher STRING confidence thresholds, network-level findings should still be interpreted as hypothesis-generating rather than confirmatory. In addition, the present analysis does not resolve cell-type specificity or disease-stage dynamics. Since bulk-level gene associations may reflect mixed contributions from cholangiocytes, hepatocytes, stromal cells, and infiltrating immune populations, future studies should incorporate single-cell and spatial-omics datasets in PBC to define cell-restricted signaling programs and stage-dependent transcriptional shifts. Although hub stability was preserved at higher STRING confidence thresholds, network-derived findings should still be regarded as hypothesis-generating rather than confirmatory. Another important limitation is that network-derived drug candidates may not always translate into clinically meaningful efficacy, as enrichment-based associations do not fully account for pharmacokinetics, tissue distribution, off-target effects, or disease-specific immune-tolerance mechanisms. Therefore, the proposed compounds should be considered hypothesis-generating rather than definitive therapeutic recommendations. Future studies should integrate transcriptomic, proteomic, and single-cell analyses in PBC patient tissues to improve target identification and biological validation.

The integrative method demonstrates how computational analysis methods speed up the

development of new treatments for complicated liver diseases. The research establishes connections between disease gene networks and drug signatures to identify particular molecular targets which leads to the validation of Tocilizumab and Budesonide and NAC for clinical and translational research applications. The established methodology enables researchers to conduct reproducible precision medicine studies in hepatology which will help develop multiple-targeted treatments for PBC in future research.

5. Conclusion

This study contributes to the existing literature by providing a comprehensive systems-level framework that integrates disease-associated gene networks with pharmacological evidence to identify repurposable drug candidates for PBC. Compared with single-pathway approaches, single pathways or isolated molecular targets, our approach systematically prioritizes central regulatory hubs and directly links them to clinically accessible drugs using both experimental binding data and structure-based interaction analysis. By bridging network biology with pharmacological validation, this work offers a reproducible strategy for prioritizing testable candidates in autoimmune liver diseases and supports the rational repositioning of existing drugs for precision hepatology.

Using this integrative network-based analysis, we identified essential molecular regulators and therapeutic targets for PBC. Analysis of 214 PBC-associated genes revealed key central hubs, including TP53, IL6, CXCL8, STAT3, IFNG, and CDKN1A, which collectively regulate immune responses, apoptotic signaling, and fibrotic pathways. Reactome pathway enrichment highlighted cytokine – and interleukin-mediated signaling as dominant biological processes. Furthermore, combined drug–gene interaction analysis and computational validation identified Budesonide, Simvastatin, Vorinostat, NAC, and Tocilizumab as potential repositionable agents targeting core mechanisms of PBC pathogenesis. These findings demonstrate that network-based analysis coupled with drug repurposing represents an efficient and cost-effective strategy to accelerate therapeutic development for autoimmune liver diseases. Future studies integrating multi-omics data with experimental validation in PBC-relevant cellular systems will be essential to support clinical translation.

Conflicts of interest: The authors declare no conflicts of interest related to this work.

Funding: This research received no external funding.

Ethics approval: Not applicable

Data availability: All data used in this study are included in the article and its supplementary files.

Author Contributions: Conceptualization, D.S.A.; methodology, D.S.A. and N.H.K.; formal analysis, D.S.A.; investigation, D.S.A., N.H.K., and F.C.; data curation, D.S.A. and F.C.; validation, D.S.A. and A.K.; writing-original draft preparation, D.S.A.; writing-review and editing, D.S.A., N.H.K., F.C., and A.K.; supervision, D.S.A. All authors have read and agreed to the published version of the manuscript.

References

1. Rawashdeh B, Couillard A, Rawshdeh A, Aziz H, Esteban J, Selim M. Primary biliary cholangitis, liver transplantation, and hepatocellular carcinoma: A mini-review. Gene Expr. 2022;21(2):34-40. https://doi.org/10.14218/GE.2022.00016.
2. Reshetnyak VI, Vinnitskaya EV, Maev IV. Primary biliary cholangitis: A historical perspective from xanthomatous lesions to modern molecular biology. World J Gastrointest Pathophysiol. 2025;16(2). https://doi.org/10.4291/wjgp.v16.i2.107347
3. Kim KA. Diagnosis and treatment of primary biliary cholangitis. Korean J Gastroenterol. 2023;81(2):86-90. https://doi.org/10.4166/kjg.2023.002.
4. Cheung A, LaRusso N, Gores G, Lazaridis K. Epigenetics in the primary biliary cholangitis and primary sclerosing cholangitis. Semin Liver Dis. 2017;37(2):159-174. https://doi.org/10.1055/s-0037.160.3324.
5. Li Y, Tang R, Ma X. Epigenetics of Primary Biliary Cholangitis. In: Gershwin ME, Vierling JM, Manns MP, editors. Liver immunology: Principles and practice. Cham: Springer; 2020. p. 259-83. https://doi.org/10.1007/978-981-15-3449-2_10
6. Xie YQ, Ma HD, Lian ZX. Epigenetics and primary biliary cirrhosis: a comprehensive review and ımplications for autoimmunity. Clin Rev Allergy Immunol. 2016;50(3):390-403. https://doi.org/10.1007/s12016.015.8502-y.
7. Prieto J, Banales JM, Medina JF. Primary biliary cholangitis: pathogenic mechanisms. Curr Opin Gastroenterol. 2021;37(2):91-98. https://doi.org/10.1097/MOG.000.000.0000000703.

8. Houri I, Hirschfield GM. Primary biliary cholangitis. Clin Liver Dis. 2024;28(1):79-92. https://doi.org/10.1016/j.cld.2023.06.006.
9. Lin CI, Wang YW, Liu CY, Chen HW, Liang PH, Chuang YH. Regulatory T cells in inflamed liver are dysfunctional in murine primary biliary cholangitis. Clin Exp Immunol. 2024;215(3):225-239. https://doi.org/10.1093/cei/uxad117.
10. Kawata K, Tsuda M, Yang GX, Zhang W, Tanaka H, Tsuneyama K, Leung P, He XS, Knechtle S, Ansari AA, Coppel RL, Gershwin ME. Identification of potential cytokine pathways for therapeutic ıntervention in murine primary biliary cirrhosis. PLoS One. 2013;8(9):e74225. https://doi.org/10.1371/journal.pone.0074225.
11. Ellinghaus D. How genetic risk contributes to autoimmune liver disease. Semin Immunopathol. 2022;44(4):397–410. https://doi.org/10.1007/s00281.022.00950-8.
12. Asuri S, McIntosh S, Taylor V, Rokeby A, Kelly J, Shumansky K, Field LL, Yoshida EM, Arbour L. Primary biliary Cholangitis in British Columbia first nations: Clinical features and discovery of novel genetic susceptibility loci. Liver Int. 2018;38(5):940–948. https://doi.org/10.1111/liv.13686.
13. Chen J, Lyu Y, Huang W, Li Z, Li Y, Yu S, Zeng R, Deng Y, Liang Z, Wang J, Leung FW, Huang J, Sha W, Chen H. Multi-omics analysis reveals potential therapeutic targets and genetic mechanisms in primary biliary cholangitis [Preprint]. Research Square. 2025 [cited 2025 Feb 1]. https://doi.org/10.21203/rs.3.rs-7186861/v1
14. Yang YC, Ma X, Zhou C, Xu N, Ding D, Ma ZZ, Zhou L, Cui PY. Functional investigation and two-sample Mendelian randomization study of primary biliary cholangitis hub genes. World J Clin Cases. 2024;12(30):6391-6406. https://doi.org/10.12998/wjcc.v12.i30.6391.
15. Fiorucci S, Urbani G, Di Giorgio C, Biagioli M, Distrutti E. Current landscape and evolving therapies for primary biliary cholangitis. cells. 2024;13(18):1580. https://doi.org/10.3390/cells13181580.
16. Ueno K, Aiba Y, Hitomi Y, Shimoda S, Nakamura H, Gervais O, Kawai Y, Kawashima M, Nishida N, Kohn SS, Kojima K, Katsushima S, Naganuma A, Sugi K, Komatsu T, Mannami T, Matsushita K, Yoshizawa K, Makita F, Nikami T, Nishimura H, Kouno H, Kouno H, Ohta H, Komura T, Tsuruta S, Yamauchi K, Kobata T, Kitasato A, Kuroki T, Abiru S, Nagaoka S, Komori A, Yatsuhashi H, Migita K, Ohira H, Tanaka A, Takikawa H, Nagasaki M, Tokunaga K, Nakamura M; PBC-GWAS Consortium in Japan. Integrated GWAS and mRNA microarray analysis identified IFNG and CD40L as the central upstream regulators in primary biliary cholangitis Hepatol Commun. 2020;4(5):724-738. https://doi.org/10.1002/hep4.1497.
17. Mitchell NE, Chan SY, Jerez Diaz D, Ansari N, Lee J, Twohig P. Evolving therapeutic landscape of primary biliary cholangitis: A review. World J Hepatol. 2025;17(7):107223. https://doi.org/10.4254/wjh.v17.i7.107223
18. Jhaveri M, Kowdley K. New developments in the treatment of primary biliary cholangitis – role of obeticholic acid. Ther Clin Risk Manag. 2017;13:1053–1060. https://doi.org/10.2147/TCRM.S113052.
19. Floreani A, Gabbia D, De Martin S. Obeticholic acid for primary biliary cholangitis. Biomedicines. 2022;10(10):2464. https://doi.org/10.3390/biomedicines10102464.
20. Floreani A, Gabbia D, De Martin S. Reviewing novel findings and advances in diagnoses and treatment of primary biliary cholangitis. Expert Rev Gastroenterol Hepatol. 2025;19(8):891-902. https://doi.org/10.1080/17474.124.2025.2537192.
21. Iljinsky IM, Tsirulnikova OM. Primary biliary cholangitis. Russ J Transplantol Artif Organs. 2021;23(1):162-170. https://doi.org/10.15825/1995-1191-2021-1-162-170.
22. Fiorucci S, Urbani G, Distrutti E, Biagioli M. Obeticholic acid and other Farnesoid-X-Receptor (FXR) agonists in the treatment of liver disorders. Pharmaceuticals (Basel). 2025;18(9):1424. https://doi.org/10.3390/ph18091424.
23. Floreani A, Sun Y, Zou ZS, Li B, Cazzagon N, Bowlus CL, Gershwin ME. Proposed therapies in primary biliary cholangitis. Expert Rev Gastroenterol Hepatol. 2016;10(3):371–382. https://doi.org/10.1586/17474.124.2016.1121810.
24. Warsop Z, Anand N, Al Maliki H, De Souza S, Kamyab A, Al Hadad A, Alrubaiy L. Up-to-date snapshot of current and emerging medical therapies in primary biliary cholangitis. J Pers Med. 2024;14(12):1133. https://doi.org/10.3390/jpm14121133.
25. arba Bernal R, Ferrigno B, Medina Morales E, Castro CM, Goyes D, Trivedi H, Patwardhan VR, Bonder A. Management of Primary Biliary Cholangitis: Current treatment and future perspectives. Turk J Gastroenterol. 2023;34(2):89–100. https://doi.org/10.5152/tjg.2023.22239.
26. Pierini E, Mazza L, Petti M, Tieri P. Exploring drug repurposing success stories through a network-based approach: ınsights from a case study. In: 2024 IEEE International Conference on Bioinformatics and Biomedicine (BIBM); 2024 Dec 3-6; Lisbon, Portugal. IEEE; 2024. p. 6959-64. https://doi.org/10.1109/BIBM62325.2024.108.22355
27. Seyath S, Arun TS, Sanjith S, Prasobh GR. A Review on Drug Repurposing: A Functional ınstrument for contemporary drug delivery. Int J Pharm Res Appl. 2025;10(4):266–271. https://doi.org/10.35629/4494.100.4266271.
28. Chikodi Ekeomodi C, Ifeanyi Obetta K, Linus Okolocha M, Nnacho S, Oluwaseun Isijola M, IfedibaluChukwu Ejiofor I. Computational approaches in drug repurposing. In: Drug Repurposing-advances, scopes and opportunities in drug discovery. IntechOpen; 2023. https://doi.org/10.5772/intechopen.110638.
29. Hong D, Kesselheim A. Strategies to advance drug repurposing for rare diseases [Preprint].DrugArXiv.2025[cited2025Feb1]. https://doi.org/10.58647/DRUGARXIV.PR000027.v1
30. Naffouj S, Wang J. Current and future opportunities for the management of primary biliary cholangitis. Front Gastroenterol. 2023;2:1241901. https://doi.org/10.3389/fgstr.2023.124.1901
31. Piñero J, Ramírez-Anguita JM, Saüch-Pitarch J, Ronzano F, Centeno E, Sanz F, Furlong LI. The DisGeNET knowledge platform for disease genomics: 2019 update. Nucleic Acids Res. 2019. https://doi.org/10.1093/nar/gkz1021.
32. Szklarczyk D, Kirsch R, Koutrouli M, Nastou K, Mehryary F, Hachilif R, Gable AL, Fang T, Doncheva NT, Pyysalo S, Bork P, Jensen LJ, von Mering C. The STRING database in 2023: protein-protein association networks and functional enrichment analyses for any sequenced genome of interest. Nucleic Acids Res. 2023;51(D1):D638–D646. https://doi.org/10.1093/nar/gkac1000.
33. Ono K, Fong D, Gao C, Churas C, Pillich R, Lenkiewicz J, Pratt D, Pico AR, Hanspers K, Xin Y, Morris J, Kucera M, Franz M, Lopes C, Bader G, Ideker T, Chen J. Cytoscape Web: bringing network biology to the browser. Nucleic Acids Res. 2025;53(W1):W203–W212. https://doi.org/10.1093/nar/gkaf365.
34. Yoo M, Shin J, Kim J, Ryall KA, Lee K, Lee S, Jeon M, Kang J, Tan AC. DSigDB: drug signatures database for gene set analysis. Bioinformatics.2015;31(18):3069-71. https://doi.org/10.1093/bioinformatics/btv313

35. Liu T, Hwang L, Burley SK, Nitsche CI, Southan C, Walters WP, Gilson MK. BindingDB in 2024: a FAIR knowledgebase of protein-small molecule binding data. Nucleic Acids Res. 2025;53(D1):D1633–D1644. https://doi.org/10.1093/nar/gkae1075.
36. Bugnon M, Röhrig UF, Goullieux M, Perez MAS, Daina A, Michielin O, Zoete V. SwissDock 2024: major enhancements for small-molecule docking with Attracting Cavities and AutoDock Vina. Nucleic Acids Res. 2024;52(W1):W324–W332. https://doi.org/10.1093/nar/gkae300.
37. Röhrig UF, Goullieux M, Bugnon M, Zoete V. Attracting Cavities 2.0: Improving the Flexibility and Robustness for Small-Molecule Docking. J Chem Inf Model. 2023;63(12):3925-3940. https://doi.org/10.1021/acs.jcim.3c00054.
38. Xu C, Rafique A, Potocky T, Paccaly A, Nolain P, Lu Q, Iglesias-Rodriguez M, St John G, Nivens MC, Kanamaluru V, Fairhurst J, Ishii T, Maldonado R, Choy E, Emery P. Differential binding of Sarilumab and Tocilizumab to IL-6Rα and effects of receptor occupancy on clinical parameters. J Clin Pharmacol. 2021;61(5):714-724. https://doi.org/10.1002/jcph.1795.
39. Rafique A, Martin J, Blome M, Huang T, Ouyang A, Papadopoulos N. Evaluation of the binding kinetics and functional bioassay activity of sarilumab and tocilizumab to the human IL-6 receptor alpha. Ann Rheum Dis. 2013;72:A797. https://doi.org/10.1136/annrheumdis-2013-eular.2360.

Cite this article: Sari-Ak D, Helvaci-Kurt N, Con F, Kural A. Integrative Analysis of Molecular Interactions and Repurposable Drugs in Primary Biliary Cholangitis Pharmedicine J. 2026;3(1): 45-60. DOI: 10.62482/pmj.40